2021•2022

Faculteit Industriële Ingenieurswetenschappen

master in de industriële wetenschappen: elektromechanica

Masterthesis

Analysis and simulation of a floating PV plant and the construction of a floating PV demonstrator

PROMOTOR :

Prof. dr. ir. Michael DAENEN

PROMOTOR :

dr. Ismail KAAYA

Marco Morelli, Michiel Voglar

Scriptie ingediend tot het behalen van de graad van master in de industriële wetenschappen: elektromechanica

Gezamenlijke opleiding UHasselt en KU Leuven

2021•2022

Faculteit Industriële Ingenieurswetenschappen

master in de industriële wetenschappen: elektromechanica

Masterthesis

Analysis and simulation of a floating PV plant and the construction of a floating PV demonstrator

PROMOTOR :

Prof. dr. ir. Michael DAENEN

PROMOTOR :

dr. Ismail KAAYA

Marco Morelli, Michiel Voglar

Scriptie ingediend tot het behalen van de graad van master in de industriële wetenschappen: elektromechanica

UHASSELT

KU LEUVEN

Foreword

This Master's thesis was part of our graduation programme in industrial engineering at UHasselt - KULeuven in Diepenbeek and commissioned by imec from September 2021 to June 2022. The choice of this thesis' topic stemmed from the interest in renewable energy technology of both of us. The fact that the subject included both an analytical side in the form of simulations and data analysis and a more practical side with the construction of a demonstrator was particularly appealing. The Master's thesis also gave us the opportunity to learn and add value in floating PV technology.

There are a few people who contributed to this thesis that we would like to thank. Firstly, our promotors prof. dr. ir. Michael Daenen and dr. Ismail Kaaya for their guidance and feedback. But also dr. ir. Joris Lemmens and dr. ir. Arttu Tuomiranta for their role as promotor before dr. Kaaya. Secondly, we would also like to thank Energyville's technical staff, Luc Vastmans, Geert Doumen and Reinoud Moors, for their support in building and designing the demonstrator.

Marco Morelli and Michiel Voglar

June 2022

Table of contents

List of tables

List of figures

Glossary of terms

DHI	Diffused Horizontal Irradiance
DNI	Diffused Normal Irradiance
FPV	Floating Photovoltaics
GHI	Global Horizontal Irradiance
GPV	Ground-mounted Photovoltaics
MAE	Mean Absolute Error
MBE	Mean Bias Error
MPPT	Maximum Power Point Tracker
POA	Plane Of Array
RMSE	Root Mean Square Error
r-value	Correlation coefficient
STC	Standard Testing Conditions

Abstract

The efficient integration of solar panels into the environment is one of the focus points of imec's energy division, based in Energyville Genk. This Master's thesis supports imec in its research on floating photovoltaics (FPV), a novel integration method that uses the free space on water bodies to generate electricity. It shows multiple benefits over ground-mounted PV (GPV). However, the claim that FPV systems perform better due to improved module cooling is still controversial. In this work, module cooling is investigated based on measured data from an FPV system in Meer, Antwerp called Clicfloats Project 600. Next to this, the accuracy of commercially available software, such as PVSyst, is analysed for use in FPV simulation. Finally, an interactive demonstrator is designed and built for promotional purposes.

To examine the module cooling, a thorough data analysis was done. The FPV simulation accuracy of PVSyst was tested on the Clicfloats system by comparing its results with both the measured data and imec's own framework. The demonstrator was built using ordered and 3D printed parts. Ultimately, the analysed data shows that nearby water has no effect on module temperature in the Clicfloats system and that cooling is more correlated to wind velocity and direction. The results of the simulations showed that both PVSyst and imec's framework underestimate the power output with a mean bias error of less than 9%. The demonstrator is a Clicfloats inspired FPV setup with working PV panels.

Abstract in het Nederlands

Integratie van zonnepanelen in de omgeving is één van de focuspunten van imec's energiedivisie, gevestigd in Energyville Genk. Deze masterproef ondersteunt imec in hun onderzoek naar drijvende zonnepanelen of floating photovoltaics (FPV) in het Engels. FPV is een nieuwe integratiemethode die van de vrije ruimte op waterlichamen gebruik maakt om energie op te wekken. De bewering dat FPV-systemen beter presteren door een betere modulekoeling is echter nog steeds controversieel. In dit werk wordt de modulekoeling onderzocht met data van een FPV-systeem in Meer, Antwerpen genaamd Clicfloats Project 600. Daarnaast wordt de nauwkeurigheid van commerciële software, zoals PVSyst, geanalyseerd voor het simuleren van FPV-systemen. Tot slot wordt er een demonstrator ontworpen en gebouwd voor promotiedoeleinden.

Een data-analyse werd uitgevoerd om de modulekoeling te onderzoeken. De nauwkeurigheid van PVSyst werd getest op het Clicfloatssysteem door de resultaten te vergelijken met de werkelijke gegevens en imec's eigen framework. De demonstrator werd gebouwd met bestelde en 3D-geprinte onderdelen. Uiteindelijk toont de data aan dat het nabijgelegen water geen effect heeft op de moduletemperatuur in het Clicfloatssysteem en dat de koeling vooral gecorreleerd is aan de windsnelheid en -richting. De simulatieresultaten tonen aan dat zowel PVSyst als imec's framework de vermogenoutput onderschatten met een gemiddelde biasfout van minder dan 9 %. De demonstrator is een, op Clicfloats gebaseerde, FPV-opstelling met werkende PV-panelen.

1. Introduction

1.1. Context

The main challenge of the ongoing global energy transition is shifting from the use of conventional fossil-based fuels to green zero-carbon solutions. Popular green solutions include the harvesting of wind, hydro and solar power. Even though they are popular and already widely used, further research is still being done. Especially in terms of solar power, there are many organizations invested into researching its integration into buildings, vehicles and other items or objects. The reason why integration has become such a big goal is because empty space is a very valuable resource. This is especially true in densely populated areas where open land is scarce and expensive.

One of the prominent research organizations working on the integration of solar energy is imec. Its energy division, which is located at Energyville in Genk, houses many experts when it comes to the research and development (R&D) of solar energy and its various applications. Therefore, this Master's thesis will be written in association with the researchers at imec.

Returning to the topic of integrated solar, one of the promising solutions to save valuable space on land is floating photovoltaics or FPV in short. This is a relatively new technology that still has several uncertainties surrounding it. The basic components of an FPV system are PV modules mounted on floating platforms, mooring lines, anchoring, a transformer and at least one inverter. A visual overview of the system is given in Figure 1.

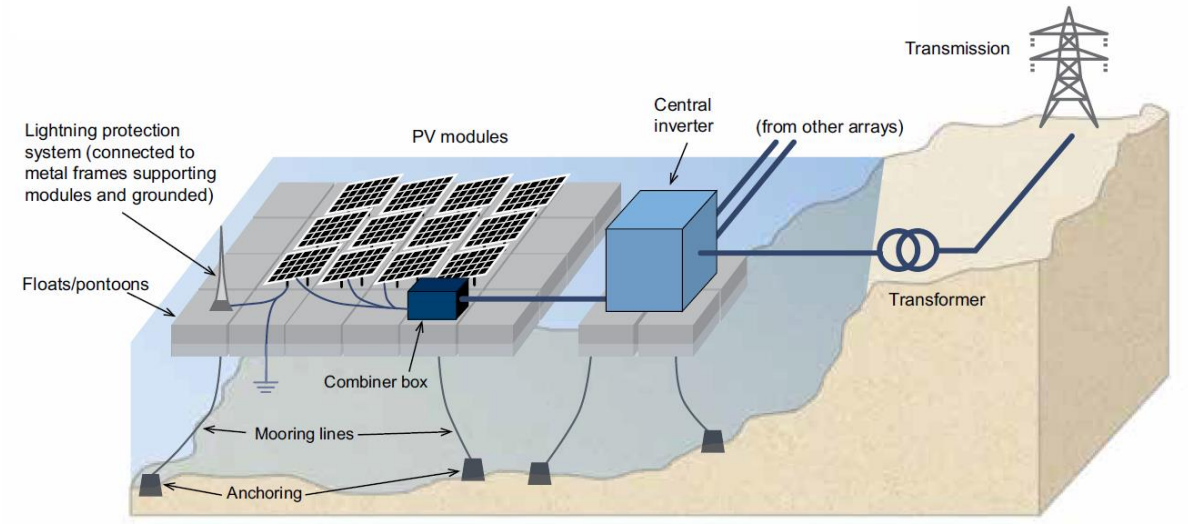

Figure 1: Drawing of a typical large FPV system [1, p. 13]

1.2. Problem statement

To save space on land and further increase green energy production, engineers have developed the concept of FPV. The first FPV system was constructed in 2007, and since then a large amount of research and testing has been done [1], [2]. This has led to advances in the technology and to researchers claiming that there is an additional benefit in the form of an increased energy yield [1], [3]–[6].

Yet to this day, it is still unclear how large this advantage is exactly. This is because of the vastly different research results ranging from an energy yield increase of 0 to 15% compared to land-based systems [7]. Therefore, further research is necessary including simulations and the analysis of data from real FPV plants.

Beside the need for additional research, it is necessary to demonstrate the potential and advantages of FPV to a broader audience. More specifically, the investors and energy companies. Promoting FPV in fairs and educational events would have a positive effect on the awareness and potential of the technology. In this case, imec is investing in a solution to promote and demonstrate FPV, as well as the research it is conducting into the application. The solution needs to be both interactive and visually appealing to draw attention at events.

1.3. Objectives

In this part of the introduction, a list of objectives is formed which should ultimately answer or solve the problems listed in the previous section.

Execute a literature review of state-of-the-art FPV applications
The first objective is performing a thorough literature study on FPV. The knowledge that is gathered from this will help understand the subject and explain the results of this work.

Determine the performance of commercially available software when simulating FPV systems
The first step to accomplishing this goal is creating a detailed simulation of a real-world FPV plant with industry-standard commercial software. Then, the results of the simulation are compared with the results of imec's proprietary solar simulation software. This is done to provide the researchers at imec with more insight on how their software compares to commercial software. The results are then also compared to the real-world data to find out the exact accuracy of the simulation.

Get a better insight on the module cooling of an FPV system by performing a data analysis
Another goal of this thesis is to challenge the hypothesis that was made in a previous Master's thesis by Mohamed Haggag; *Exploring the Thermal Dynamics of a Floating Photovoltaic System* [7] using real-world data. This involves going through every possible aspect that can have a positive impact on the energy yield (e.g. wind speed, water temperature, etc.) and checking if the data from a real plant confirms the theory.

Design and construct a realistic FPV demonstrator
Beside the analysis and simulation part of the thesis, the design and construction of a demonstrator is also one of the goals. This demonstrator will have an informational and promotional purpose at fairs or events. It will consist of a scaled-down, functional representation of an FPV plant where some of the important aspects of FPV are demonstrated including real-time monitoring of the energy yield.

1.4. Materials and methods

General information about the subject is obtained by conducting a literature study. The information starts off more general but then delves deeper into topics that are relevant for the further thesis.

At Energyville, the opportunity is given to be a part of Clicfloats project 600 in Meer, Antwerp in which imec is involved [8]. The project uses smaller, modular FPV elements that can be assembled to create a full-size FPV plant. The plant in Meer is extensively monitored with inverter readings and various sensor measurements (e.g., irradiance, temperature, etc.). Simulations of this FPV plant are made in PVSyst, which is a widely used commercial software. Python is the programming language used to process and analyse the data, make calculations, and create plots.

The FPV demonstrator is designed using Autodesk Inventor. The necessary parts are bought, or 3D printed. Construction of the setup is supported by the technical team of Energyville.

1.5. Content preview

The content of this thesis is separated into five main chapters. The first is an extensive literature study on the different aspects of FPV. This will provide general knowledge on the topic and introduce terms and principles necessary to better understand the remainder of the thesis. Next, the Clicfloats FPV system is introduced. This includes general information about the plant, as well as the system characteristics and various measurement devices. The third chapter discusses the simulation of an FPV plant and elaborates on the process of simulating the Clicfloats plant in PVSyst. The results of the simulation will be discussed and compared to measured data and imec's framework. This chapter is followed by the data analysis. This will try to provide answers to two questions using data from the Clicfloats system. Namely, what the influence of water temperature and wind speed is on module temperature. Chapter five deals with the design and building process of the FPV demonstrator. Finally, in the conclusion, the main results are summarised and final thoughts on the thesis are addressed.

2. Literature study

The purpose of the literature study is to gather the knowledge necessary to understand the subject and to aid in explaining the results of this work. The first topic of this literature study addresses a technology overview of FPV. Here, the different components of an FPV system are discussed and an overview of the benefits and drawbacks of FPV is given. A second topic analyses the energy yield. It addresses the conditions and losses that may affect the energy yield. The third topic explains thermal inertia of PV modules and its presence in an FPV environment. In this manner, the structure of the literature study starts with more general information and then goes deeper into the topics that are specifically interesting for this thesis.

2.1. Technology overview

2.1.1. State of the art

FPV is a relatively new method of generating solar energy with the first FPV system being built in 2007. Since 2016 the technology's market has grown rapidly and promises to grow even more in the future [1]. The rise of FPV has brought a lot of dynamism to the sector, making it difficult to group or categorize FPV systems. However, the configuration of an FPV system can usually be divided into several key components. These components are the floating structure, the anchoring and mooring system, cables, electrical components, and the solar panels themselves [8]. Figure 2 gives an overview of these components.

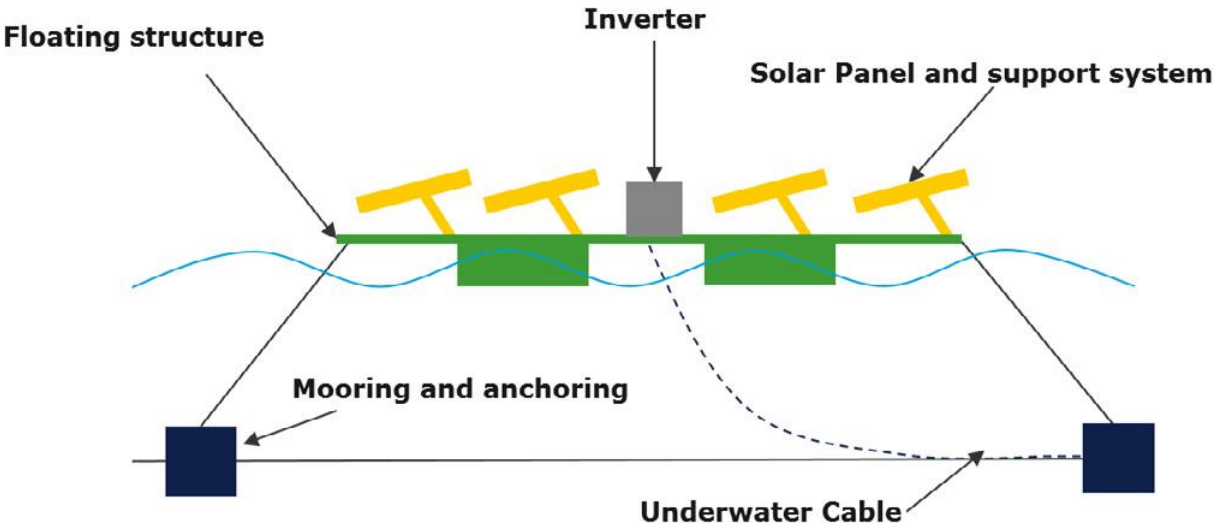

Figure 2: Overview of FPV components [8, p. 3]

FPV applications are currently mainly deployed on freshwater bodies like reservoirs and lakes. But technologies are being developed to implement FPV offshore as well. Offshore FPV adds complexity due to the additional challenges posed by the harsh marine environment and extreme wave loading. The number of offshore applications and concepts is rising but is still limited to this day [8]. The following sections of this literature study go more into detail on the key components of FPV.

2.1.2. Floating structures

The floating structure of an FPV system makes sure that the power generating equipment can float and is accessible [9]. The design is project specific and considers multiple variables such as the scale of the project, suitability of the water body's bed, cable routing, accessibility, etc [1]. Different floats are used for different components. For the module array three types are commonly used:

Pure floats

With this type, PV modules are mounted directly onto the floats. Each float usually holds one module [9]. They are easy to assemble and manufacture because arrays are made up of a number of these floats. This is also the reason why an array made up of these floats adapts well to wave motion and is thus less prone to stress. On the contrary, this wave-following design also introduces wave-induced losses, current mismatch, and cross-array shading. Another possible downside of this type is that the PV modules are very close to the water. This could have a negative effect on module cooling by wind (see section 2.3.2) [1]. Figure 3 illustrates the basic idea of pure floats.

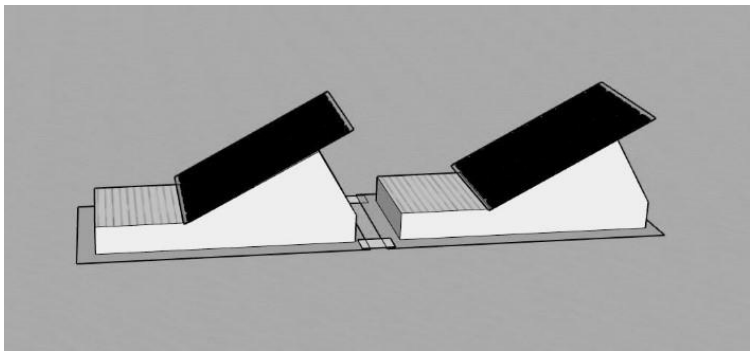

Figure 3: Illustration of pure floats [9, p. 78]

Modular rafts/pontoons + metal framing

This type uses metal framing that holds the PV modules and is supported by floats. Such a modular raft carries several PV modules and can also support combiner boxes, inverters and/or transformers [10]. This type does not require specially designed floats because here the floats are present just to provide buoyancy. Because it is a rigid structure, waves cause more stress at certain points [1].

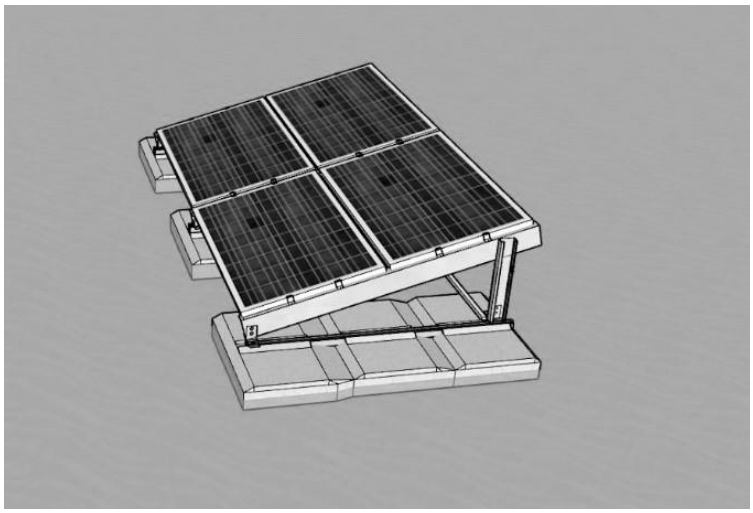

Figure 4: Illustration of modular pontoons [9, p. 78]

Membranes

This is a less common type of floating system where the PV modules are attached to a membrane. This membrane is supported by an additional structure that provides buoyancy [9]. An added benefit of the membrane is that it covers a large area of the water which helps prevent evaporation and saves water for drinking or irrigation. The direct contact with the water also helps with cooling [1]. Figure 5 shows the principle of membrane floats. Here, the membrane is supported by a tubular ring.

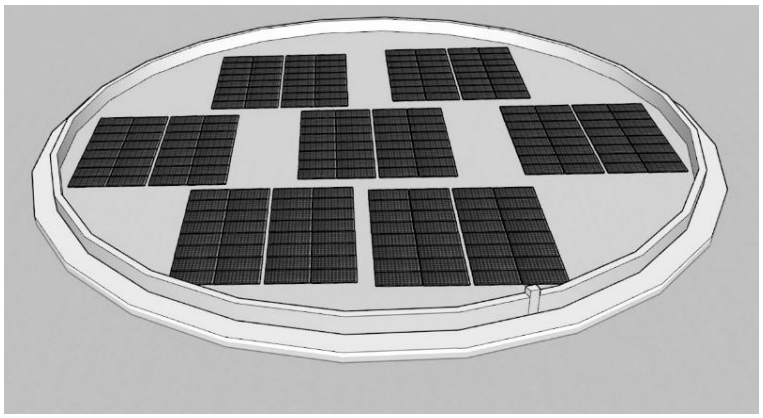

Figure 5: Illustration of membrane floats [9, p. 79]

Other components, such as inverters, combiner boxes, transformers, walkways and cables usually have their own unique floats.

The materials that are used for making floating structures mostly consist of synthetic polymer (heavy duty plastics) and metals. The most common material for floats is high-density polyethylene (HDPE). Framing and other mounting structures are made of metals like aluminium, stainless steel or carbon steel. The plastic material in the floats must be hard-wearing, UV-stable, and rot- and fire-resistant. It also aims to be recyclable. Key performance indicators are stability, strength, and long-term reliability. The PV modules used for FPV are tested to last 20 to 25 years, so the floating structure should also be able to last for the same time period. In addition, the floats must meet the environmental requirements. In the case of

drinking water reservoirs or lakes with wildlife, the plastic floats must not affect the water quality [9], [10].

2.1.3. Anchoring and mooring

The anchoring and mooring of an FPV system keep the floating system in place. It tries to keep the horizontal excursions of the array within acceptable levels, so it stays at a safe distance from the shore or doesn't bump into any obstacles or infrastructure [9]. How the mooring system is arranged and what anchor type is used depends on the site conditions. Mooring lines can be submerged, on shore or a combination of both. Because failure of the lines can lead to catastrophic damage, it is important to ensure redundancy. If one mooring line fails, the others should be able to hold the load. To ensure this, factors such as strength, stiffness, durability, and degradation must be taken into account while selecting the mooring line components.

The components that are a part of the mooring line assembly are the line material, connecting elements and possible mooring line segments. Common materials to be used are fiber rope, chain, or steel wire cable. Additionally, segments like elastic elements, buoyancy elements and clump weights can be added [9]. Buoys and auxiliary weights for example help to keep the mooring lines tight and accommodate for water-level changes. The length of mooring lines is an important factor as well. They should be long enough to accommodate for water-level changes while still limiting the lateral movement [10].

To anchor FPV arrays there are several options. Anchors can be installed at the bank and/or at the waterbed [9]. Anchoring at the bank is almost always the better option because it usually is more cost-effective [1]. This of course must be possible for the site. Mooring lines are then secured to shore points that can be drilled, gravity based, poles, bollards, etc. When choosing anchors at the waterbed options are; gravity-based anchors, embedded anchors and drag anchors [9]. Gravity-based anchors are most commonly used and can be as simple as heavy concrete blocks. Embedded anchors consist of screws or helical objects that are screwed into the substrate. They are generally used when terrain and soil conditions are more complex, or where loads are larger [1]. Drag anchors rely on frictional resistance of the surrounding soil [9].

An intermediate solution to anchoring at the bank and at the waterbed is anchoring on piles. Here, piles are drilled into the basin floor and mooring lines are attached to the top of the pile. This solution is especially useful for installations with special features like tracking and concentration. The pile can be used here as a central pole which the FPV platform resolves around. The platform can also slide up and down the piles which is a great response to water-level changes [1]. Figure 6 gives an illustration of the most common anchoring types.

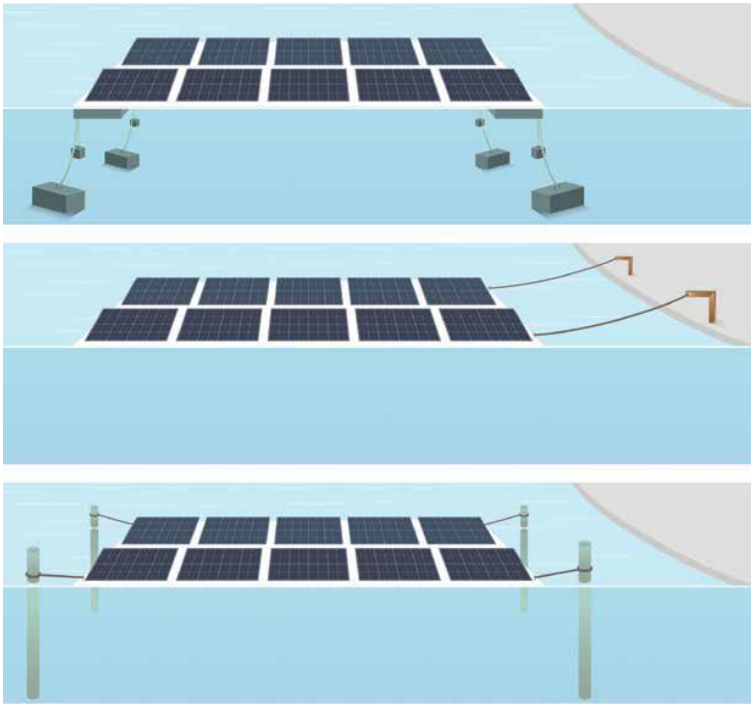

Figure 6: Anchoring types for FPV [1, p. 39]

2.1.4. Electrical layout and components

The specifics in electrical layout and components of an FPV system differ a bit from its ground mounted counterpart. This is due to the different environmental conditions that sometimes cause additional requirements.

Let's start with the PV modules. The stress factors of FPV modules can be quite different from ground mounted PV modules. Moisture, mechanical stress, hot-spots/shading, UV, high- and low temperature and temperature cycling can accelerate the degradation rate of a module and should be taken into consideration when choosing PV modules for an FPV site. Because of the robustness of existing module designs, a module suitable for tropical environments is able to be used in FPV with minimal or no modification [10].

Yet to improve reliability, a couple of mitigation strategies can be applied to minimize failure due to environmental stresses. To address increased moisture hardening, improved encapsulants and back sheets are available. Improvements to deal with mechanical stress can be made by enhancing panel stiffness or by mounting and placing strings and cells on the tensionless axis. Cutting cells in half will address fatigue because of the strain reduction on ribbons. For hotspots, a reduction in the number of cells on a diode can lower the temperature and use of higher rating material will improve heat resistance. Finally, to help prevent the formation of shading, there are antifouling coatings, antireflective coatings, and cleaning technologies being developed [10].

The other electrical components on an FPV system are grouped as "balance of system" and consist of inverters, combiner boxes, cabling and connectors, transformers, high voltage and medium voltage switchgear and enclosures, earthing, lightning protection, SCADA and

CCTV, and fire protection [9]. For all these components there are standards on the requirements.

Inverters
An inverter converts direct current (DC) electricity to alternating current (AC) electricity. This is necessary because the solar panels generate DC electricity and electricity grid lines use AC electricity for distribution. Inverters can either be central inverters or string inverters. With central inverters, one inverter is used to transform the DC electricity from all solar panels of the system. With string inverters, every string in the solar array has its own inverter. There is also the third and more expensive option of using micro inverters. Here, every solar panel has its own small inverter. Using micro inverters results in a higher energy yield. This is because every solar panel produces a different current and the current through a series string is always limited to the lowest current produced by a solar panel in said string [11].

When the FPV system is large and the distance to shore is long, it is recommended to position the inverters on a floating structure near the FPV array. When the distance to shore is short, it is better to place inverters on land. If inverters are placed on floats, it is important the inverters are properly enclosed so the electrical components cannot interact with the water [9].

Combiner boxes
The output of the solar strings is brought together in a combiner box. Inside the combiner box, the string conductors are connected to a fuse terminal. As an output, the fused inputs are combined onto a single conductor that connects to the inverter. Additional equipment such as disconnect switches, monitoring equipment, and remote rapid shutdown devices can also be integrated [12].

Cabling and connectors
Cables between the PV modules and combiner boxes are made of copper and are dual insulated [9]. The management of cables in an FPV installation requires careful planning. Cable lengths and cable routes are important because the right amount of slack must be provided to allow for movement of the floating array and variations in water levels. Large-scale FPV systems have the inverter and transformer floating close to the solar array. In these situations, cables will be routed to a substation on land. This can be done with the cables floating on the water or with submarine cables. When possible, floating cables are chosen because it is the less expensive option.

Transformers
Transformers are used to step-up the voltage of the solar panels to a voltage that is suitable for transmission. The transformer is usually placed close to the inverter and can be placed either on land or on floats. There are two types of transformers that are used, oil type transformers and dry type transformers. When harsher conditions are expected on the waterbody, dry-type transformers are preferred because when oil type transformers are damaged, they can potentially leak and spill to the water.

Earthing
The non-current-carrying exposed conductive parts of an installation must be grounded properly. Earth cables are usually routed to shore where they are grounded to an earth pit [10]. The design of the earthing is determined by a risk assessment. Here, all potential fault situations are considered [9].

Lightning protection
A lightning protection system has the purpose of protecting the PV installation from direct strikes and possible fires caused by lightning. External lightning protection intercepts direct lighting strikes and discharges lighting current to the ground. Internal lighting protection protects equipment from lightning strikes with surge-protection devices and equipotential bonding for metallic parts and frames. Lightning can induce large currents in the circuit when in proximity to cables. This effect is more severe for long cables. Therefore, it is important to keep the wiring distance as small as possible [10].

SCADA
SCADA stands for supervisory control and data acquisition. A SCADA system can be implemented in an FPV system to allow owners to monitor power generation and the condition of equipment. It can also perform maintenance checks on devices and send alarms.

CCTV and fire protection
Fire detection and fire extinguishing should be present in an FPV system as required by local codes and standards [9]. CCTV stands for closed circuit television and is used for monitoring and security purposes.

2.1.5. Benefits and drawbacks

Tables 1 and 2 respectively give an overview of the benefits and drawbacks that come with floating PV [1].

Table 1: Benefits of FPV

Benefit	**Explanation**
Land-use	In countries where land is scarce or not suited for PV, the cost of building ground-mounted PV systems rises. In countries where a lot of open land is available for PV, populated areas with high energy demand are sometimes far away from PV farms. In this case, far distances must be bridged to transmit the energy resulting in losses and high costs. In these cases, FPV provides a viable solution. FPV can utilize water surfaces that are otherwise unused at low cost.
Utilizing hard-to-access terrain	In some terrains it is not possible to deploy ground-mounted PV, for example mountainous regions. Man-made lakes or reservoirs in these areas can be used for FPV.
Reduced water evaporation	Evaporation causes a significant loss in water resources. Reducing water evaporation can be very beneficial where water is scarce. FPV helps with this because it covers parts of a water body's surface with its solar panel array. The FPV array also limits the effects of wind on the water surface with the cover it provides. And because wind is also part of the evaporation process, this helps as well.
No effect on water quality	Most floats that are used in FPV are made of HDPE. This same material is used in drinking water applications and has no degradation or contamination effects on water.
Potential environmental impacts	Because FPV covers parts of a water body's surface, it will let less light through to the water. This will discourage algae growth and can, in certain cases, improve water quality. However, there can also be adverse environmental effects from blocking sunlight.

Increased energy yield	One of the most important advantages of FPV is the potential increase in energy yield. The cause of this increase could be due to some of the following four elements: 1. *Evaporative cooling effect of water* The ambient air temperature on water is lower than the nearby land environment. This causes lower operating temperature for the PV modules and thus a higher efficiency. The magnitude of this cooling effect is dependent on the air ventilation underneath the floats. Good thermal contact with water can improve the cooling effect even more. 2. *More wind* Wind speeds over open water are usually higher than over land. Higher wind speeds provide better air ventilation around the PV modules and allow the modules to be cooled more easily. 3. *Less shading* FPV systems are less prone to shading because water bodies rarely have buildings or other objects in proximity to the solar panels. Tilt angles on FPV systems are usually kept low to reduce wind loads. This helps reduce inter-row shading. 4. *Less dust* There tends to be less dust on water bodies than in some ground-mounted PV plant locations. The complications of dust accumulating on panels are thus minimized.
Synergy with existing electrical infrastructure	Many inland water bodies that are used for industrial purposes or agriculture have a grid connection nearby. When FPV is installed on these water bodies, the length of medium-voltage power lines is thus likely to be short and will reduce costs. Furthermore, the energy-intensive infrastructure that uses the water body can use the solar energy of the FPV system for self-consumption which would further decrease costs and energy losses.
Complementary operation with hydropower	The combined and integrated operation of hydropower stations and FPV promises great potential. In dry seasons there is less water flow but high solar insolation and in wet seasons the opposite is true. A hybrid of hydropower and FPV would thereby reduce seasonal variations because one complements the other. Moreover, the natural variability of solar radiation can be largely compensated for by fast-acting water turbines, improving power quality and reducing power outages. Also, the diurnal cycle can

	be optimized by leveraging more solar power during the day and more hydropower at night.
Easier installation and deployment	When complicated anchoring and mooring is not required, the installation process for FPV is in many cases simpler than for ground-mounted PV. The deployment times are shorter, and costs are lower.

Table 2: Drawbacks of FPV

Drawbacks	**Explanation**
Capital expenses	Overall, the costs of FPV are still slightly higher than the costs of ground-mounted PV. This is because of the expenses for floats, mooring and anchoring, and extra requirements for electrical components. The cost of the floats is expected to lower over time, but the installed capacity today remains small to profit from economies of scale.
Anchoring and mooring	In some reservoirs, water depth and the terrain of the water body's bed can make anchoring difficult. In these cases, more complex solutions may be required that add to the cost of the installation.
Operation and maintenance	O&M is generally more difficult to do on water than on land. Often boats are required to access the floating array. Cables for anchoring and mooring must be regularly inspected and may require divers. FPV islands may also attract birds that sit on the solar panel and leave droppings. These factors increase the cost of O&M.
Electrical safety and long-term reliability	Electrical systems that are exposed to humidity and possibly salinity for long periods of time are at a higher risk of failure. Degradation and corrosion occur faster than on land and also biofouling can bring additional challenges. Because of this, periodical reinforcement or replacement of components might be necessary throughout the lifetime of the system.
Floats transportation	Most floats are difficult to ship because they are bulky and have a low weight-to-volume ratio. This causes the cost of transporting them to be high.

2.2. Energy yield analysis

This second chapter of the literature study reviews the step-by-step process of carrying out an energy yield analysis on an FPV system. While the overall process is similar for both ground-mounted PV (GPV) and FPV, there are a few key differences that should be considered [10].

For PV systems in general, an energy yield analysis is performed to accurately predict the energy production over a certain period of time. The different steps of the analysis do not only cover the efficiency loss due to the system design and components, but also various environmental factors. A full rundown of the various steps can be summarized in a loss diagram.

In the industry, an energy yield analysis is usually done with simulation software utilities such as PVsyst, PVSol, HelioScope, Solarfarmer and SAM. Commonly, the first step in any of these software packages is to input the environmental and site condition data. This is done for the specific location where the analysis is being carried out. The next section covers this first step.

2.2.1. Environmental and site conditions

Data that contains the environmental and site conditions of an FPV site is used as a basis for the energy yield analysis [9]. Therefore, it is important that the data which is used is reliable. Ideally, the data is gathered at ground weather stations that are located on or near the FPV site. However, if there are no weather stations in the vicinity, site-adapted satellite-derived data can be used instead.

To make predictions for longer periods of time, it is necessary that the input data spans at least twelve months. This is needed to ensure that seasonal effects are properly captured. Preferably, measurements over a time span of twelve years are used to also capture long term climatic conditions. Even so, for most locations, such historic data is not available. In practice, when high accuracy is required, it is common practice to use a twelve-month-long measuring campaign in correlation with long-term satellite-derived data.

When running simulations for FPV systems specifically, there are additional factors that are present. Most notably water temperature, waves, water current and, if applicable, water depth. A list of influential environmental and site conditions used in the modelling process of FPV systems are covered in Table 3.

Table 3: Influential environmental and site conditions used in the modelling process of FPV systems

Irradiance	In general, irradiance refers to the solar energy which arrives at a specific area [13]. Irradiance, measured in W/m², can be expressed in multiple different ways. Commonly the following: • Direct Normal Irradiance (DNI) or beam radiation • Diffuse Horizontal Irradiance (DHI) or diffuse sky radiation • Global Horizontal Radiation (GHI) or total solar radiation The GHI is the sum of the DHI and the product of the DNI and the solar zenith angle. Therefore, it is sufficient to measure only two of the factors above when the zenith angle is known.
POA irradiance	Alternatively, a few of the early simulation steps can be avoided by directly measuring and using the Plane of Array (POA) irradiance [9]. This avoids any errors that could be made during the transposition of the solar waves, the application of the incidence angle modifier losses and the far shading losses. However, based on the surroundings, near shading losses can be very different depending on the FPV module in question.
Module temperature	Module temperature, measured in degrees Celsius, is the temperature inside the enclosure of an FPV module. Commonly, when designing an FPV system, this temperature is calculated by the simulation software. That is the case because it can not be measured unless a test setup is made or if the system is already operational. When accurate module temperature data is available, it can increase the accuracy of the simulation.
Ambient temperature	Ambient or dry bulb temperature, measured in degrees Celsius, is the temperature of the air around the FPV system.
Water temperature	Water temperature, measured in degrees Celsius, is the temperature of the water below the FPV system.
Wind speed and direction	Wind speed, measured in meters per second, is the speed of the wind at the same altitude at which the modules are placed. Another component of wind is the wind direction which is measured in degrees from the north.
Water current	Water current has, just like wind, a velocity and direction.

Waves	Waves are separated into the categories of regular and irregular waves. Regular waves are characterized by wave height and wave period. Irregular waves on the other hand are characterized by significant wave height and peak wave period.
Water depth	Water depth, measured in meters, is the difference in height between the bottom of the water body and the water level.
Precipitation	Precipitation is the amount of water vapor in the atmosphere that falls down from the clouds under the gravitational pull of the earth [14].
Relative humidity	The relative humidity is the current absolute humidity divided by the maximum humidity at the ambient temperature [15]. It is commonly expressed as a percentage.
Soiling	The contamination of the surface of the solar cells [9].

2.2.2. Optical losses

The optical losses in an FPV system refer to the energy lost as a result of reduced irradiance in the plane of the array [9]. Four common optical losses are addressed in this section.

Far shading losses

Far shading losses are a type of optical losses that are caused by the obstruction of the horizon line at the FPV site. Typically, these losses are caused by mountains or large faraway structures. Inside simulation software, the horizon line can either be imported or calculated using satellite data.

Near shading losses

Near shading losses are a type of optical losses that are caused by shadows as a result of local objects obstructing the sunlight. Local objects can be nearby buildings, trees, or other objects. During simulation, the near shadings can be accounted for in two ways. In a scenario where the FPV system is on a large open waterbody, a 2D modelling approach can be used. However, when there are objects in and around the FPV system, the system and its surroundings should be modelled in a 3D environment. This is done so the near shadings can be properly calculated and accounted for.

It should also be noted that in FPV systems the near shading can change depending on the water level [10]. Lower water levels can result in higher shading losses because even more sunlight is blocked by nearby objects. Most commonly, the borders of the basin the FPV system is floating on.

Soiling losses

Soiling losses are a type of optical losses that are caused by the accumulation of substances on the surface of the PV modules [9]. Examples of these substances are dust, dirt, leaves, and

bird droppings. In tropical areas, irrigation ponds and ponds close to nature, biofouling may be present as well. In colder areas, snowfall can also cause large soiling losses. Especially when the PV modules are close to the supporting structure [9], [10]. During simulation, a flat percentage can be used to account for soiling losses. However, in some locations it can be beneficial to use a measurement based soiling profile [9].

IAM losses
The incidence angle modifier (IAM) losses are a type of optical losses caused by the incident light reflecting off the surface of the PV module. A reliable loss factor can be retrieved from third party tests or via a theoretical modelling approach. If the modelling approach is taken, it is important to note whether or not the PV module is covered with an anti-reflective coating.

2.2.3. Water surface albedo

It is common for modules used in FPV plants to be bifacial modules because of the improved water resistance [16]. However, water generally has a lower surface reflection, or albedo, compared to rooftop materials [10]. A comparison is shown in Figure 7 based on measurements from a Singaporean testbed with an albedo meter placed two meters above the surface.

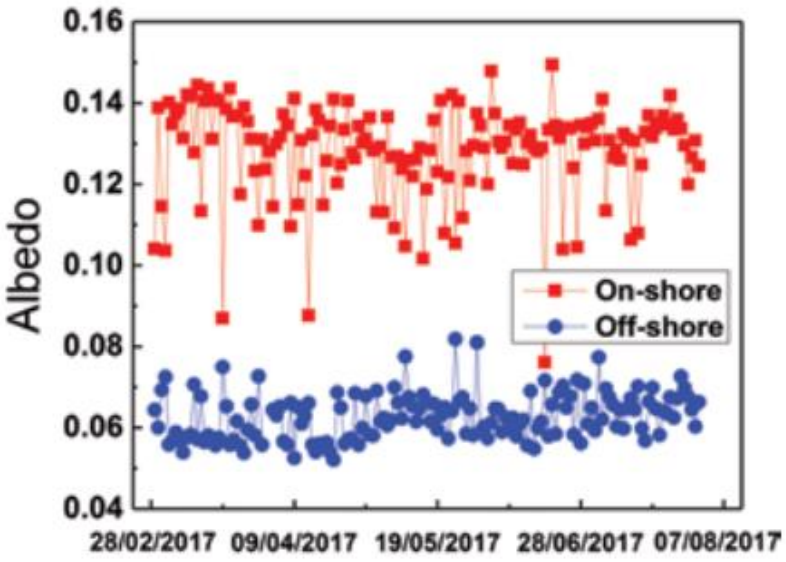

Figure 7: Average daily albedo (weighted against irradiance) of water compared to a concrete rooftop surface over a timespan of four months [10, p. 32]

Next to this, it is common in FPV systems to use a low module tilt angle, further reducing the potential for an increased irradiance input. For these reasons, the diffuse irradiance measured at the rear side of modules in FPV systems is minimal. As a result of this, there are no large power gains because of the bifaciality.

2.2.4. Module losses

Module losses are a result of various real-world influences acting on the PV modules [9]. Three common module losses are assessed in this section.

Low-light loss

Low-light losses are a type of module losses that are present when the PV module is collecting an irradiance lower than what is used during standard testing conditions (STC) [9]. The material out of which the PV module is made affects its low light performance [17]. To account for the loss in performance, a value found on the module's datasheet can be used [9]. However, to get a more accurate result, real world testing at the desired system location should be performed.

Temperature-dependent performance

The power output of a PV module is heavily influenced by its temperature [9]. Temperatures higher than the one seen in STC result in a smaller energy yield. This loss of power is a result of a decrease in voltage while the current only increases marginally as is shown in Figure 8.

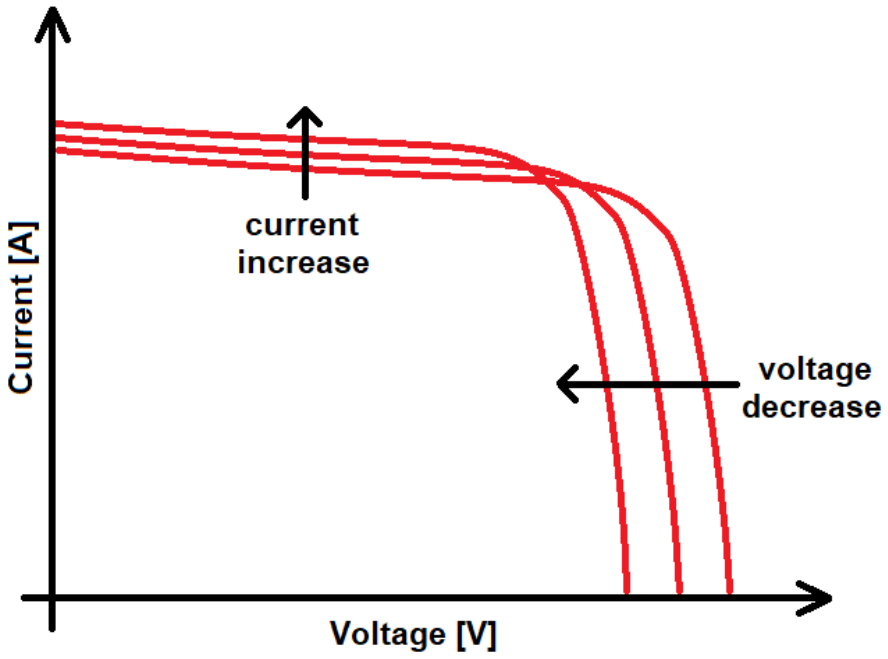

Figure 8: The effect of temperature on the IV-curve of a PV module [18, p. 3]

For this reason, a temperature coefficient of power is listed on all PV module datasheets. The module temperature is determined using thermal loss factors in combination with calculated or measured temperature and wind data. The thermal loss factors that are used should be adapted to the specific system and float design. A higher thermal loss factor indicates that more heat is able to be dissipated because of the way the system is designed.

In practice, the thermal loss factor of an FPV system is ideally determined using real-world on-site measurements. The key factors that should be included in a measurement campaign are the POA irradiance, the ambient temperature, the wind speed, and the module

temperature. The water temperature can also prove useful beside the previously mentioned factors. Especially when the PV modules are mounted close to the water level.

The thermal loss factor U, in [W/m²K], can be calculated by using the real-world data in combination with the equation [9] shown below:

$$U = \frac{\alpha \cdot G_{inc} \cdot (1 - \eta(T_{module}))}{(T_{module} - T_{ambient})} \tag{3.1}$$

With

α = solar irradiation absorption coefficient, in []

η = efficiency of the PV module dependant on T_{module} , in []

G_{inc} = plane of array irradiance, in [W/m²]

T_{module} = module temperature, in [°C]

$T_{ambient}$ = ambient temperature, in [°C]

The solar irradiation absorption coefficient and the PV module efficiency are both module characteristics and can therefore be derived from the datasheet or a third-party test.

Once the general thermal loss factor U has been calculated, it can be further split up into a constant component U_C and a component U_V which is proportional to the measured wind speed. The accompanying equation [9] is shown below:

$$U = U_C + U_V \cdot v \tag{3.2}$$

With

v = wind speed, in [m/s]

In practice, U_C and U_V are calculated by applying a linear regression model onto U in function of v. Once they have been determined, they can be implemented into the simulation so it can accurately work out the thermal losses in the system. It is however important to keep in mind that module temperatures can vary depending on its location within the system. Modules on the outer edges of the system are likely to see lower temperatures due to being more exposed to wind.

All of the aforementioned literature in this section assumes the ideal scenario where the necessary real-world data is available to determine the thermal loss factors. However, in some cases certain, or all data, might not be available and other ways of creating an accurate simulation must be explored. When there is no accurate wind data available, using the factor U_V might result in an inaccurate result. Therefore, a different approach must be taken. In cases when there is a complete absence of real-world measurements, thermal loss factors can be derived from third party research papers covering an equivalent system.

Even though module performance is often worse than what is measured during STC, it is possible to see an energy output higher than what is listed on the datasheet. For this to be the case, the module temperature has to be lower than the one used in STC, and the irradiance has to be the same or higher.

LID losses
Light-induced degradation (LID) is a phenomenon that permanently affects the solar conversion efficiency of crystalline PV modules [9]. It occurs in the very beginning of the module's lifecycle when it is first exposed to sunlight. A loss factor provided by the manufacturer, or a third party can be used to account for the loss in module performance.

2.2.5. Inverter losses

Inverter losses are losses that occur when the DC power generated by the PV modules is converted to AC power so it can be transported using the distribution grid [9]. A list of substantial inverter losses is covered in this section.

Inverter loss during operation
The power that is lost during the conversion from DC to AC due to the inverter efficiency [19].

Inverter night consumption
The power consumed by the inverter during the night for powering status screens or communication.

Inverter loss due to power threshold
The power that is lost during times where the DC power produced by the PV modules is below the minimum threshold for the inverter to work.

Inverter loss over nominal inverter power
For economic reasons it is common to use an inverter with a maximum power output that is lower than the peak power output of all the PV modules connected to it [20]. However, this introduces power clipping on sunny days when power on the DC side exceeds the maximum inverter power.

Inverter loss due to voltage threshold
The power that is lost during times when the DC voltage is lower than the minimum maximum power point (MPP) voltage [19].

Inverter loss over nominal inverter voltage
The power that is lost during times when the DC voltage is higher than the maximum (MPP) voltage.

2.2.6. Electrical losses

Electrical losses are any losses that occur during power transmission between the various components as a result of sub-optimal electrical behaviour [9].

Mismatch losses

Mismatch losses are losses as a result of a voltage or current mismatch within the electrical system [10]. This type of loss can have multiple root causes which are summarized below.

Voltage mismatch occurs when multiple strings connected to the same maximum power point tracker (MPPT) are made to operate at a common voltage [9]. However, this type of loss is negligible unless the strings connected to the MPPT have a different number of modules connected to them due to a failure or design flaw.

Current mismatch can originate from a quality difference between different modules [10]. It can also emerge due to a difference in irradiance received by different modules within the system. This can happen due to shading or soiling for example. Another cause can be the temperature variance between the various modules within the system. As discussed previously, it is common for modules on the outer edges of the system to see lower temperatures due to the extra exposure. Finally, there are also current mismatch losses specific to FPV systems which are wave-induced mismatch losses. The cause for these, as the name suggests, are the waves pushing against the PV arrays resulting in a misaligned orientation.

Cabling losses

Cabling losses are any losses that occur in the cables connecting the various system components [10]. When calculating the cabling losses, it is important to know cable lengths, cross-sections, and materials. Therefore, it is important to have data covering cable-routing schemes as well as the distance to the shore. The location of the inverter also has an effect on cabling losses as it dictates how much of the cabling is carrying DC vs AC power.

2.2.7. Long-term system degradation

Long-term system degradation refers to any performance losses as a result of components aging over time [9]. The main system component that faces a loss in performance due to degradation is the PV module. The pace at which a module degrades can be different for any specific module. This results in additional mismatch losses being introduced into the system. Therefore, further reducing system performance when the system is nearing the end of its life span.

At this point a lot of historical data on long-term degradation has been collected for normal PV systems. There is however uncertainty over how well this data carries over to FPV systems due to the high-humidity aquatic environment [10].

2.2.8. Summary: loss diagram

All of the previously discussed losses can be summarized in a loss diagram. An example made using the simulation software PVSyst is shown in Figure 9 below.

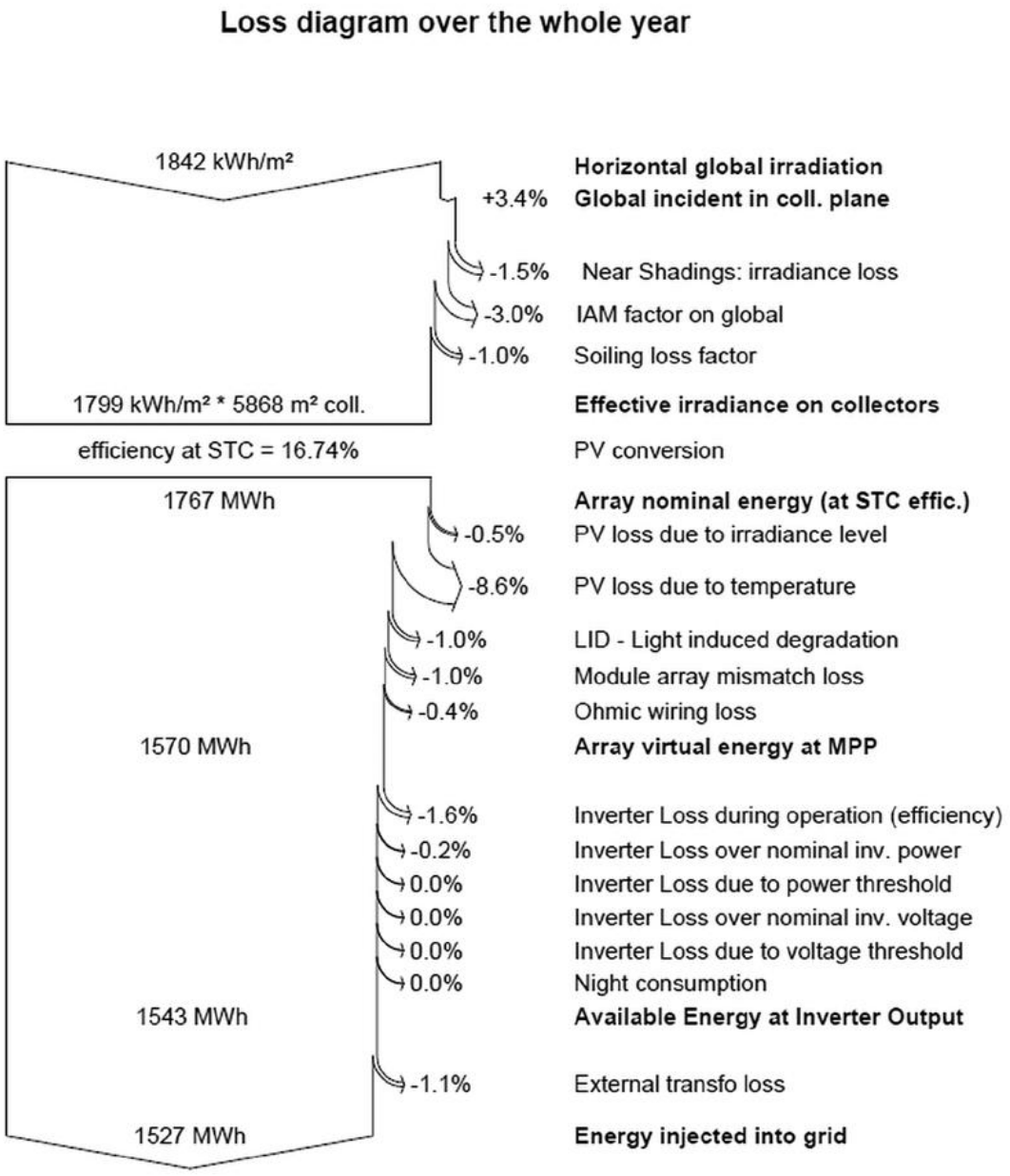

Figure 9: Loss diagram example made using PVSyst [10, p. 28]

2.3. External factors impacting module temperature

An important aspect to consider when comparing GPV and FPV systems is the potential increase in module efficiency. In section 2.2.4, it was mentioned that there is a negative correlation between module efficiency and module temperature. In this chapter of the thesis, a number of possible external causes for a change in module temperature will be covered in further detail. These are divided into two chapters, namely site conditions and system setup.

2.3.1. Site conditions

Module temperature is affected by the ambient conditions present at the site of the FPV installation. In this section, various site conditions will be discussed in detail.

Absorption of solar irradiation

Although solar irradiation is necessary for solar panels to work, part of it also directly contributes to the increase in module temperature [21]. When the energy carried by the incoming light is lower than that of the bandgap of the module, it is unable to be converted to electricity. Instead, this infrared light causes the module to heat up. Besides that, any light that is absorbed by parts of the module which are not solar cells will contribute to heating up the module. In this case the wavelength of the light does not matter. The solar irradiation absorption is accounted for by the coefficient as seen in equation 3.1.

Ambient temperature

The importance of the ambient temperature was already discussed in section 2.2.4. However, the manner in which the heat is transferred was not. Heat from the module can be transferred to the air around it in three different ways [22]. Commonly, as per the laws of thermodynamics, it is required that the ambient temperature is lower than the module temperature to see any beneficial cooling effect.

The first way the module can transfer heat to the ambient air is by means of conduction. The main driving factor in this case is the temperature difference between the air and the module. Besides that, the effectiveness is also determined by the thermal resistance of the module.

Convection is another way of transferring heat. Although ambient temperature plays an important role in it, wind is also a necessary component for convective heat transfer to occur. Therefore, it will be covered further in a section about wind speed.

Finally, heat transfer can also happen by means of radiation. Here the emissivity of the module, which is usually in the range of 0,03, decides the effectiveness of the heat transfer.

Water temperature

There is still no consensus in literature on the exact impact of water temperature on module temperature. The results of [23] and [24] show that there is a reasonably strong relationship between the two parameters while [25] claims there is no correlation at all. In [7], it is made clear that the effectiveness of the cooling depends on the air gap between the module and the water body. This clarifies why more commercially used pure floats and modular pontoons combined with metal framing, like the ones used in the aforementioned literature, see different levels of effectiveness.

It is however clear that FPV setups, making use of the membrane design, can see improvements in module temperature consistently. Resulting in a gain in energy yield of 5 to 7% on average [26]. The reason for this is the conductive heat transfer that can take place from the module through the membrane to the water. A larger temperature difference between the module and the water will once again result in more heat being transferred.

Wind speed

Wind plays an important role in module cooling for both ground-mounted PV and FPV systems [9]. On top of that, average wind speeds are usually higher above bodies of water due to there being fewer obstructive objects and the water surface having a lower friction than most surfaces present on land [27]. This means FPV installations can potentially see lower module temperatures due to the increased convective cooling as a result of higher wind speeds. There is however no clear consensus in literature on how much more beneficial the effect is in FPV systems. With a theoretical model, it was concluded in [28] that it is indeed beneficial. Besides that, in [29], the results showed that there was no significant difference between an FPV and GPV system that were located close to each other. The likely reason for this is that there was not enough open space or water around the FPV system for the effect to be noticeable.

There is also still uncertainty over the exact relationship between the module temperature and the wind speed. In [30], it is stated that there is a linear relationship between the two variables. While in [31], the conclusion is that there is a logarithmic relationship. The reason for this, as described in [7], is that natural convection has a larger impact at wind speeds below 2 m/s. Therefore, drastically reducing the temperature of the module. However, at higher wind speeds, the effectiveness of the cooling will decrease as the temperature difference between the module and the air being moved by the wind becomes smaller. A comparison between both relationships is shown in Figure 10. This figure is a simplification of the one shown in [7].

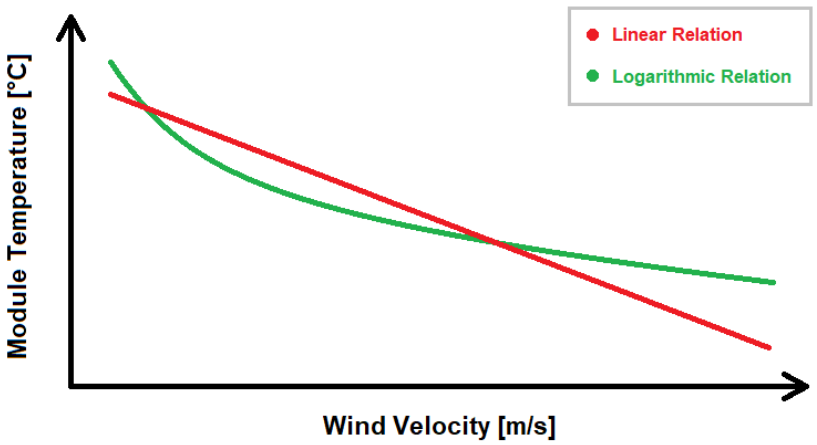

Figure 10: Linear vs Logarithmic relationship between module temperature and wind velocity

Wind direction

The final site condition to be discussed is wind direction. It is an important factor in determining the effectiveness of convective cooling done by wind [32], [33]. In Figure 11 the relationship between module temperature and angle of attack is shown for a single module. The figure is a simplified version of the one shown in [7].

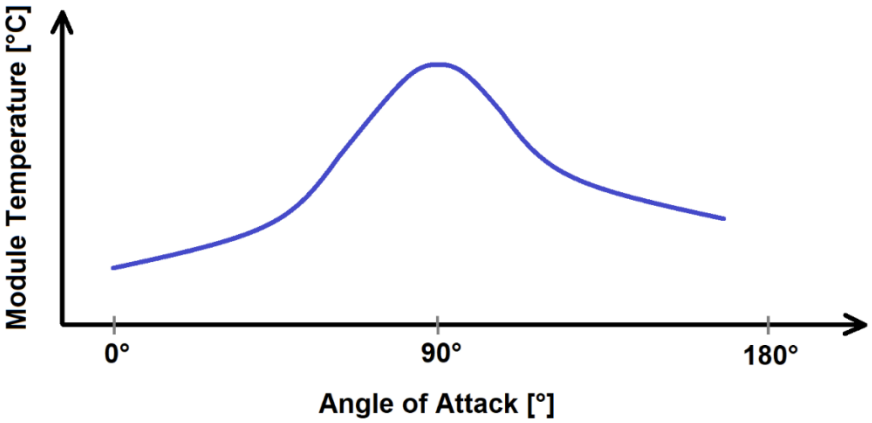

Figure 11: Relationship between module temperature and angle of attack for a single module

The horizontal axis, representing the angle of attack, is used to specify the angle at which the wind hits the solar module. An angle of attack of zero degrees indicates the wind hits the frontal area of the module. This is where the solar cells are located. When the angle of attack is 90 degrees however, the wind is moving in parallel to the module. Finally, if the angle of attack is 180 degrees, the wind is impacting the back of the module. Knowing this, it is clear by observing Figure 11 that it is beneficial for convective cooling if the wind hits the front of the module.

2.3.2. System setup

The way a solar system is set up can have a major impact on the cooling of the PV modules. A module's tilt angle and air gap above the water are design choices that have an impact. Besides this, adding active cooling methods is also a beneficial option. The following points dive deeper into these elements of the system setup and how they have an impact on module cooling.

Tilt

The tilt angle of a solar module is the angle between the module and a horizontal line. For optimal energy yield, the tilt angle of PV modules corresponds to the local latitude. Regardless, for floating PV modules, the tilt angle is usually kept quite low. This is to minimize self-shading losses and exposure to wind loads [8]. A low tilt angle will also cover more water, which helps to prevent evaporation [34].

The tilt angle plays a role in cooling because it affects the amount of wind captured by the modules. Higher tilt angles provide more surface area for the wind to act on and therefore will generally have a better cooling effect [35], [36]. This beneficial effect however is very minimal, so keeping the angle low for reasons mentioned above is acceptable.

Air gap

The air gap, in this context, is the distance between the underside of a solar panel and the underlying surface (water for FPV). For ground-mounted modules, module temperature decreases as the air gap increases. This is because more space under the module means air can pass through easier and air velocity is higher allowing for better convection of heat. This decrease in module temperature however stagnates if the air gap becomes greater than 12 cm. Keeping this gap as a minimum is thus optimal to prevent overheating [37].

For floating PV, the surface underneath the PV modules is water. This changes things because water has a possible beneficial effect for module cooling. For most cases of FPV in open water, the water temperature is lower than ambient temperature. Air above the cold-water surface will mix with water molecules and create a blanket of vapor. The temperature of this vapor blanket is cooler than the ambient temperature but only has a thickness of 2 cm maximum. So, in order for PV modules to benefit from this, the modules would need to be laying very close to the water. This is contrary to the thermal benefit that wind has, because when the PV modules are very close to the water, the air doesn't have enough room to have an optimal effect [7]. Therefore, PV modules tend to have higher temperatures this close to the water compared to when the air gap is larger.

Array configuration

Different array configurations are possible for FPV. In general, three different options are considered:

- all modules facing one direction;
- modules gable configuration;
- modules in V-configuration.

An illustration of all three configurations can be seen in Figures 12, 13 and 14.

Figure 12: Configuration where modules face one direction [38]

Figure 13: Modules in gable configuration [39]

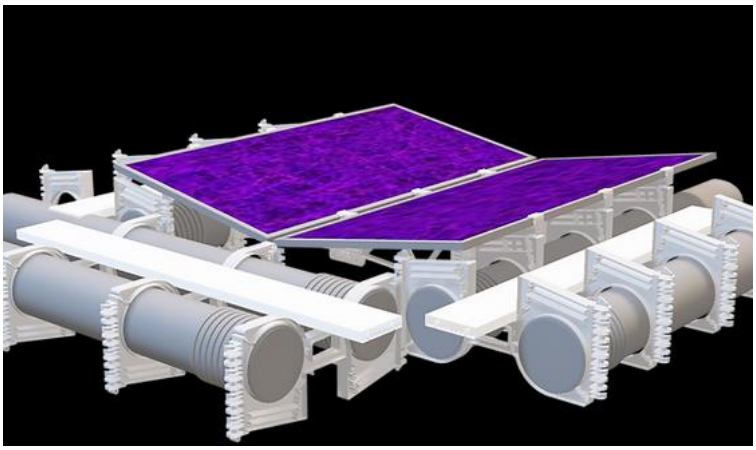

Figure 14: Modules in V-configuration [40]

Depending on global location, solar panels are usually placed either north- or south facing. A rising trend however are east-west configurations. This configuration is most appropriate for larger installations, as an east-west configuration allows more panels to be installed on the same surface area. In terms of pure power output per module, one sided array configurations still perform better [41].

To see what thermal effect the array configuration has, it is crucial to look at the wind direction in relation to the configuration. This is because other factors in relation to the array configuration do not influence the temperature as much. Haggag M. [7] simulated the difference between the different configurations by setting up four situations, each with two modules in different configurations, where wind comes from one direction (see Figure 15).

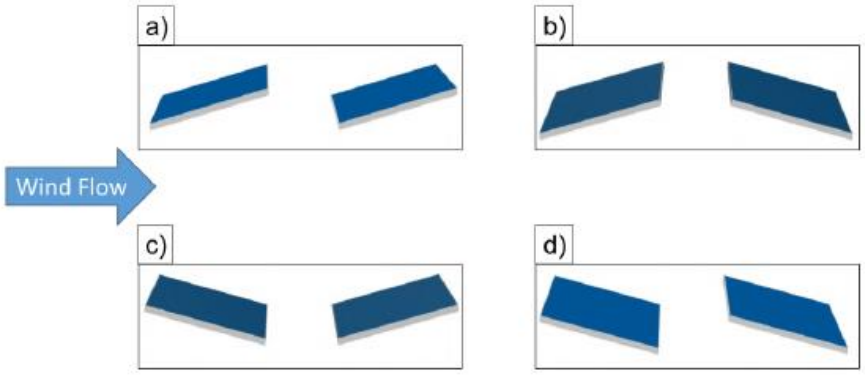

Figure 15: Thermal effect of module configuration considering wind [7, p. 71]

He found that:

- for configuration A, similar temperatures can be seen in both panels;
- for configuration B, both panels experience more heating than in configuration A (~0,5°);
- for configuration C and D, the first panel sees remarkable heating while the second panel cools down marginally.

Water cooling methods

Cooling FPV modules with water is an effective way to decrease module temperature. It is an active cooling method because it needs an external mechanism to initiate the cooling. Two elements are critical for water-based solutions: enough available water and low energy consumption for pumps. Both of these conditions are met in FPV [42].

Having water on top of PV modules causes three things to happen: a reduction in module temperature, modification of the solar spectrum and change in reflection. The first effect is desirable and is the goal of a water-cooling method. The second effect is due to water being a strong light absorber. The light spectrum that is absorbed however is luckily mostly in the infra-red region while the solar radiation that is converted to energy is mainly in the visible spectrum. The effect of water absorption is negligible for water of a few mm. This means that no corrections need to be made to the PV modules for techniques such as water veil cooling.

The third effect happens because water has a different refraction index than glass, making it behave like a graded glass. This is beneficial because less light is reflected, and more light is transmitted to the PV module. High incident angles cause for even more transmitted light making water cooling methods interesting at high altitudes.

The most popular methods of water cooling are water veil cooling and water spray cooling. Pumping systems are used here to pour water over the PV modules when module temperature reaches a certain threshold [1]. This will cool down the PV modules and can ultimately increase module efficiency by 10% or more [42]. Water quality of the reservoir must also be suitable for proper use of these methods because filthy or salty water may cause soiling after repeated cycles of spraying and drying [1].

Submersion
Submerged FPV systems have their modules in direct contact with water. Because of this, they benefit from the cooling that water provides [1]. The same effects as the ones observed in water veil cooling apply here. Submerged FPV systems with a thin water layer can have an efficiency gain of around 20% compared to a dry panel without cooling system [43].

2.4. Thermal inertia of PV modules

In this chapter, the effect of a varying irradiance on the temperature of a PV module will be covered.

A fast change in irradiance can be a result of clouds moving over a PV system. Clouds reduce the solar irradiance that reaches the system which results in less heat being generated inside the PV modules [21]. PV modules do however have a certain heat capacity, causing the module temperature to drop slower than expected. This phenomenon is also referred to as thermal inertia. The thermal inertia is defined as the degree of slowness with which the PV module temperature approaches its surroundings [44].

To understand if thermal inertia should be considered when analysing data, it is important to first look at the daily irradiation curve of the PV system that is being analysed. The usual daily curve for sites with ideal climates consists of a single smooth line that shows small fluctuations in the solar irradiance value [45]. An example with a 5-s resolution is shown in Figure 16 (left). In this type of climate, the dynamics of the thermal processes are not very influential. In Central Europe however, the climate is not as ideal. Because of the clouds, the irradiation curve will look more like the example which is shown in Figure 16 (right). This graph is also based on data with a 5-s resolution. In this case, the thermal inertia of PV modules does play a more significant role in the thermodynamic process.

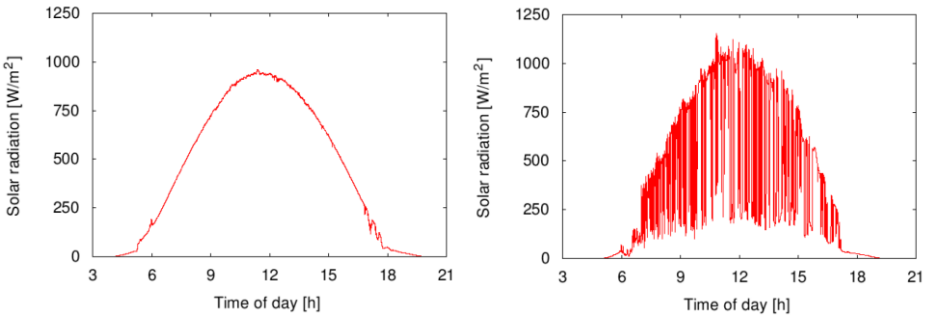

Figure 16: Solar irradiation in function of time for a single clear sky day (left) and cloudy day (right) [45, p. 462]

The significance can be visualized by plotting the temperature difference between the module and the environment in function of the solar irradiation. Figure 17 (left) shows the resulting graph for a clear sky day and Figure 17 (right) for a cloudy day.

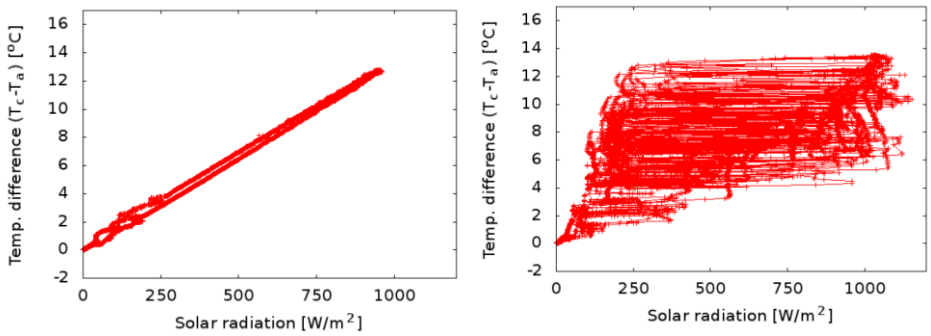

Figure 17: Temperature difference in function of solar irradiation for a single clear sky day (left) and cloudy day (right) [45, pp. 462–463]

From these results it can be concluded that, due to thermal inertia, unexpected temperatures can be observed when the irradiance is rapidly changing. Finally, it is important to note that thermal inertia does not have an impact on typical PV forecasting because of the low time-resolution data that is used [46].

3. The Clicfloats FPV system

Clicfloats Project 600, referred to as the Clicfloats FPV plant, is the system on which the simulation and data analysis is performed. This unique system is located in Meer, Antwerp and is installed on two irrigation ponds for greenhouses. An aerial photo of the plant is illustrated in Figure 18. The information below was obtained during a visit to the system on the 4th of November 2022 and from a report on the data acquisition written by the researchers from Energyville and KU Leuven [47].

Figure 18: Aerial photo of Clicfloats FPV plant [40]

3.1. Parties involved

Multiple parties are involved in this project. The first one is tomato company VW Maxburg. It owns the system and uses the ponds for watering its greenhouses. The energy generated by the solar panels is used to cover its own consumption. In the future, VW Maxburg will add more FPV on its ponds and will exchange power with a neighbouring company. The next company involved is Connectum which made the floats for this system. Connectum is known for its Clics-toys but started developing a unique modular floating structure with clickable connections. Another company which is involved is Pulsar Power. It was responsible for installing the solar modules and data acquisition system. Finally, imec and KU Leuven were tasked to measure the performance of the system. They installed several additional sensors and retrieved data in the period starting at the 7th of August 2021 until the 16th of January 2022.

3.2. System setup

The complete FPV system consists of 600 solar modules divided between two basins. 480 of these modules are placed in the biggest basin of the two. Of the 480 modules in this basin, 300 are connected to one inverter and are gridded in 20 strings of 18 to 20 modules. The remaining 120 modules are installed on a smaller basin and are connected to a second inverter together with the 180 modules of the bigger basin. No measurements or models are made for the modules of this second inverter.

The modules that are used are the JAM72D30 modules from JA Solar. These are bifacial and have a rated maximum power of 535 W. The inverters are Huawei's SUN2000-100KTL-M1 inverters and have a nominal AC output power of 100 kVA. The inverter can receive inputs from 20 PV strings. These inputs are grouped into 10 MPPT circuits to track the maximum power point of the PV strings.

3.3. Measurement devices

Power monitoring

The Huawei inverter provides AC and DC parameters with an accuracy of 1% in 5-minute intervals. Parameters that are measured include the DC voltages and currents as well as the AC voltage, current, cos(φ), line frequency, active output power and reactive output power.

Irradiance

Irradiance was measured in two ways. With a RaZON+ sun tracker and with plane-of-array sensors. The sun tracker was located on the wall of the basin and captured averaged data at a 1-min resolution. It functioned as a pyrheliometer, tracking the sun and capturing the full spectrum of the direct solar irradiance. It also captured the integral hemispheric diffuse irradiance by using its thermopile pyranometer. As a function of these two irradiances, the global horizontal irradiance is calculated.

The plane-of-array sensors were positioned among the PV modules in both east and west facing planes, on both the front and rear side of the modules. These also captured averaged data at a 1-min resolution.

Temperature

Module temperature was measured using 4-wire Pt100 type sensors that are distributed over several PV modules. At two locations, three sensors were used to acquire temperatures on the top side, on the bottom side and in the middle of the module. The three sensors were placed on east and west facing modules. At one other location, only one sensor was placed on both an east and a west facing module.

Water temperature was measured using a rod-type sensor that was located on one of the walkways at the centre of the system. An air temperature sensor was also located on a walkway near the water temperature sensor.

All temperature data was captured at an averaged 1-sec resolution.

Wind

Wind speed and wind direction were measured with an ultrasonic wind sensor that was positioned next to the sun tracker. The measurements were taken approximately 1 metre above the top of the basin's wall and were captured at a 1-sec resolution.

Water depth

A differential-pressure sensor, that captures data at a 1-sec resolution, was used to measure water depth.

Overview

Figure 19 gives an illustration of the bigger basin and shows the location of the measurement devices.

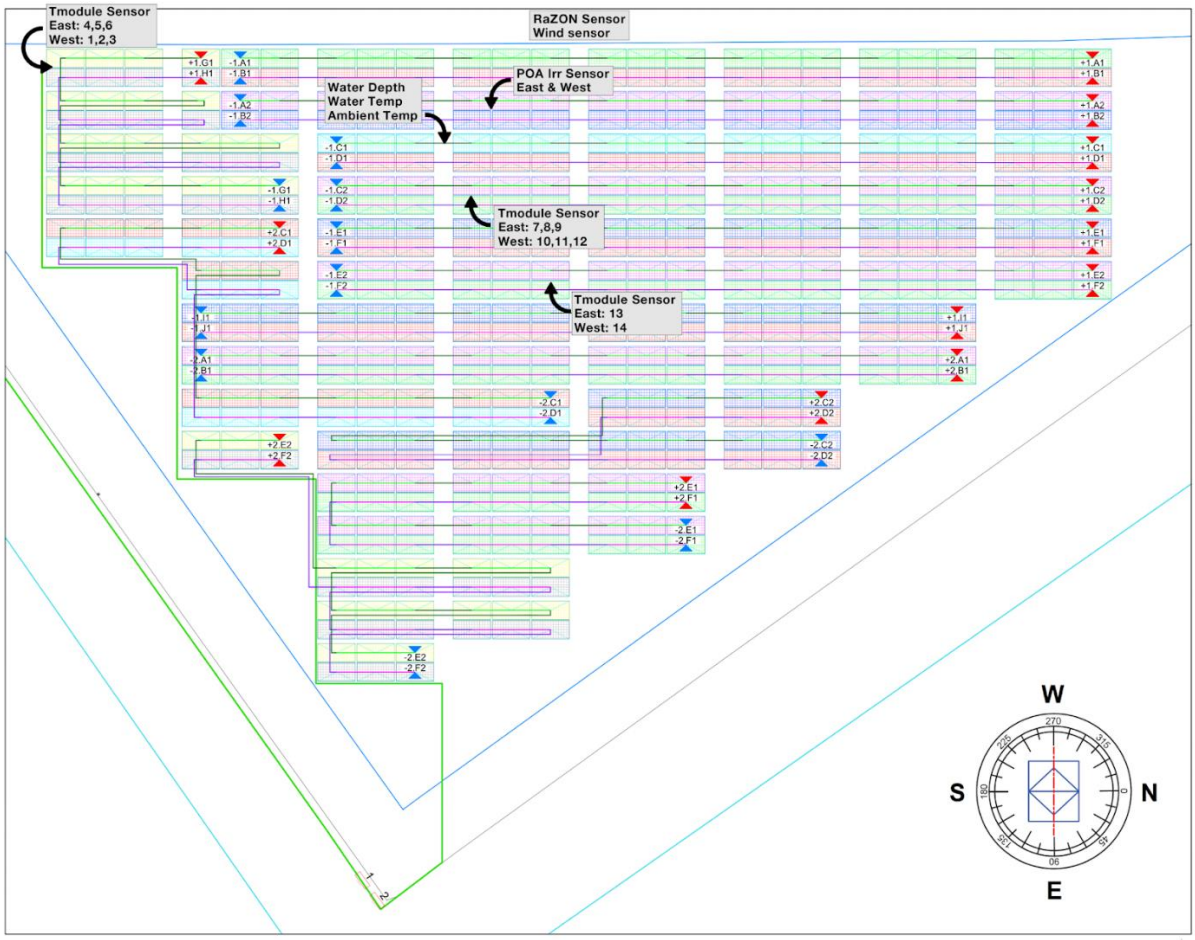

Figure 19: Overview of big basin with device locations [47, p. 7]

3.4. Data processing

The data from all the devices in the system was collected by a National Instruments data acquisition unit. This unit was connected to a PC that saved all the data in a database. The data could then periodically be downloaded via a web link. This raw data was however not ready for use straight away. It first had to be processed into a uniform format before it could be imported into the simulation software and used for the data analysis. This section covers the steps that had to be taken during the data processing. All data processing was done using Python scripts.

RaZON (DNI, DHI, GHI data)

The 1-min resolution output data of the RaZON sun tracker were separated into files that included a small number of days (two to five). These files were combined into a single file for use in the data analysis and simulations.

POA (POA Irradiance data)

The POA data missed a number of datapoints which were filled in by NaN values to make sure the length of each day was correct. The daily files with a 100-ms time resolution were averaged over 1-min. These daily 1-min resolution files were then combined into a single file accounting for the entire measurement campaign. This file was then ready for use in the data analysis.

Tback (Temperature and wind data)

Also, for these files, the gaps in the dataset were filled in by NaN values to make sure the length of the dataset is accurate. The daily files with a 1-s time resolution were then combined into one file for use in the data analysis. For the simulations however, the data was averaged over one minute. As was mentioned before, this is the highest resolution that PVSyst can use as an input.

Inverter data

The inverter data used two different formats over the course of the measuring campaign. The first format, which was used until the 10th of September 2021, saved data in a separate file for each inverter. One file contained all data for that particular inverter in a 5-min time resolution. Power values of zero were added at times when no data was being recorded as the inverter was on standby due to the lack of sunlight. This means night-time inverter losses are not accounted for.

The second format, which was used starting the 10th of September 2021 up until the end of the measuring period, required more work. This format alternated between the data of both inverters every timestep. The data in each timestep only included non-zero values and was measured anti-chronologically. Every day was also saved in a separate file. A script was written to reformat this data into the same format in which the first data was converted.
Both reformatted files were then combined into one file. Finally, the time zone of the data was changed to UTC+0 from UTC+1 with daylight saving time.

PVSyst input file

Using the properly formatted files, a PVSyst input file was constructed. This included the RaZon data, ambient temperature, wind velocity and wind direction at a 1-min resolution.

3.5. System characteristics

This final section of chapter three includes basic system characteristics that are made using the on-site data. These characteristics should provide a better insight into the usual operating conditions of the system.

First, the POA irradiance for the western and eastern modules, as well as the total generated AC power at inverter one, are shown in Figure 20. The data was recorded on the 5th of September 2021 which was a clear sky day. As expected, the eastern POA irradiance curve starts, peaks, and ends earlier than the western one. The power curve is located in between both irradiance curves. The result of shading provided by the nearby greenhouses is also visible in the curves. Especially in the evening, the POA irradiance drops drastically.

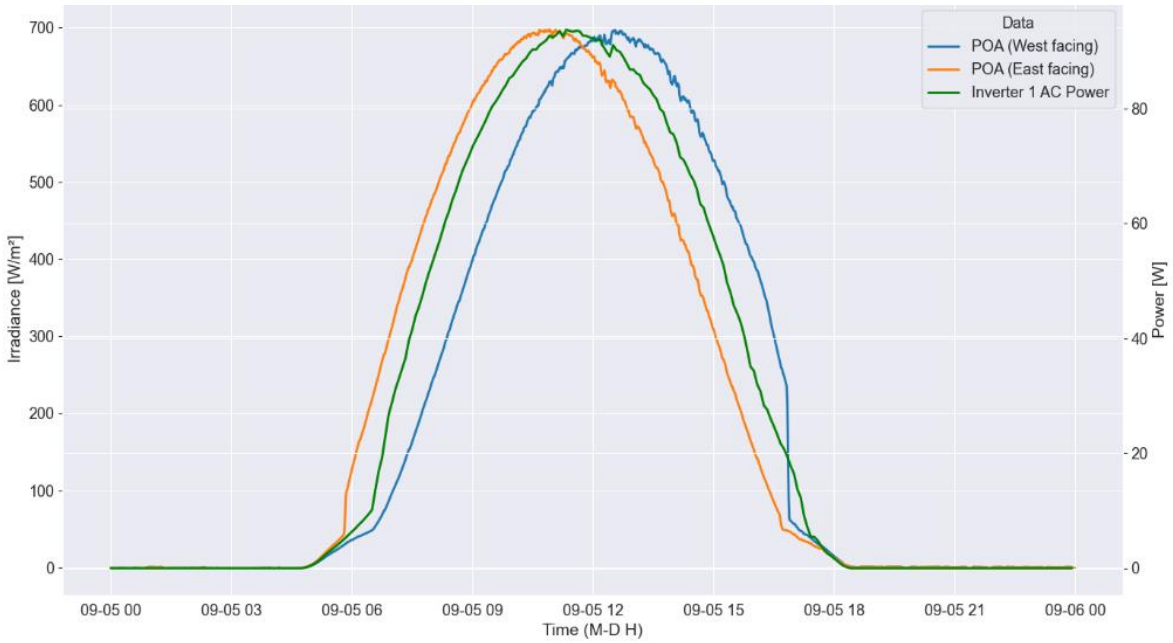

Figure 20: Power and irradiance data for a clear sky day

In Figure 21, various system temperature curves are shown for the first week of September 2021. During daytime hours, the module temperatures for each wind direction show the same behaviour as the irradiance in Figure 20. At night, the module temperatures more closely resemble the ambient temperature as there is no heat being absorbed or generated. The water temperature is also shown, however it only changes by one or two degrees over the entire week.

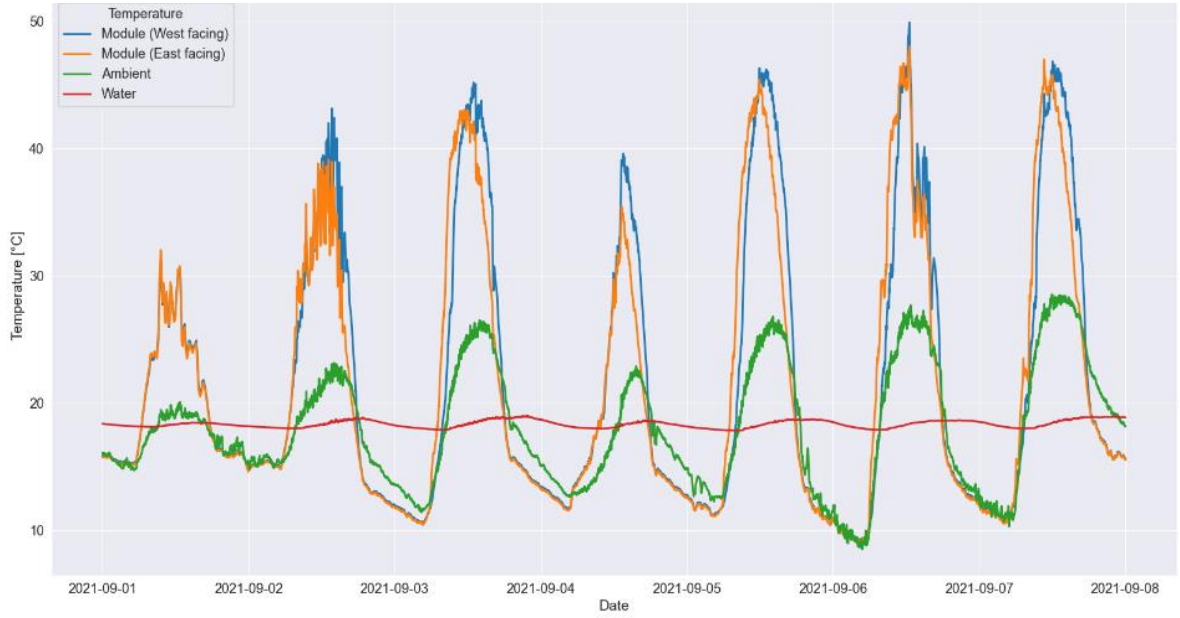

Figure 21: Temperature data for 01/09/2021 up to 07/09/2021

Next, in Figure 22, a normalised wind rose is shown which visualises the wind speeds, in m/s, and the wind direction from which it originates. Wind speeds higher than 10 m/s are filtered out to make the data more presentable. By looking at the wind rose, it becomes clear that higher wind speeds usually originate from the southwest while the wind almost never originates from the north. This is as expected since southwestern winds are most common in Belgium.

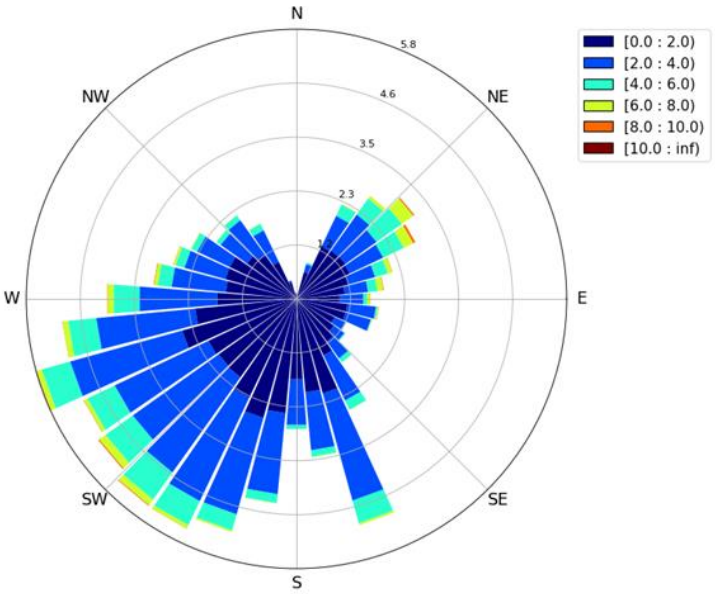

Figure 22: Normalised wind rose

Complementary to the wind rose, Figure 23 shows a histogram of the wind speeds up to 10 m/s. The histogram peaks at a wind speed of about 1,5 m/s and then drops down to around zero at 8 m/s. The shape of this wind speed histogram looks as expected. Similar results can be found in literature [48].

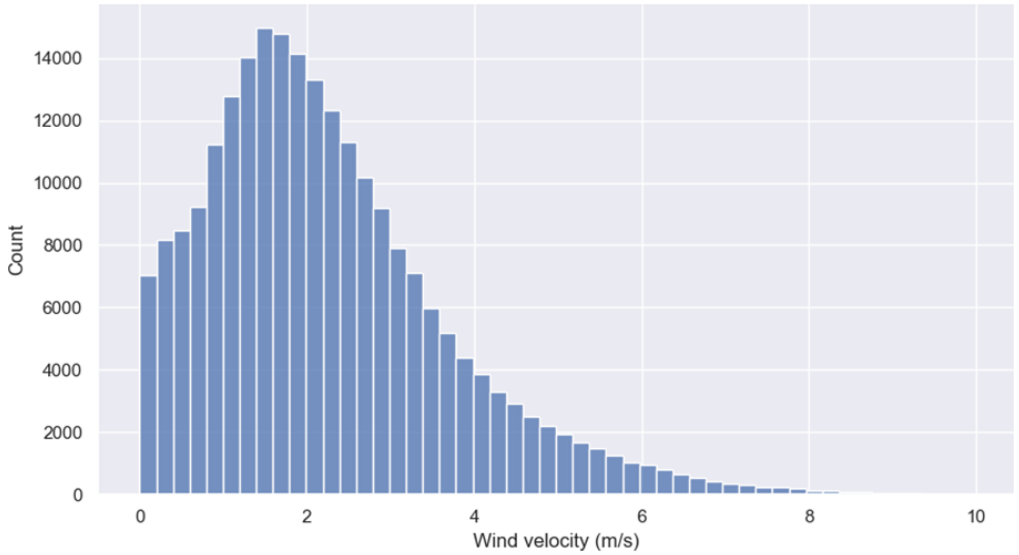

Figure 23: Histogram of wind speeds

The next characteristic covered in this section is the water level in the basin. As was described in a previous section, the basin is used as an irrigation pond. Therefore, the water level changes when the farmer is watering the tomatoes in the greenhouses nearby. A histogram of the water level is shown in Figure 24. It stays between a range of 1,9 and 3,5 m. However, it is common for the water level to be either around 2 m or higher than 3m.

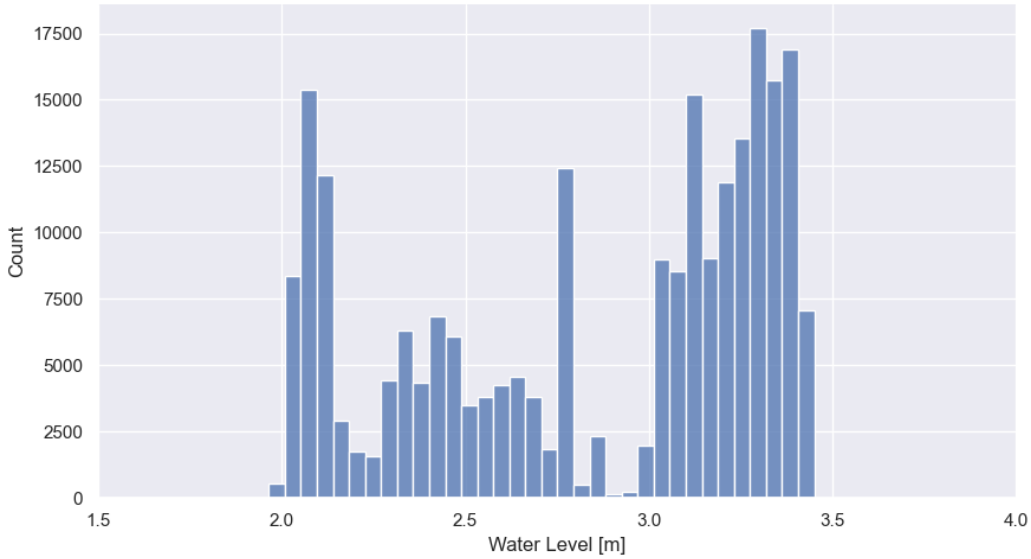

Figure 24: Histogram of water levels

The final characteristic covered in this section is the AC power plotted in function of the POA irradiance for eastern facing modules. This plot, shown in Figure 25, also contains a trendline with an r-value of 0,961. Only the POA irradiance for the eastern panels is shown here because there is very little difference between the eastern and western characteristic.

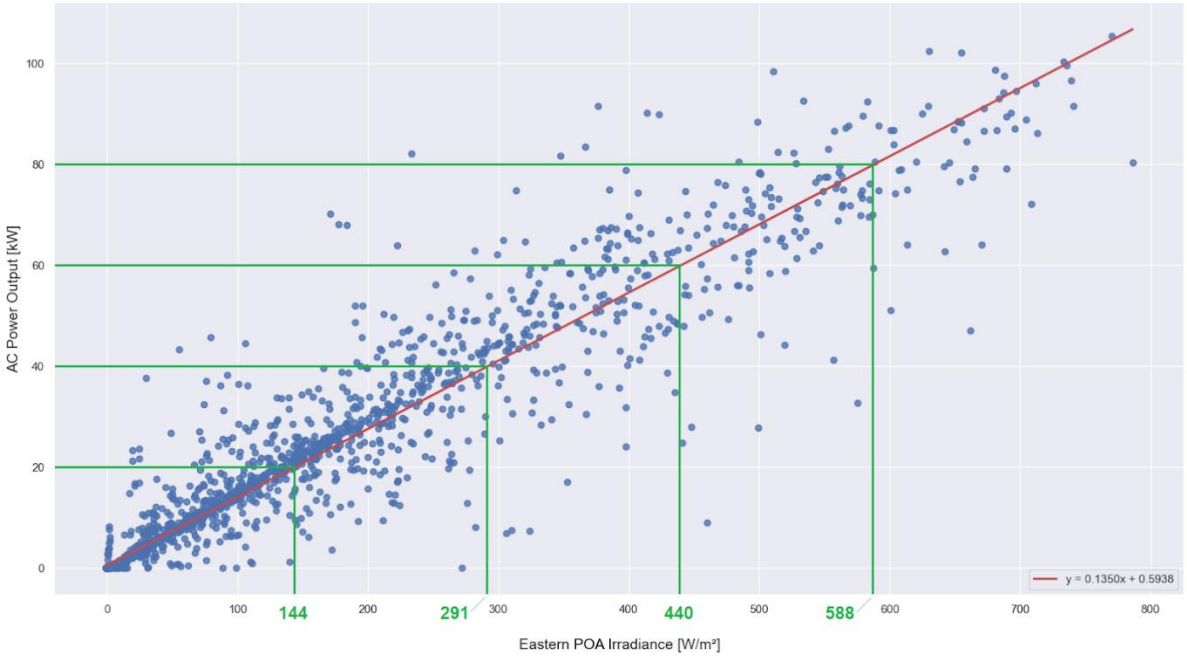

Figure 25: AC power output in function of the eastern POA irradiance

This plot is also used to determine the range of irradiances that is the most impactful on the total energy yield. To do this, the AC power output is divided into bins of 20 kW, with the exception of the high end where the bin is 30 kW. The portion of the energy yield which is generated in between these bins is then calculated using the dataset. After this, the linear formula of the trendline, shown in the bottom right of Figure 25, is used to calculate the corresponding POA irradiance ranges. The results of both these calculations are compiled in Table 4.

Table 4: Portion of energy yield for irradiance and power ranges

Irradiance range [W/m²]	Power range [kW]	Portion of the energy yield
0 to 144	0 to 20	18,3%
144 to 291	20 to 40	24,2%
291 to 440	40 to 60	22,6%
440 to 588	60 to 80	22,9%
588 to max	80 to max	12,0%

By studying the table above, it can be concluded that irradiances from 144 W/m² up to 588 W/m² will account for just under 70% of the total energy yield of the system. The same can be deduced for the power range of 20 kW to 80 kW. Knowing which irradiance and power range is the most impactful on the total energy yield will prove useful in analyses later on.

4. Simulation of an FPV plant

4.1. Simulation software

Simulation software can provide very useful tools in the development of renewable energy systems. Several software have been developed for simulating and optimising photovoltaic systems. They are used for PV plant sizing, technical, economic and pre-feasibility analysis and optimisation. This is done to avoid poor reliability, oversized plants, and high installation costs. Several popular simulation software packages are SAM, PVsyst, HOMER, PVSol, RETScreen, Solarius PV, HelioScope, Solar Pro, SOLARGIS, and PV F-Chart [49]. In this thesis, PVSyst and a proprietary software designed by imec are used to simulate the Clicfloats plant. The following sections go into further detail about both of these software packages.

4.2. PVSyst simulation

PVSyst is considered a worldwide standard for PV system design and simulation. It can be used to study, size, and analyse data of complete PV systems. Possible system configurations include grid-connected, stand-alone, pumping and DC-grid systems. The software also includes extensive databases of meteorological data and PV system components as well as general solar energy tools. According to [49], PVSyst is considered to be one of the most effective software tools.

The remainder of this section discusses the process of simulating the Clicfloats plant in PVsyst. This process is divided into different steps, starting with the site file.

Site file

When starting a project, the first step is creating a site file. This contains basic information of the system site such as coordinates and the corresponding time zone. Using this info, PVSyst can determine the sun path as well as retrieve basic meteo data from PVGIS.

Meteo file

Next, a meteo file is imported. In this case, the meteo file consists of measurements made at the Clicfloats site. It includes minute time-resolution data of the GHI, DHI, ambient temperature and wind velocity. Here, it is important to make sure that the time zone settings are accurate so PVSyst can interpret the measurements correctly. A time-resolution of 1 min is the highest possible resolution PVSyst can use as an input.

Project settings

Only two parameters are changed in the project settings. First of all, the albedo is set to 0,06. This value is retrieved from [10] where it was measured at the water surface below an FPV system. The next setting which has to be changed is part of the design conditions. Here, ‘limit overload loss for design’ has to be increased. This is needed because the base value of 3% will prevent multi-MPPT inverters from being simulated [50]. In this case it was set to 50%.

Orientation
In this part of the setup, the orientation of the system is assigned. Two values have to be set for the Clicfloats system, because there are eastern and western facing panels. The exact azimuth which is used is 90° for the eastern and -90° for the western panels. Besides this, the tilt angle of the panels is set to 10° for both orientations.

System
In the system settings, the PV module and inverter need to be selected. Next to this, multiple subarrays have to be created to make use of the multi-MPPT converter.

First, a new database entry is made for the JA Solar JAM72 D30 535 MB module. This needs to be done because it isn't included in the PVSyst database. The required information about the module is retrieved from the module's datasheet and similar modules that are included in the PVsyst database. There are no optimizers used in the system, so the corresponding setting is left off. The setting to simulate bifacial modules is also set to off. This is done because PVSyst is not yet able to simulate bifacial modules which are part of a 3D shading model.

Next, the inverter is selected and configured. In this case, it is not required to manually enter the specifications because the Huawei SUN2000 100KTL M1 is part of the PVSyst database. Then, the multi-MPPT feature is enabled to allow for power sharing between the ten MPPT inputs of the Huawei inverter. The grid frequency is also set to 50Hz because the system is connected to the Belgian grid.

The following step is creating the necessary subarrays. This is needed because the number of modules in a string and the number of strings connected to a single MPPT differs between MPPTs. The PVSyst help page [51] explains how to set up the subarrays in order to get the desired result. Table 5 shows all ten MPPTs and the strings which are connected to them. MPPTs can only be assigned to the same subarray if it has the same amount of strings connected to it and if those strings have the same length. For example, the MPPTs marked in orange both have two strings of twenty modules connected to them. Therefore, they are assigned to the same subarray.

Table 5: Inverter 1 MPPTs with corresponding strings and string lengths

Inverter 1		
MMPT#	**East**	**#Modules**
MPPT-7	1A1	20
	1A2	20
MPPT-6	1C1	18
	1C2	18
MPPT-4	1E1	18
	1E2	18
MPPT-9	1G1	20
MPPT-1	1I1	18
MMPT#	**West**	**#Modules**
MPPT-8	1B1	20
	1B2	20
MPPT-5	1D1	18
	1D2	18
MPPT-3	1F1	18
	1F2	18
MPPT-10	1H1	20
MPPT-2	1J1	18

Table 6 shows which subarrays are to be created in PVSyst. The used colours correspond to the strings and MPPTs in Table 5.

Table 6: PVSyst subarrays with corresponding MPPTs and strings

PVSyst Subarrays	
Subarray 1	4x20 over 2 MMPT
Subarray 2	8x18 over 4 MMPT
Subarray 3	2X18 over 2 MMPT
Subarray 4	2X20 over 2 MMPT

The final setting that has to be adjusted in the system tab is the orientation distribution. This is set to 50/50 for every subarray. As can be seen in Table 5, every subarray has the same amount of eastern and western facing strings.

Detailed losses

The thermal loss factors of the system are set to the values recommended by PVSyst. In [52], it lists a constant loss factor of 25 W/m²K and a wind loss factor of 1.2 W/m²K / m/s in case reliable wind data is available. Besides this, all settings are left as default due to either a lack of information or it being of less importance to the comparison.

Near shading

PVSyst uses a 3D model to calculate the near shading losses. This model can either be imported from a 3D modelling software or made in PVSyst's own environment. In this case, it is opted to build a model inside of PVSyst. Dimensions of the plant were retrieved from CAD drawings and empirical measurements. The final model that was used for the simulations is shown in Figure 26. It is important to note that only the light blue modules are accounted for in the simulation. The dark blue modules are connected to the second inverter. Therefore, they have been turned into dummy modules. The water level in the model, shown in the figure, is the average value during the measuring campaign.

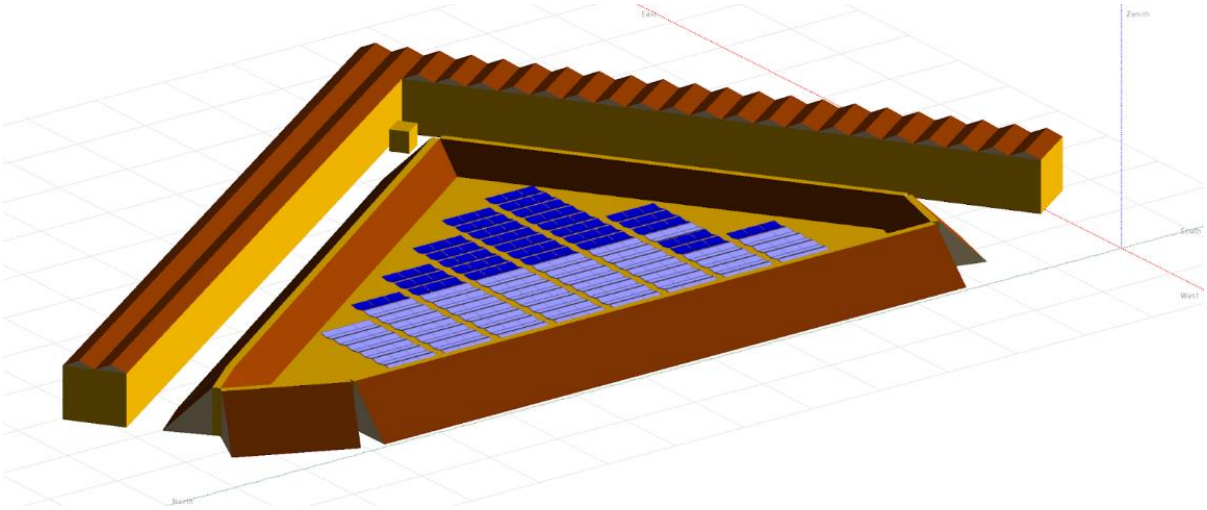

Figure 26: 3D model in PVSyst to calculate near shading losses

Once the model of the system is completed, the shading factor table is calculated. PVSyst can plot these losses on top of the solar path as is shown in Figure 27. This gives a useful visual representation of how much solar irradiation is lost due to shading.

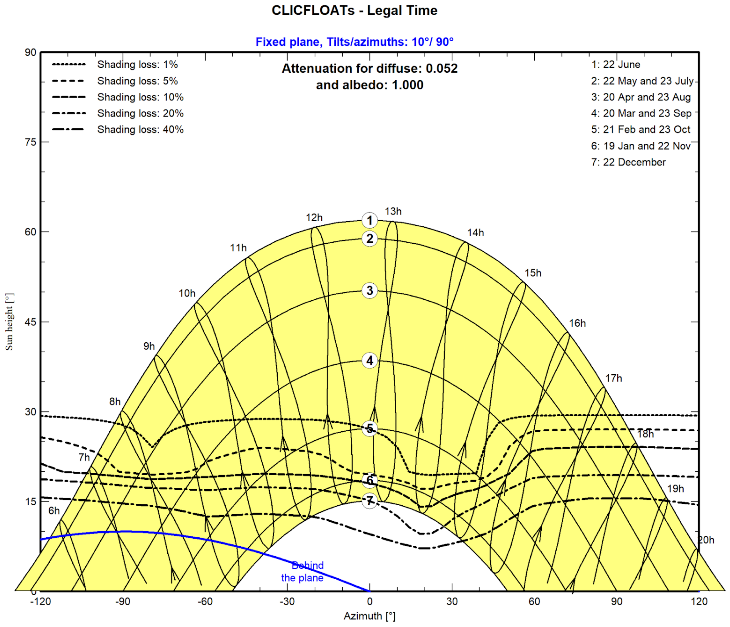

Figure 27: Solar path with shading losses

Finally, the manner in which shading should be applied in the simulation is assigned. This is set to ‘detailed electrical calculations’, which makes use of the module layout to get the most accurate results possible. The module layout is covered in the next section.

Module layout

The last part of the simulation process is the module layout. Here, the system attributes are linked to the 3D model. This is done based on Table 5. Figure 28 shows the final result with the MPPT and string names on the left and the modules from the 3D model, in the corresponding colour, on the right. All the eastern facing modules are shown in the top right rectangle and all the western facing ones are shown in the bottom right rectangle.

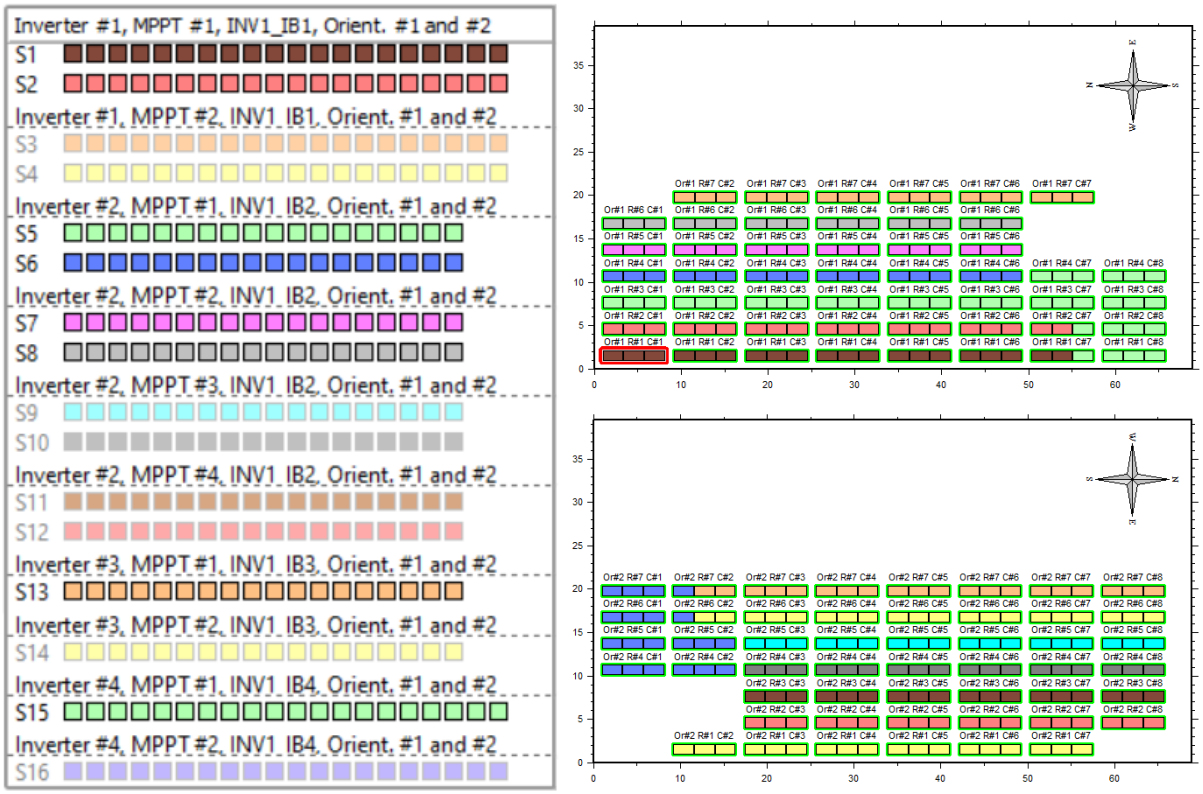

Figure 28: Module layout with system attributes linked to the 3D model

Simulation and data export

PVSyst is now fully set up to simulate the Clicfloats system. However, the necessary output parameters need to be selected before the simulation can be started. In this case, the array temperature, the array current, the array voltage and the generated power at the AC side are selected to be included in the output file. The highest time resolution that PVSyst can output is 1 hour. Finally, the simulation can be executed after which a csv file will be generated with the requested output parameters. These will be used in the comparison which will be covered in part 4.4.

4.3. Imec’s simulation framework

This third chapter about the simulation of an FPV system goes into more detail about imec’s own simulation framework. It is beneficial to have a basic understanding of the framework, even though the simulation of the Clicfloats plant was made by a researcher at imec. Understanding the strengths and weaknesses of the framework will help interpret the results of the comparison.

Figure 29 gives a visual representation of imec’s simulation framework. The inputs of the model are shown in blue at the very top. The first inputs the model needs are the 3D geometry of the PV plant and the electrical layout of the various components. Next to that, it also requires the meteorological data as well as the properties of the components and materials. As a first step, the model uses the data to calculate the POA irradiance. This is done using a state-of-the-art ray tracing calculation. This should provide better results than the view factor technique used by PVSyst. Next, the POA irradiance is used by the optical absorption model to determine the photo-generated current and the generated heat. In the next step, a modelling cycle is started which includes both the thermal and the electrical model.

In the first part of the cycle, the thermal model determines the cell temperature using the heat generated during absorption and the environmental factors. These include the ambient temperature and the wind velocity. The model is also capable of accounting for the effect nearby water might have on the cell temperature. Next, the cell temperature is used in the electrical model in combination with the photo-generated current calculated by the optical absorption model. The electrical model determines the DC output voltage and current as well as the heat dissipation by the components. In the next timestep, the thermal model will also include this heat dissipation in the calculation of the cell temperature. Finally, the DC output values are used to calculate the AC output. This is done using the inverter and wiring characteristics.

The framework has more features than those covered here. However, due to confidentiality these are left out.

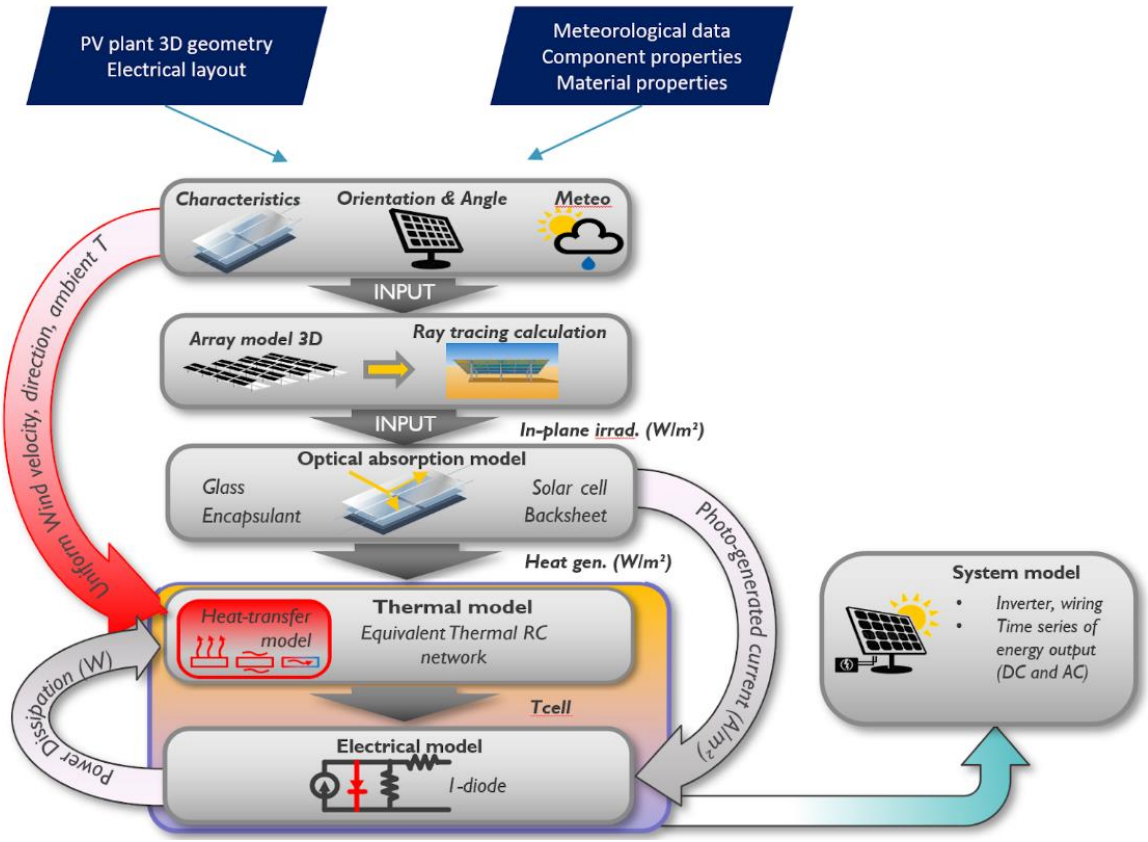

Figure 29: Visual representation of imec's simulation framework [53]

4.4. Results and discussion

4.4.1. How accurate is PVSyst in modelling the Clicfloats FPV plant?

To answer this question, a comparison is made between the results of the PVSyst simulation and the data from the inverter. This comparison is based on the power output at the AC side of the inverter. In Figure 30, the capacity factor of the modelled PVSyst data is plotted in function of the measured inverter capacity factor. To calculate the capacity factor, the power data is divided by 110 kW, which is the maximum power the Huawei inverter can output on the AC side. The black solid line resembles what an ideal model would look like.

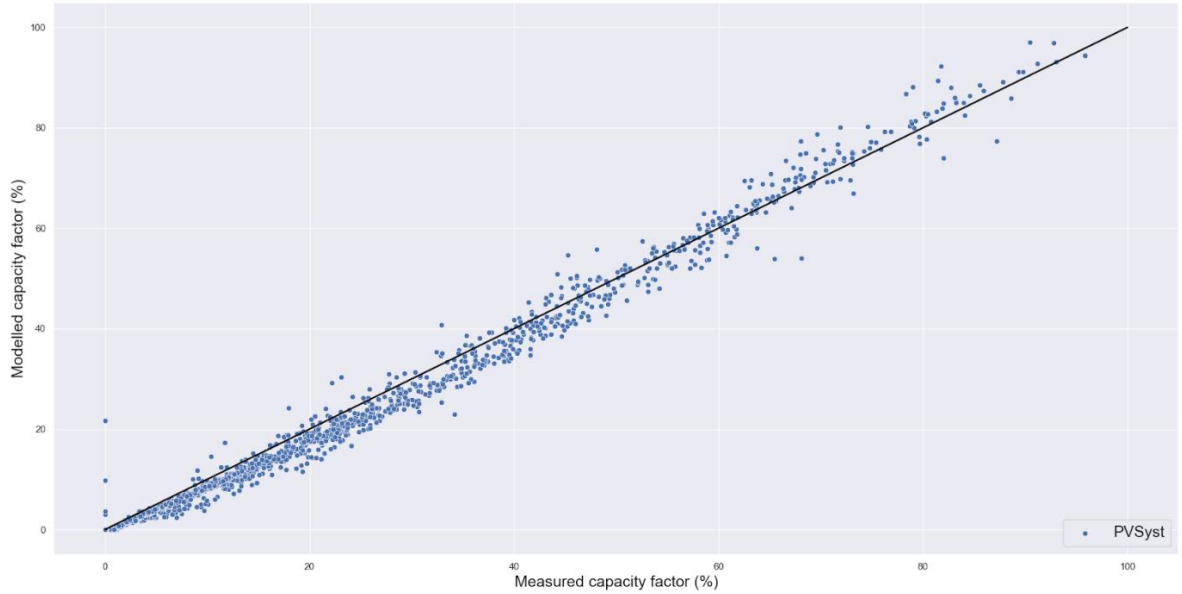

Figure 30: Capacity factor comparison PVSyst - inverter

Overall, it can be observed that the model is effective at estimating the power output. It does however tend to underestimate, especially below a capacity factor of 60%. Higher power outputs seem to be more commonly overestimated

Three error metrics are used to quantify the error between the model and the real data. Figure 31 shows the absolute errors on the left and the normalised errors on the right. The mean bias error (MBE) is positive which means that the model underestimates the real power output. The accuracy of the model can be judged using the mean absolute error (MAE) and the root mean square error (RMSE). The normalised MAE is just under 9% and the normalised RMSE is just under 12,4%. These are excellent results when compared to literature. In [54], a mean absolute percentage error (MAPE) of 15% was obtained when modelling an FPV plant in SAM. This error is also an underestimation. While in [55], a normalised RMSE of 39% was achieved also using PVSyst to model an FPV system. This, on the contrary, was an overestimation.

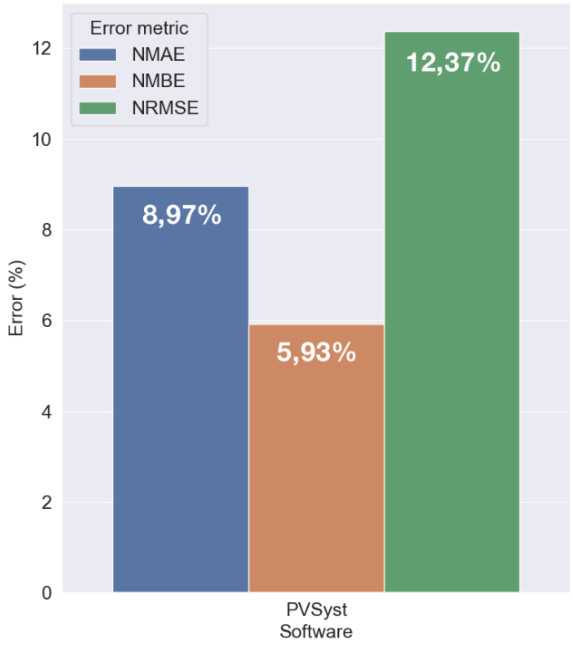

Figure 31: Normalised error metrics PVSyst - inverter

There are multiple possible reasons as to why the model underestimates the power output at a capacity factor below 60 %. The first reason is the fact that the simulation does not specifically account for any additional cooling that might occur due to the fact that the system is floating on water. Figure 32 shows the modelled module temperature from PVSyst in function of the measured module temperature.

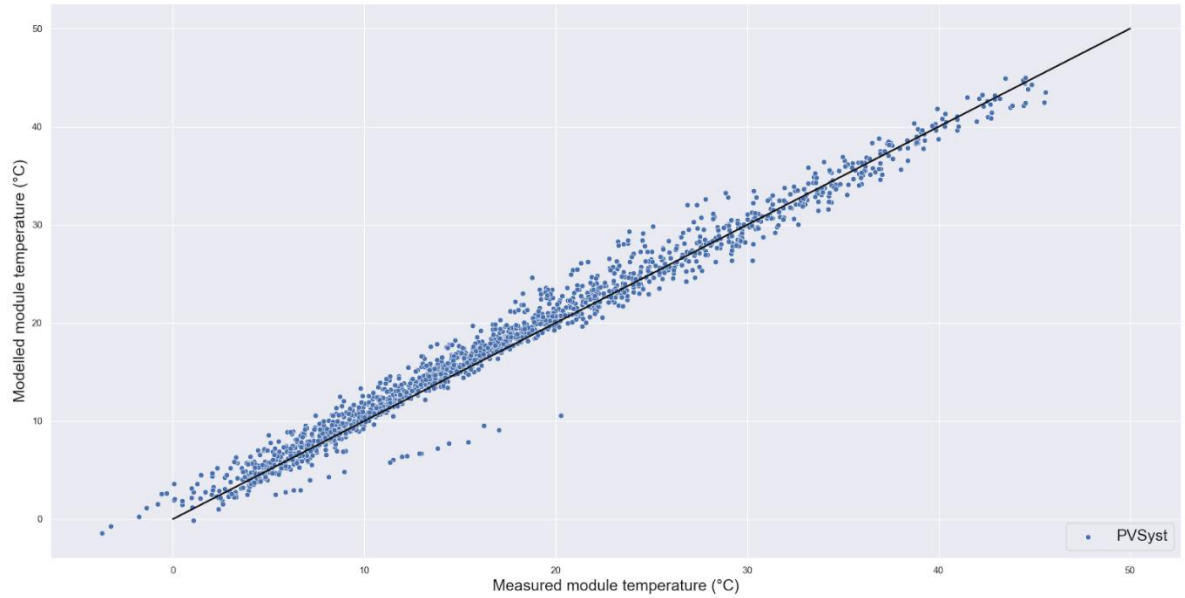

Figure 32: Modelled module temperature in function of the measured module temperature

In this figure, it can be seen that lower temperatures are overestimated by PVSyst. Therefore, if it is assumed that at lower temperatures there is a lower irradiance and thus a lower power output, the power output is underestimated due to a temperature overestimation. This could be improved by calculating the thermal loss factors using the environmental data instead of using the default PVSyst values. Next to this, there is no dynamic model to account for the change

in water level. Therefore, the PV array is kept constant at the average water level as was mentioned in section 4.2. The result of this is that the shading losses might not always be fully accurate.

A reason for the overestimation at capacity factors above 60 % could be the importance of cable losses at higher currents. The cable losses in PVSyst are calculated with a default loss factor of 1,5 % at STC. If more detailed data about cable lengths, diameter and material were available, this could be improved.

In section 3.5, the most important power range for the total energy yield was discussed. It was determined that just under 70% of the total energy is generated between the power range of 20 to 80 kW. Therefore, it is important that the model excels at simulating the power output between these ranges. Figure 33 shows the previously discussed model but highlights the aforementioned power range.

Figure 33: Capacity factor comparison PVSyst - inverter with highlighted important power range

Within the highlighted range, it can be observed that most data points underestimate the power output. Figure 34 shows that the normalised MAE and normalised MBE drop by more than two percent compared to the full range while the normalised RMSE drops by more than four percent. Therefore, it can be concluded that the PVSyst model performs even better at the important range.

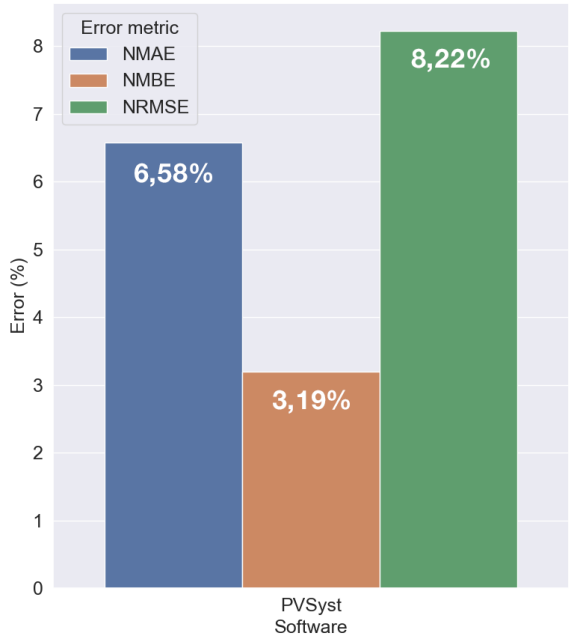

Figure 34: Normalised error metrics PVSyst - inverter for important power range

4.4.2. How well does PVSyst perform compared to imec's framework?

The simulation in imec's framework was done for only two strings due to time constraints. These two strings are connected to the same MPPT and consist of twenty eastern facing modules each. To make a comparison with PVSyst, the PVSyst simulation was repeated but this time including only the same two strings.

A similar plot to the one in section 4.4.1 is made in Figure 35. However, this time it includes the results of both PVSyst and imec's framework. Another difference is the fact that the comparison is based on the DC power output. This means inverter losses are not accounted for. It also changes the way the capacity factor is calculated. The DC power is now divided by the total maximum power of the modules, which is 40 (number of modules) times 535 (maximum power of a single module in watts), to get the capacity factor. Figure 36 also shows a direct comparison between the modelled capacity factors from PVSyst and imec's framework.

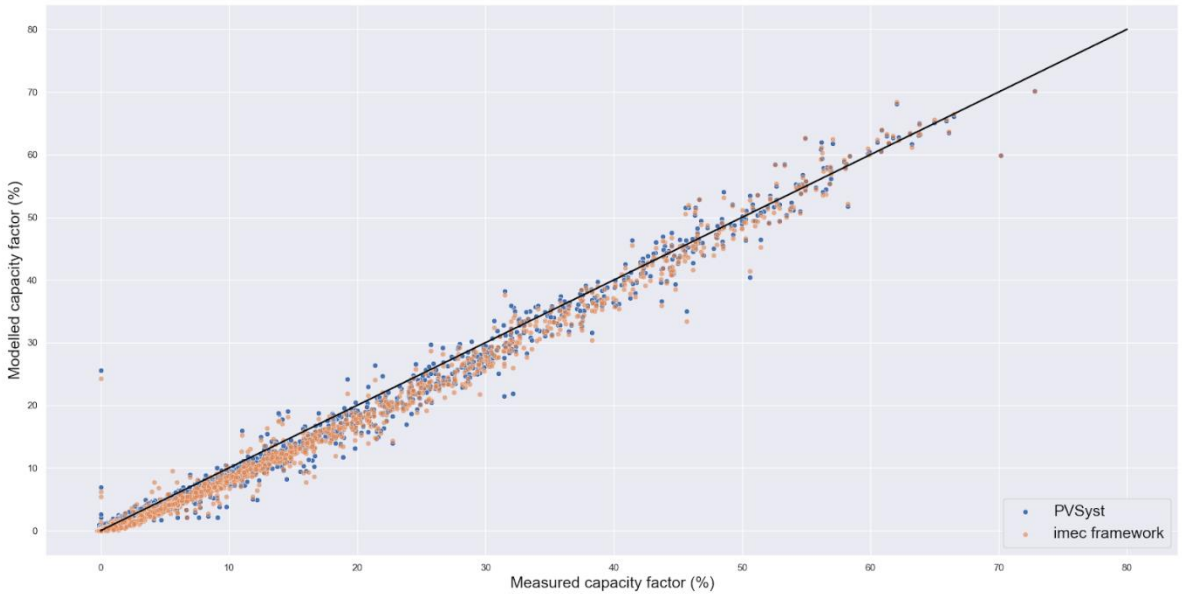

Figure 35: Capacity factor comparison PVSyst and imec's framework - measured

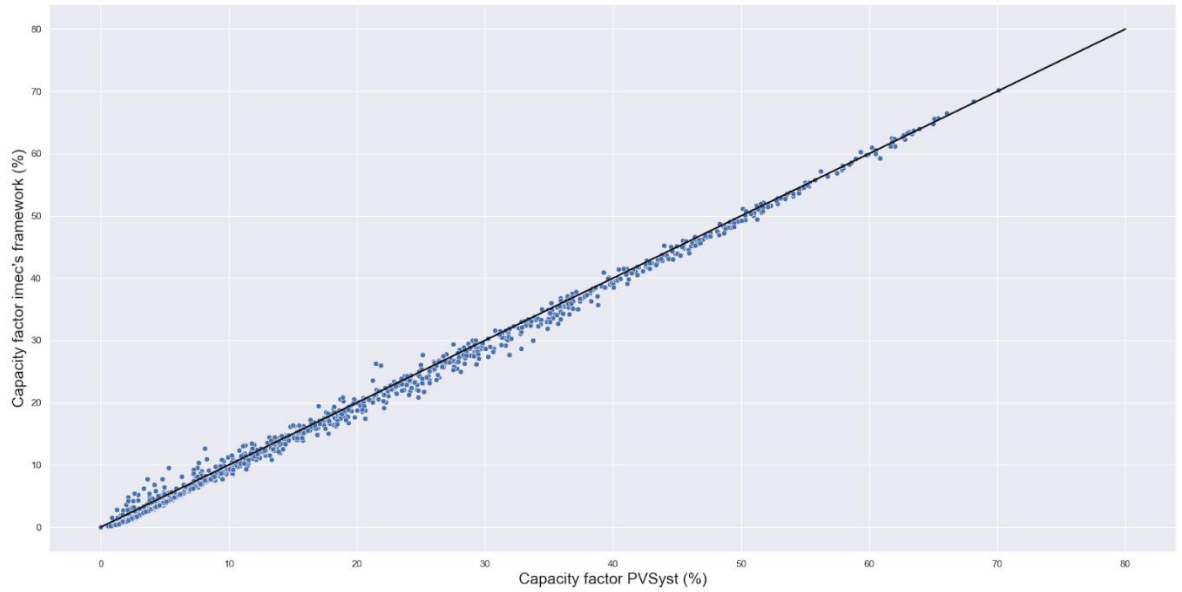

Figure 36: Capacity factor comparison PVSyst - imec's framework

It can be observed that both models do well at estimating the power output. There is however a clear underestimation visible for both. Figure 36 also shows that the estimated values of both simulations are very similar. Looking at Figure 37, PVSyst outperforms imec's framework by less than 4% in every error metric.

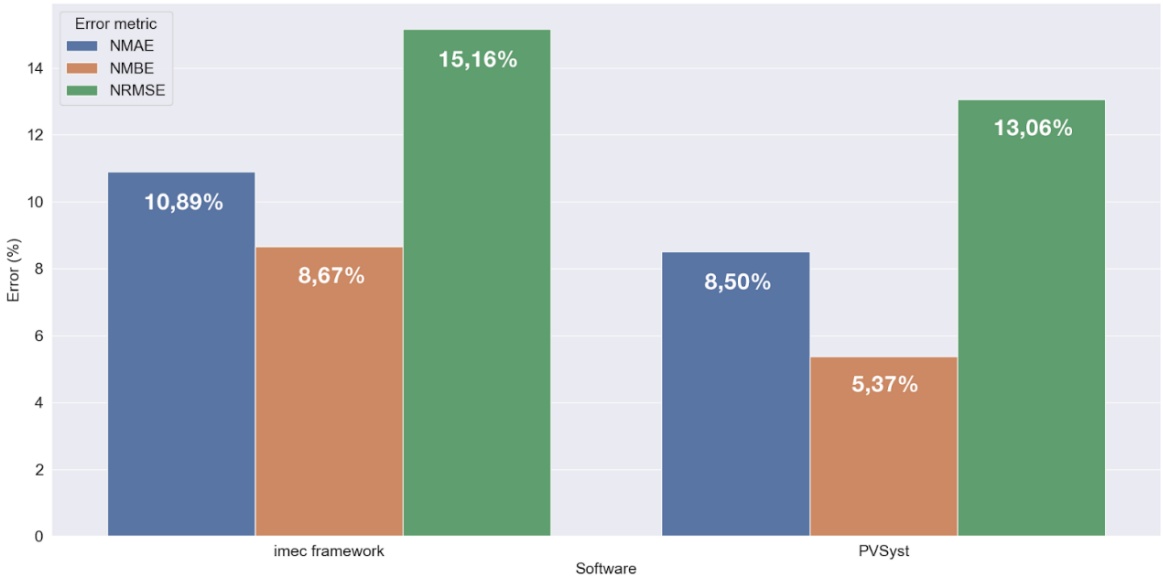

Figure 37: Normalised error metrics PVSyst and imec's framework - measured

A reason for this could be the fact that imec's framework is known to be worse at accurately calculating the shunt resistance. This is mostly visible at low irradiance since the shunt resistance is more prominent here. This is an issue imec is actively working on and should already be improved in the latest version of the framework.

To confirm the error exists due to the performance of the electrical model, the simulated module temperatures are compared in Figure 38. The measured module temperature used in this comparison is the average of temperature sensors 2 and 5 (see Figure 19). These are located at the edge of the system and should therefore give a better representation of the temperatures seen in the two strings being analysed here.

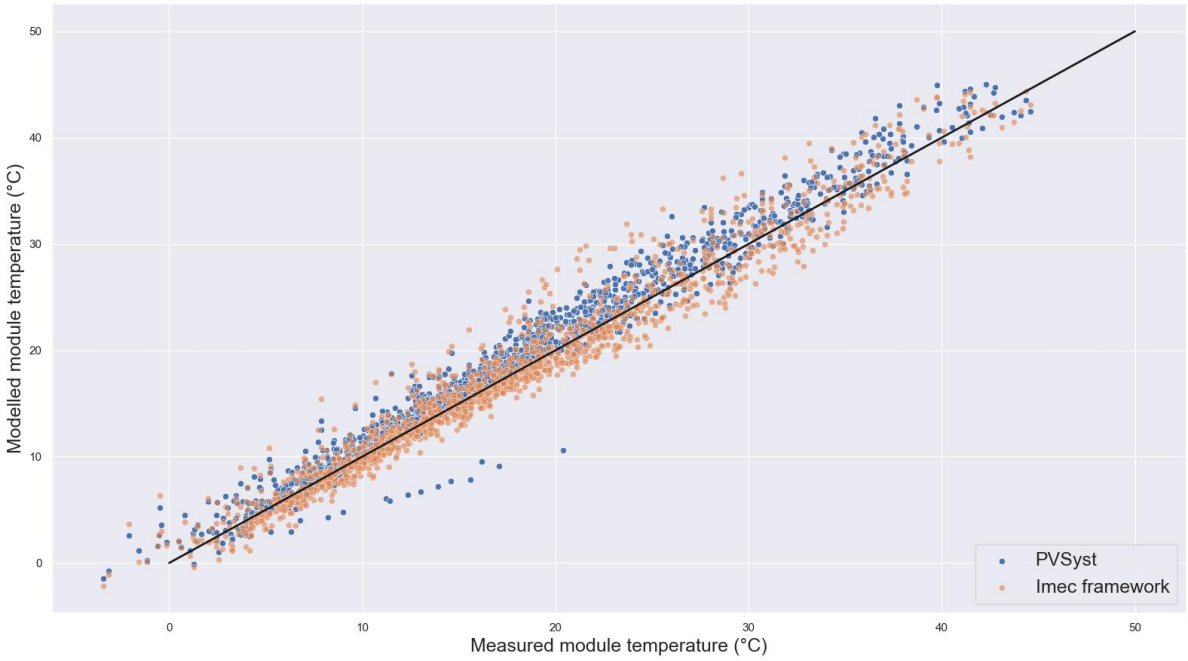

Figure 38: Module temperature PVSyst and imec's framework - measured

This figure shows that imec's framework performs very well at estimating the module temperature. The NMBE confirms this observation as it is only -0,82%, which means there is a slight underestimation. Besides this, PVSyst underestimates with a NMBE of -6,48%. Both have an NRMSE of around 11%.

With these results, it can be concluded that one of the reasons for PVSyst being better at estimating the power output is the fact that it underestimates the module temperature. Lower module temperatures increase the power output and will therefore cause the model to underestimate the actual power output by a smaller amount. Next to this, it can be concluded that if imec improves the electrical model of their framework, a generally more accurate simulation can be made.

The important power range that was determined is section 3.5 is no longer valid here. Therefore, the portion of the energy generated between the same irradiance range has to be recalculated. The result is that just under 69% of the energy is generated between an irradiance of 144 and 588 W/m². This is very similar to the important power range covered previously. The error metrics of both simulations in this range are given in Figure 39.

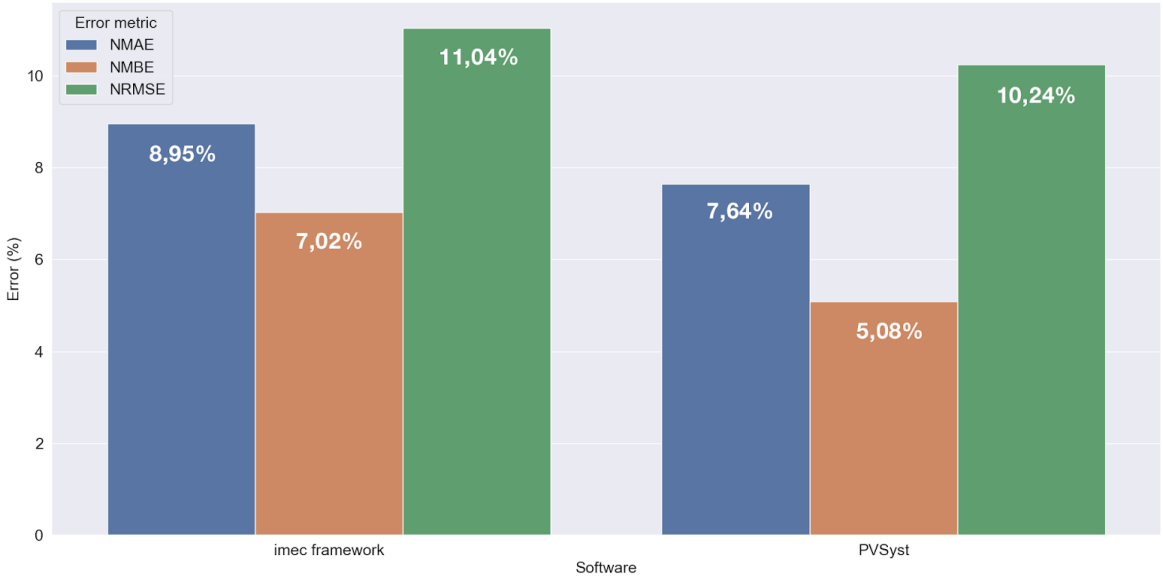

Figure 39: Normalised error metrics PVSyst and imec's framework – measured for important power range

Here, it can also be concluded that the simulations perform better within the important power range. PVSyst does however still outperform imec's framework by less than 2 % in each error metric. The same reasoning as the one given previously applies here as well.

4.5. Conclusion of simulation results

From the simulation results, it can be concluded that PVSyst is effective at simulating the Clicfloats system. It underestimates the AC power output with an NMBE of 5,93 %. This underestimation is likely due to an overestimation in module temperature. Next to this, it is concluded that the model performs even better within the predetermined important power range. The comparison between PVSyst and imec's framework shows that both models perform well at simulating two strings of the Clicfloats system. However, PVSyst performs slightly better on estimating the power output, which is likely due to two reasons. The first reason could be the poor calculation of the shunt resistance within the electrical model of the imec framework. This error is already being addressed by the researchers at imec and should be improved in the latest version. A second reason may be the fact that PVSyst underestimated the module temperature with an NMBE of 6,48%, while imec's framework estimated this very accurately.

5. Data analysis of an FPV plant

Chapter five of this thesis discusses the results of the data analysis. As was mentioned before, the data was measured at the Clicfloats FPV system. The goal of the data analysis is to answer three main research questions. The first question sought to be answered is whether or not the nearby water in the basin has a positive cooling effect on the PV modules. Secondly, a similar question is addressed but instead of water, the effect of wind is analysed. The third and final section looks into a possible combined effect of both the water and the wind working together to cool down the modules.

5.1. Influence of water temperature on module temperature

As was mentioned in the introduction, this section analyses the effect of nearby water on the temperature of PV modules. In order to find a qualitative correlation between the module temperature and the water temperature, other influential factors should stay constant. This is not possible however because when factors are kept constant at one value, there are too few data points. Therefore, specific bins are assigned for both the ambient temperature and the POA irradiance. For the ambient temperature this range is 2°C and for the irradiance this is 50 W/m². Only the data where the wind speed is 2 m/s or less is used here. This makes sure that only the effect of water temperature is looked at. The correlation coefficient between the module temperature and water temperature is calculated for each combination of ambient temperature and POA irradiance. This is then summarised in a heatmap. The minimal amount of data points in a bin required for the correlation to be shown in the heatmap is 60. The heatmap for the eastern facing modules is shown in Figure 40 and the map for the western facing modules is shown in Figure 41.

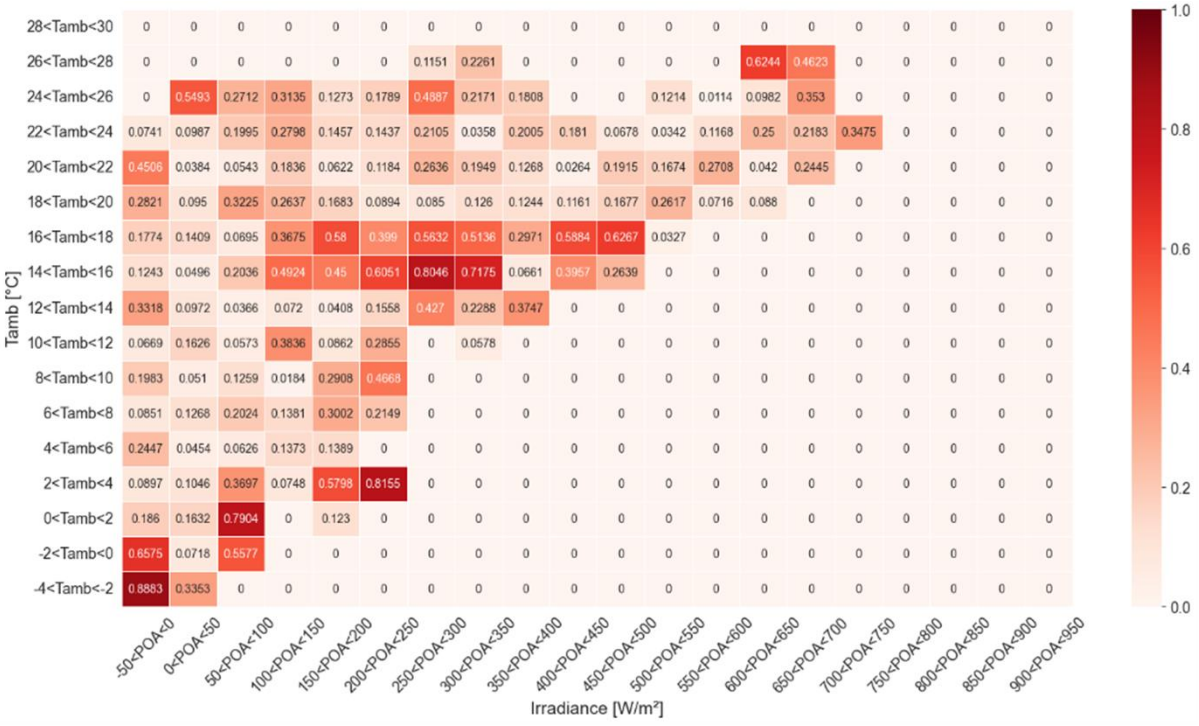

Figure 40: Heatmap of correlations between module temperature and water temperature on east facing modules

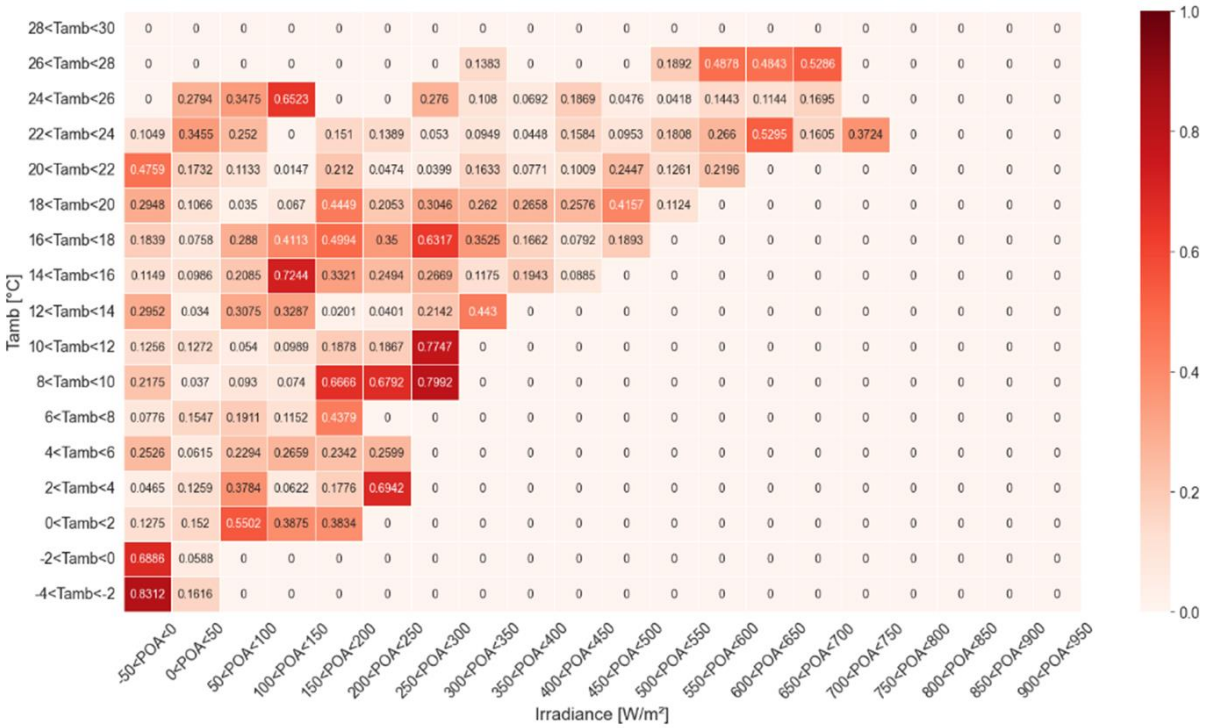

Figure 41: Heatmap of correlations between module temperature and water temperature on west facing modules

The first thing to note is that the POA irradiance data includes negative values in the first vertical column. These are most likely measurement errors and do not exceed -3 W/m². Then, looking at the heatmaps in general, it can be observed that most correlations are very weak. There are a few situations where the correlation is higher, but there seems to be no trend in what situations this is the case.

Regression fits were done on the scatter plots of each cell in the heatmap to further analyse the correlations. These include a regular linear regression fit and a Huber fit. The Huber fit is a robust fitting method that attributes a lower weight to outliers and thus gives a more relevant fit for situations where multiple outliers are present. The correlation coefficient of the Huber fit is also the one shown in the heatmaps. Figures 42 to 45 show plots for a few situations.

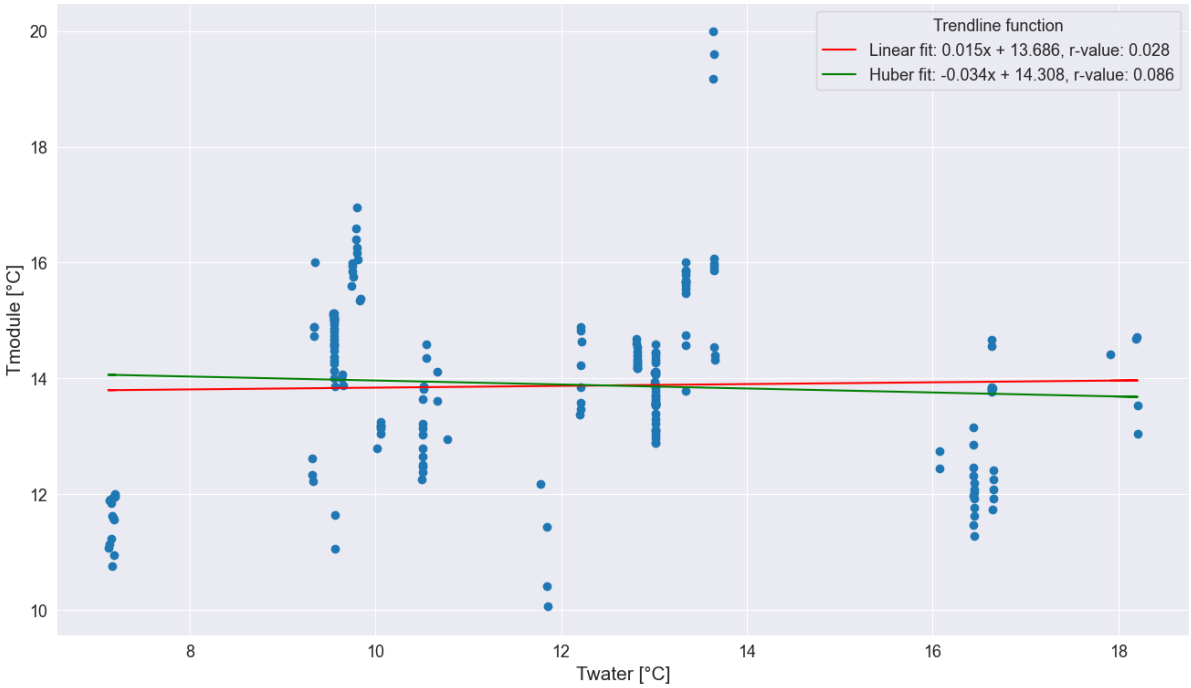

Figure 42: Module temperature in function of water temperature, east facing, 150<POA<200 W/m², 10<ambient temperature<12 °C, 0<wind velocity<2 m/s

This first regression plot includes data points for a POA irradiance range of 150 to 200 W/m² and an ambient temperature range of 10 to 12 °C. The plotted module temperature is from an eastern facing module. The trendlines and the r-value clearly show there is no correlation. When observing the plot, it is also clear that the data is shaped in vertical lines. This confirms that the module temperature varies while the water temperature stays constant. It is worth noting that most regression plots with a low correlation coefficient look similar to this one. Therefore, the observations about this plot already represent a large portion of the heatmap.

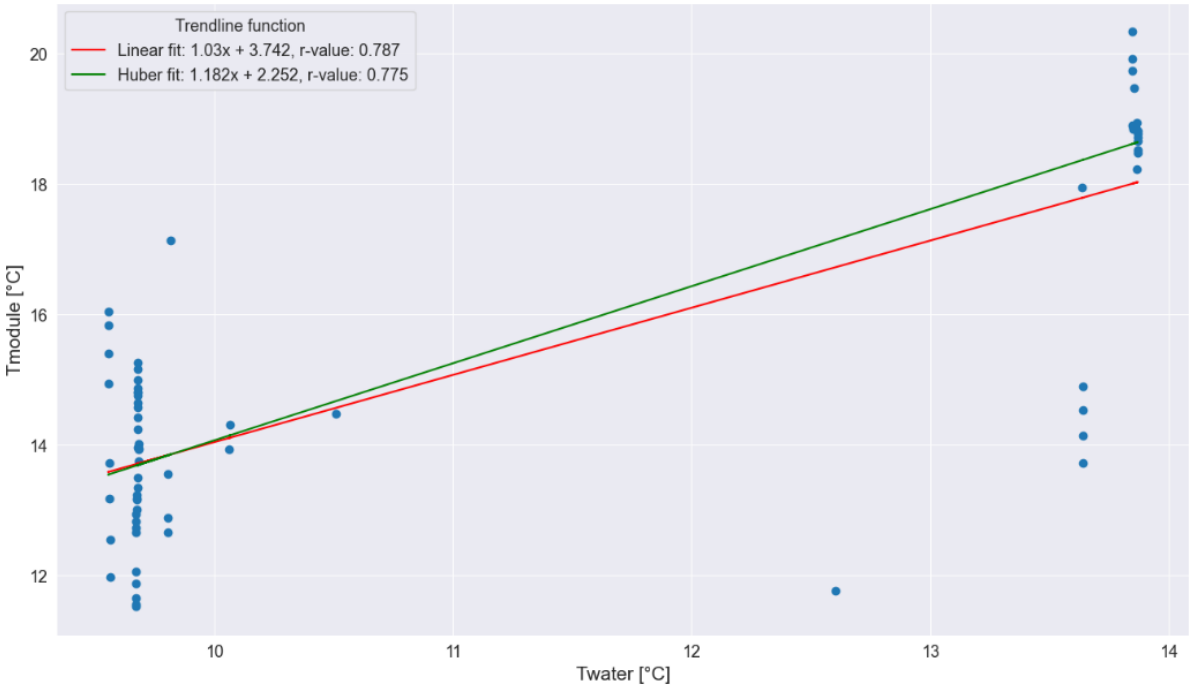

Figure 43: Module temperature in function of water temperature, west facing, 250<POA<300 W/m², 10<ambient temperature<12 °C, 0<wind velocity<2 m/s

In this second plot, the trendline for a POA irradiance range of 250 to 300 W/m² and an ambient temperature range of 10 to 12 °C is shown. Once again, vertical lines can be observed in the data. However, the trendline shows a high, positive correlation for this particular situation. The data in this range is however inconsistent with a gap between low and high water temperatures. Therefore, this plot is less relevant.

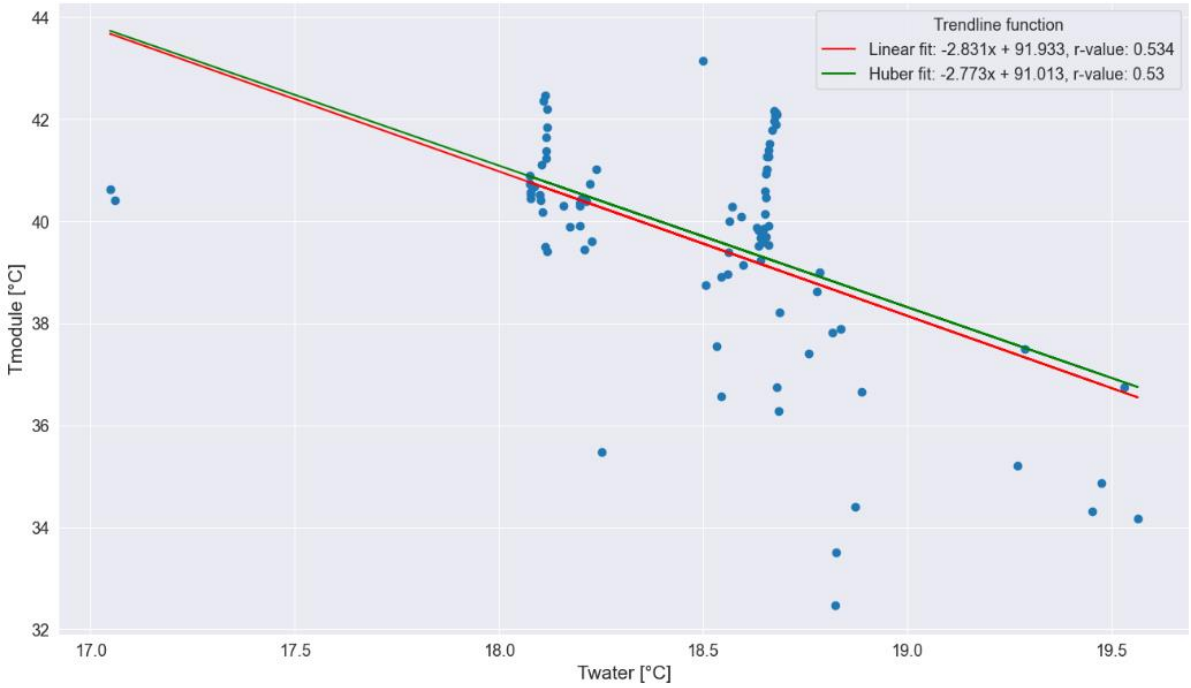

Figure 44: Module temperature in function of water temperature, west facing, 600<POA<650 W/m², 22<ambient temperature<24 °C, 0<wind velocity<2 m/s

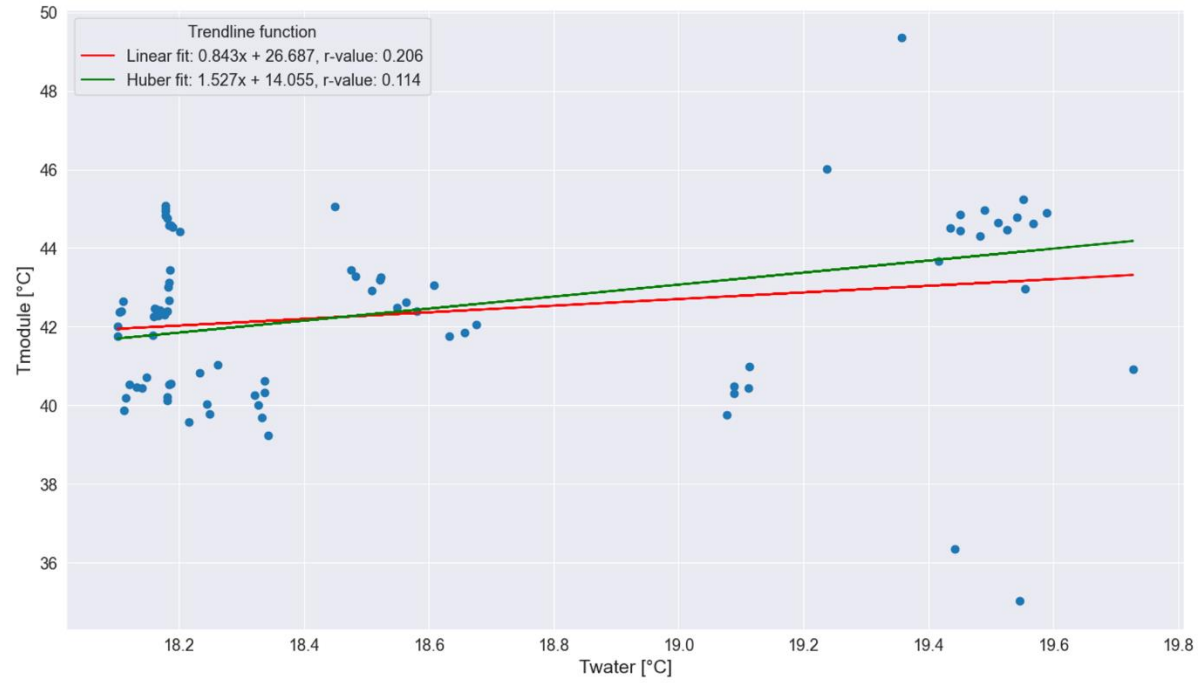

Figure 45: Module temperature in function of water temperature, west facing, 600<POA<650 W/m², 24<ambient temperature<26 °C, 0<wind velocity<2 m/s

These last two plots show situations for a POA irradiance range of 600 to 650 W/m² and ambient temperature ranges of 22 to 24 °C and 24 to 26 °C. The two trendlines are very different and show that correlations are not consistent.

From this analysis it can thus be concluded that, for the observed data from the Clicfloats plant, water temperature on its own does not seem to have a statistically significant effect on the module temperature.

5.2. Influence of wind speed on module temperature

Similar to the previous section, heatmaps of correlation values are made to see what the correlation is in different situations. Here, the heatmaps, illustrated in Figures 46 and 47, show correlations between module temperature and wind velocity. The same bins for POA irradiance and ambient temperature are used. The water temperature is not kept constant in this case since the previous section concluded that water temperature has no direct impact on module temperature.

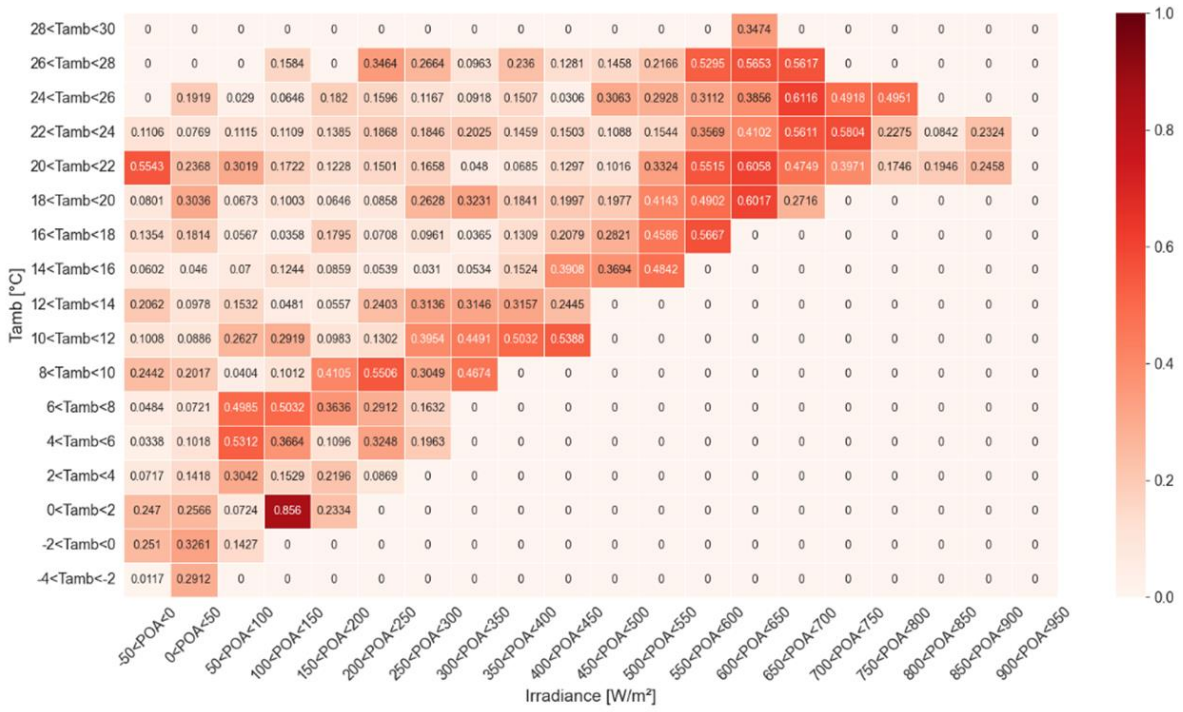

Figure 46: Heatmap of correlations between module temperature and wind velocity on east facing modules

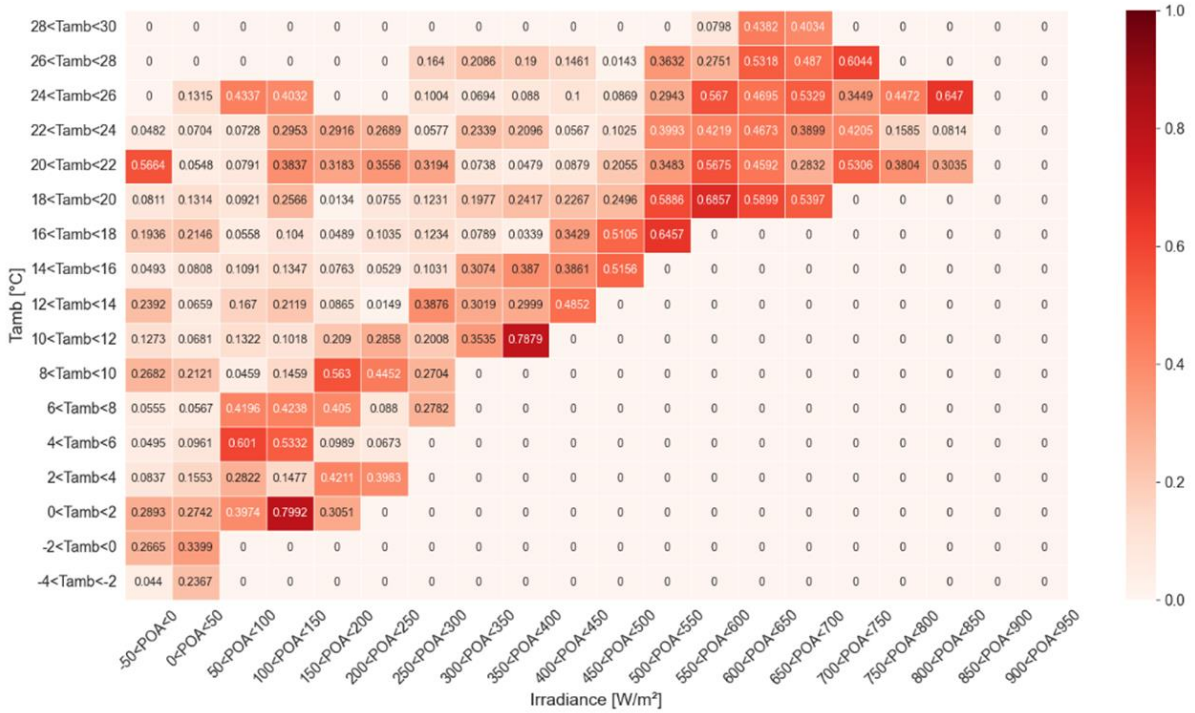

Figure 47: Heatmap of correlations between module temperature and wind velocity on west facing modules

From these heatmaps, it can be concluded that correlations are generally higher and show up more consistently. Especially at the higher irradiance ranges, there tends to be a higher correlation. A logical explanation for this is that the temperature difference between the ambient temperature and the module temperature is higher at high irradiance levels. Therefore, convective cooling done by wind will be more effective. Additionally, the correlation is at its highest when the irradiance is high and the ambient temperature is low, which further confirms the previous statement.

These conclusions are also visible in the scatter plots. Figure 48 shows a situation with a lower POA irradiance of 200 to 250 W/m² and ambient temperature of 8 to 10 °C. While Figure 49 shows a scenario with a higher POA irradiance of 550 to 600 W/m² and ambient temperature of 18 to 20 °C.

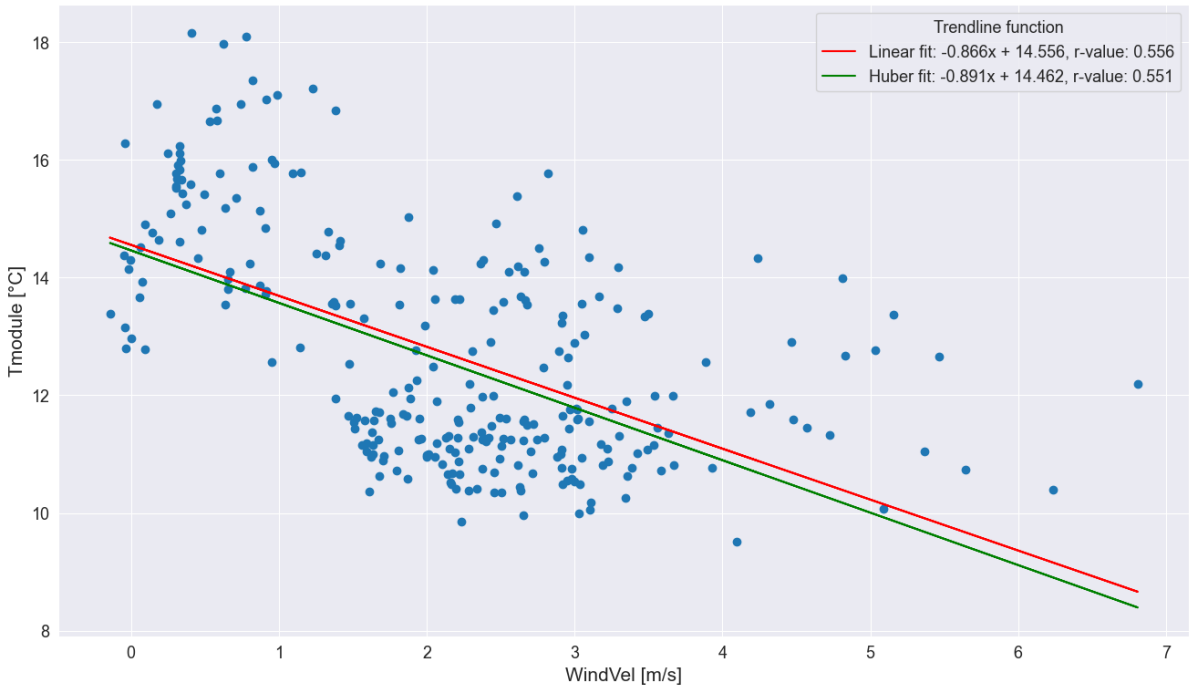

Figure 48: Module temperature in function of wind velocity, east facing, 200<POA<250 W/m², 8<ambient temperature<10 °C

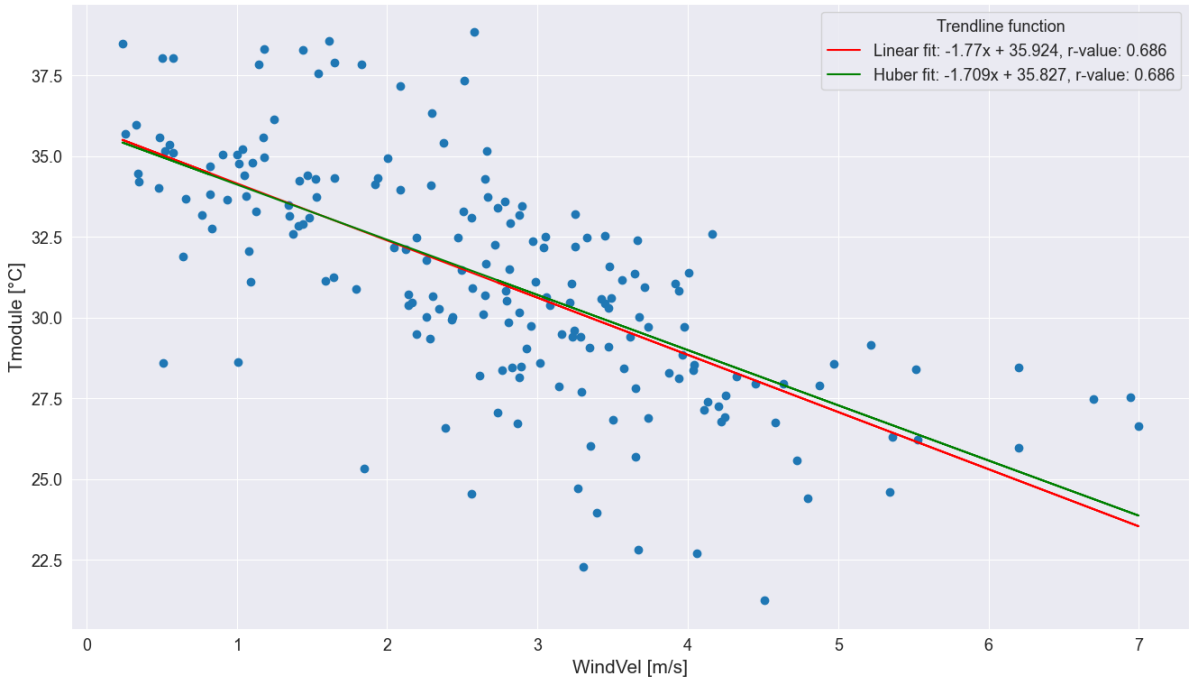

Figure 49: Module temperature in function of wind velocity, west facing, 550<POA<600 W/m², 18<ambient temperature<20 °C

In both situations, a clear negative correlation exists. It clearly indicates that module temperature lowers when wind velocity increases. This result was to be expected since the same conclusion was made in various literature [7], [48], [56].

Generally, it can be seen that the trendline in plots with lower irradiance became steeper as the ambient temperature decreased. The trendline in plots with higher irradiance kept a steep decline throughout all the temperature ranges.

To make the positive effect of wind even more clear, two more figures were made. Figures 50 and 51 show the module temperature on the y-axis and solar irradiance or wind speed on the x-axis. The different lines show different wind speed ranges and irradiance ranges.

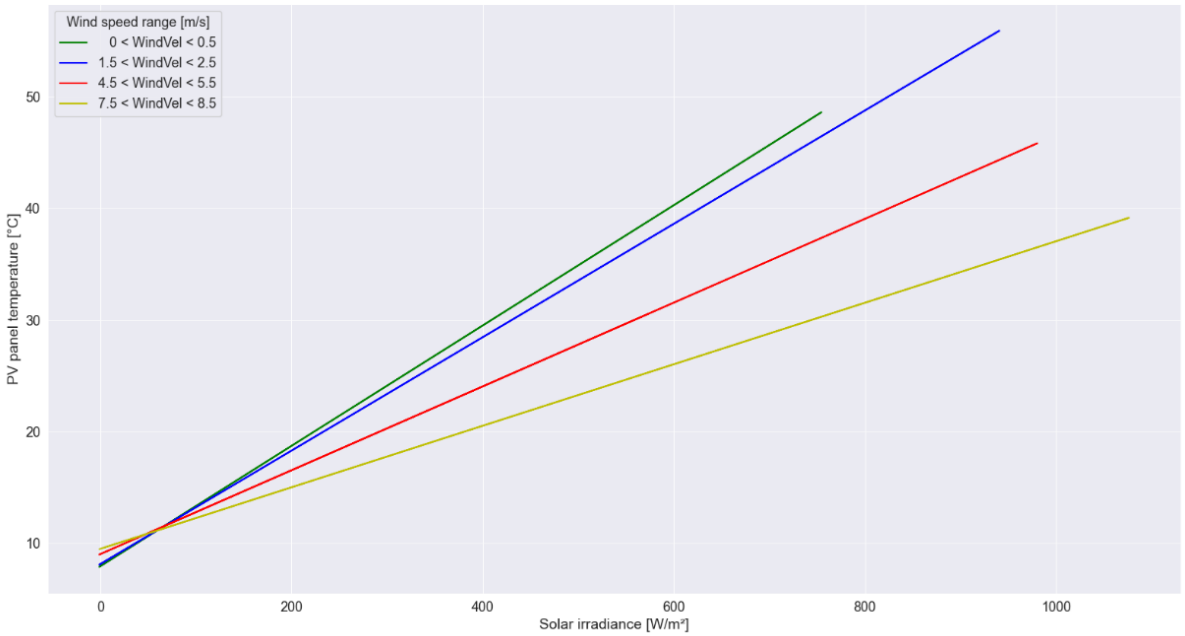

Figure 50: Effect of solar irradiance on PV temperature

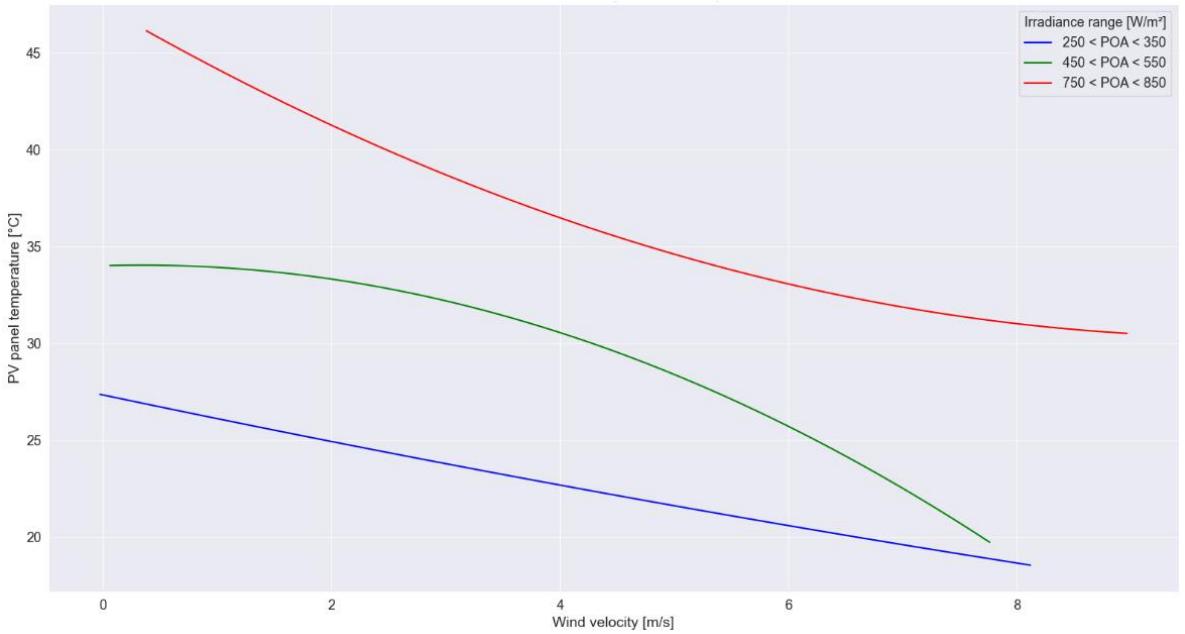

Figure 51: Effect of wind velocity on PV temperature

The figures show that there is a clear correlation between wind speed and module temperature in all irradiance ranges. These findings correspond to the concussion that was made in [57].

In the remainder sections of this chapter, the effect of the water level in the plant's basin and the effect of wind direction are discussed.

5.2.1. Effect of water level

The basin of the Clicfloats plant has a trapezium shaped border around the water which could potentially form a barrier for the wind. The ultrasonic wind sensor that measures the wind velocity is located on top of this border as was mentioned in section 3.3. Therefore, the wind speed that reaches the modules might differ from what is measured on top of the basin border. This also means that the water level in the basin can influence how much of the wind reaches the modules and at which speed. To see if the water level has an effect on the correlation between wind speed and module temperature, a plot was created. A picture of the basin's border can be seen in Figure 52. The plot is shown in Figure 53.

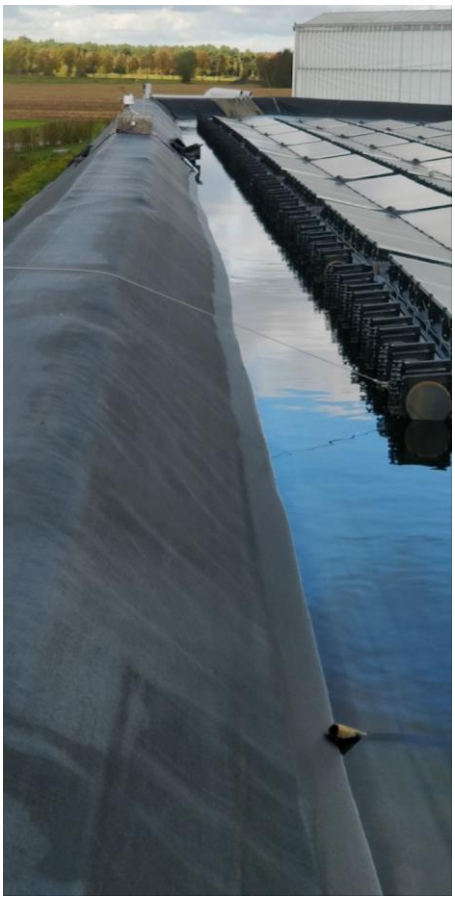

Figure 52: Border around the basin

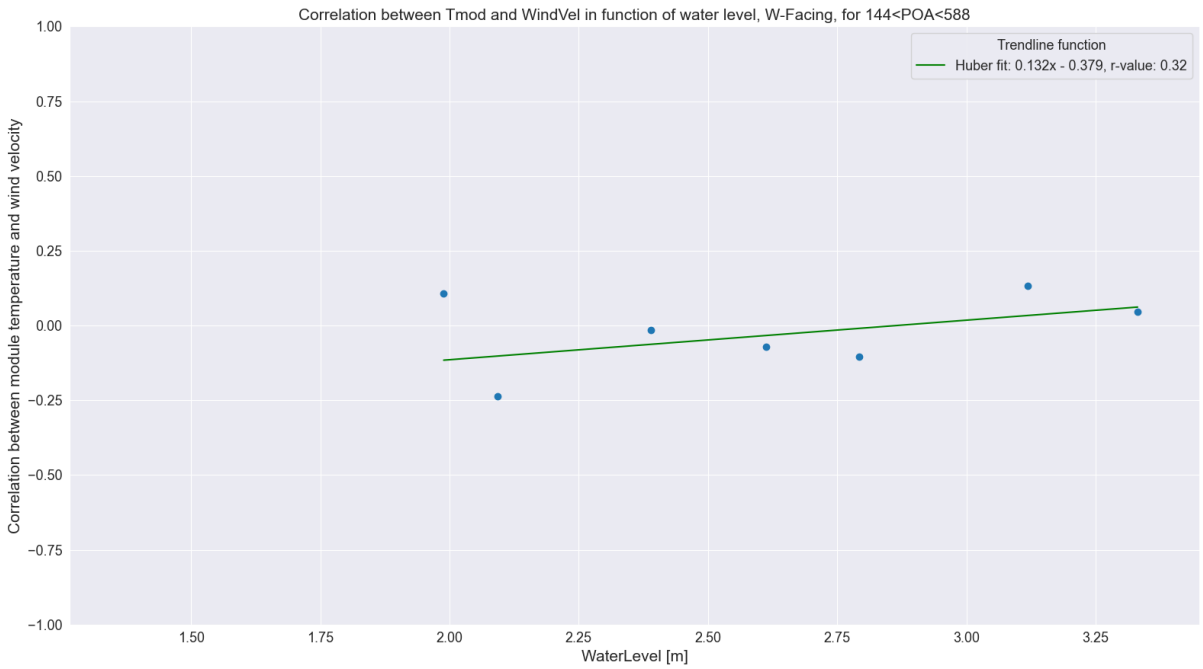

Figure 53: Correlation between module temperature and wind velocity in function of water level, west facing, 144<POA<588 W/m²

This plot shows the correlation between module temperature and wind velocity on the y-axis and the basin's water level on the x-axis. The POA irradiance is kept in the important range (see section 3.5) from 144 to 588 W/m² and the fit is a Huber fit.

This plot shows that there is a low correlation. It can thus be concluded that the water level of the basin has no significant effect on the cooling effect of the wind on the modules.

5.2.2. Effect of wind direction

The wind direction might also have an impact on the cooling of the modules. To see the influence of wind direction on module temperature, a normalised histogram is made. This histogram plots the normalised distribution of the module temperature for each wind direction. Figures 54 and 55 show the histograms for east facing modules and west facing modules.

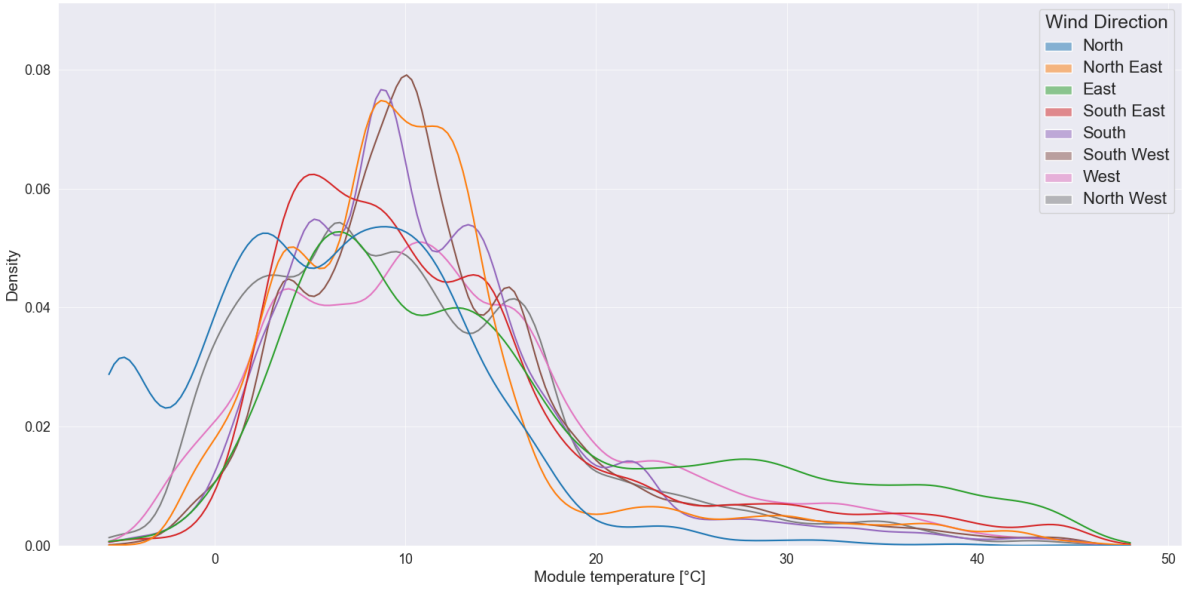

Figure 54: Normalized module temperature distribution for each wind direction, east facing modules

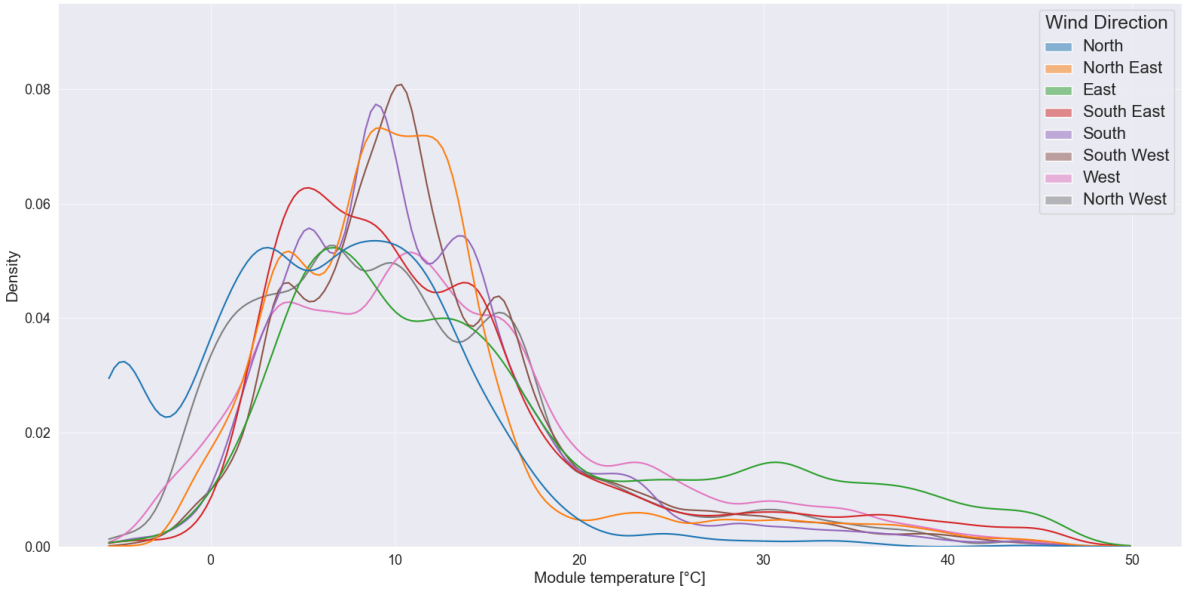

Figure 55: Normalized module temperature distribution for each wind direction, west facing modules

Both histograms look very similar. At the lower temperatures, the northern and southern wind directions are the most present. This indicates that wind from northern and southern directions has a more positive effect on module temperature compared to eastern and western winds. This result is not to be expected because in literature study section 2.2.9 it was concluded that when wind hits the face of the modules, it would provide better cooling. A possible reason for the conclusion being different here could be contributed to the system configuration. If wind arrives from the eastern or western directions, it will likely flow upwards after colliding with the modules around the outer edge of the system. Therefore, preventing the modules in the middle from getting the full benefit of the cooling. When the wind originates from the north or south however, it can flow through the walkways while pulling the hot air out from underneath the modules. This hypothesis makes sense since the temperature sensor that recorded the data in the graphs above, was indeed located more towards the middle of the PV array.

5.3. Combined effect of water and wind

It has already been concluded that, for the Clicfloats plant, water temperature on its own does not have a significant effect on module cooling. However, the velocity of the wind does. This final section of the data analysis will look at a possible combined effect of the two.

To do this, 3D plots have been created that include the module temperature in function of both the wind velocity and the water temperature. In the plots, POA irradiance and ambient temperature are kept constant in bins like in the first sections of the data analysis. Figures 56 to 58 show the plots for a few situations. Surface plots were drawn through the data points to better visualise the relation.

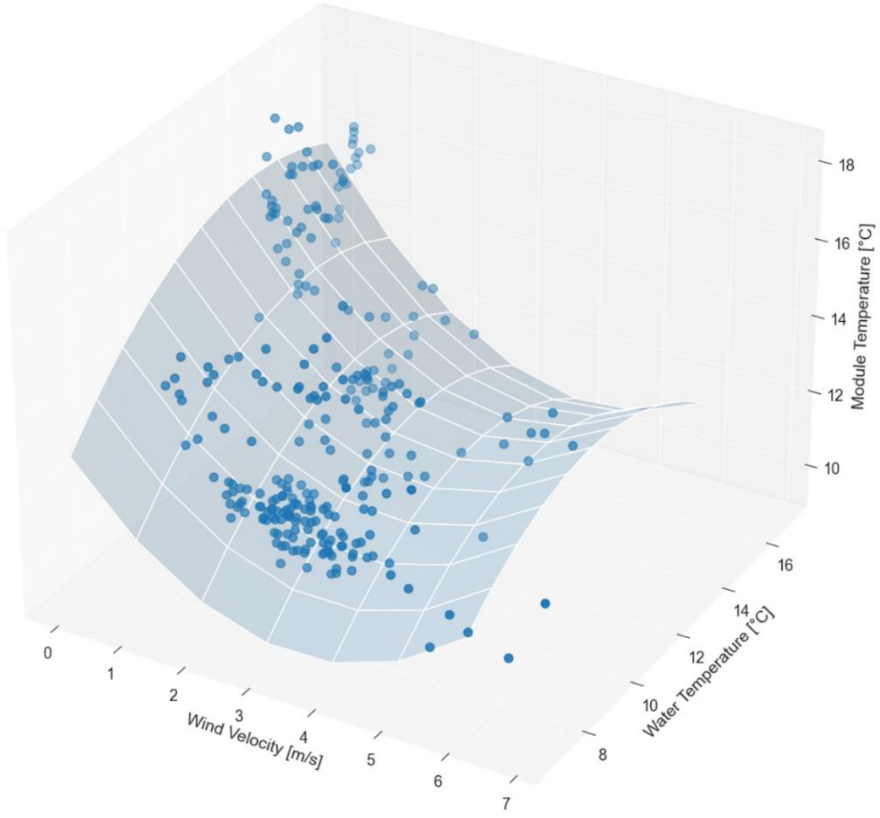

Figure 56: 3D plot of module temperature in function of wind velocity and water temperature, surface fitted quadratic polynomial, east facing, 0<wind velocity<10 m/s, 200<POA<250 W/m², 8<ambient temperature<10 °C

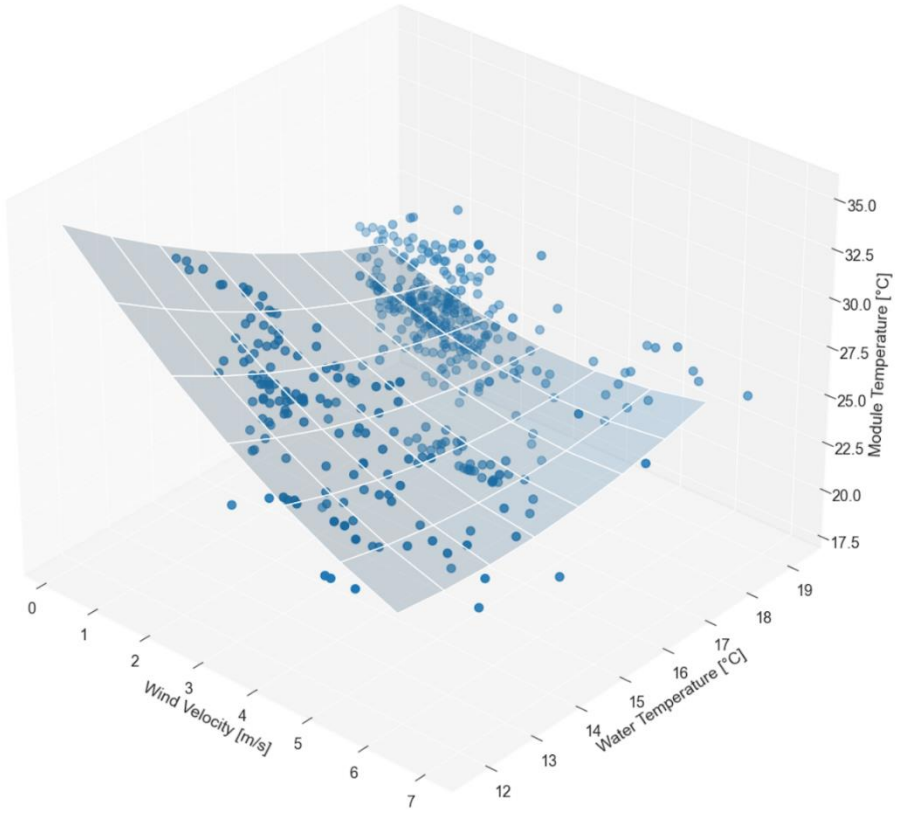

Figure 57: 3D plot of module temperature in function of wind velocity and water temperature, surface fitted quadratic polynomial, east facing, 0<wind velocity<10 m/s, 400<POA<450 W/m², 16<ambient temperature<18 °C

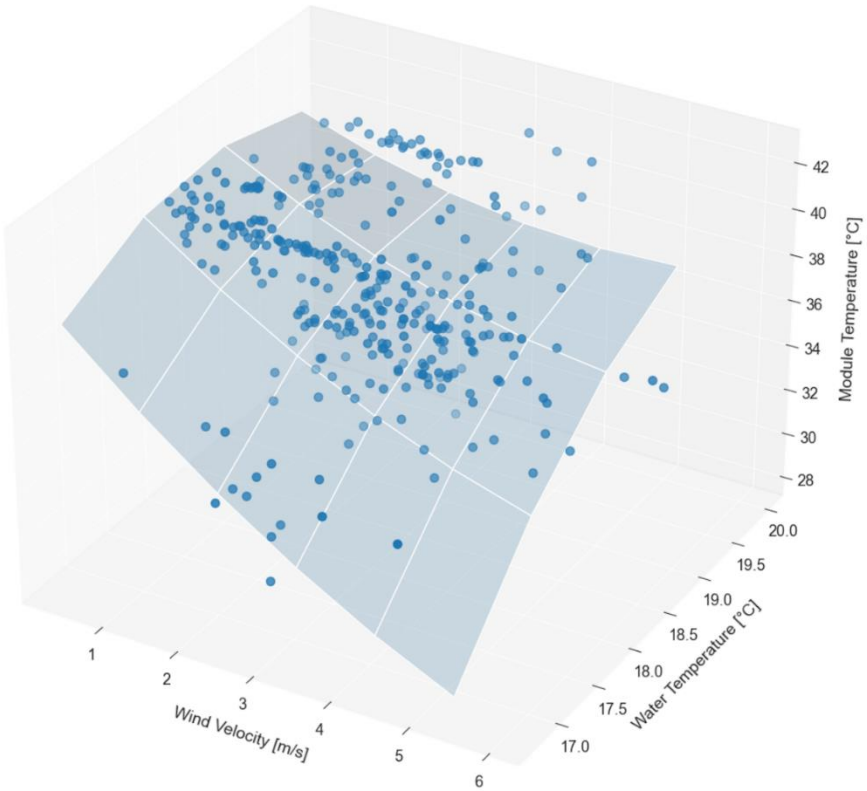

Figure 58: 3D plot of module temperature in function of wind velocity and water temperature, surface fitted quadratic polynomial, east facing, 0<wind velocity<10 m/s, 600<POA<650 W/m², 22<ambient temperature<24 °C

If there was a clear combined effect of water and wind, module temperature would decrease with decreasing water temperature and increasing wind velocity. In the 3D plots, this would mean that the surface plot's highest point is located at the lowest wind velocity and the highest water temperature. The lowest point would be located where the wind velocity is the highest and the water temperature is the lowest. For the first two plots above, this expected pattern is not clearly visible. Only for Figure 58, this pattern is present. This is however the only case where this occurred over the twenty 3D plots that were examined. Since most situations don't show this pattern clearly, a definitive conclusion about a combined cooling effect between wind and water cannot be made.

5.4. Conclusion of data analysis

The conclusions from this data analysis are in line with what Mohammed Haggag stated in his Master's thesis [7]. His theory that cooling of FPV is mostly caused by wind is now confirmed with real world data. This however does not mean that water has no influence entirely. The temperature of the vapour blanket on water bodies is usually lower than the ambient temperature and can therefore lower the temperature of the wind flowing over it. A clear conclusion on the combined effect of water and wind could however not be drawn in this thesis. Next to this, it was concluded that wind originating from the north and the south provided better cooling for the system layout used in the Clicfloats plant. The effect of the water level on the cooling done by wind was also analysed and it was concluded that there was no clear correlation. Besides this, the claim that cooling done by wind is more effective in FPV systems compared to GPV systems was not able to be verified. This is due to the lack of data of a nearby GPV plant. It is expected however that the Clicfloats system would not show an improvement over GPV due to the small water surface area and the nearby greenhouses.

6. Design and construction of an FPV demonstrator

This next chapter of the thesis describes the design and construction of an FPV demonstrator. This demonstrator will make it possible for the specific structure, advantages and technical challenges related to FPV to be presented to a wide audience in a tangible and interactive way. Ultimately, this miniature setup will be used for promotional purposes at fairs, open days and in education. Energyville's technical staff offered their support and guidance in both the designing- and building phase.

6.1. Design process

To start off the designing process, a meeting was arranged with the thesis promotors and technical staff of Energyville to discuss the purpose and requirements of the demonstrator. Following this meeting, a list of requirements was made, and brainstorming started for the realisation of a first design. An overview of the list of requirements is given in Table 7. This table separates the requirements into fixed, variable, and desirable.

Table 7: Requirements list for demonstrator

Fixed	Variable	Desirable	Requirement
x			Working solar modules must be used
	x		Some sense of power output must be shown on a display (either short-circuit current or power with an MPPT)
x			The demonstrator is easily movable
	x		The demonstrator can fit through a door
x			The floating structure looks realistic and is functional
x			Anchoring and mooring is included with the floating structure
		x	Additional environmental features (like wind, waves, water temperature, etc.) to make the demonstrator more interactive

From this list of requirements, it can be concluded that there is a lot of freedom in designing this demonstrator.

The following sections go over the evolution of the design. Each section discusses the choices that were made, issues that came up and feedback that was given. Autodesk's CAD software Inventor was used to create 3D designs of the demonstrator.

6.1.1. First design

The first design consisted of a steel table frame mounted on wheels. Steel profiles were chosen because then the dimensions of the table could be customised. Wheels are a convenient way of making the setup mobile and are included in all designs. The dimensions of the table are 700 by 1000 mm². A front panel and two side panels serve as cover for the inside of the table. The back of the table is open, so the inside is accessible. Stickers will be placed on the cover panels to represent the parties involved.

An extended portal above the table frame holds the lamp in place. This lamp will be recovered from an older demonstrator setup Energyville has. The idea was that the lamp could be put in any position. So higher or lower positioning, but also sliding in x and y directions and adjusting the angle at which the lamp emits light. The mechanical details on these movements were not yet devised.

The miniature FPV system is placed on top of the table frame. It was agreed upon that the system would be based on the Clicfloats system. This way all three parts of the thesis are about the same system. Directly on the top panel of the table, there is an artificial basin with water in it. On the water floats the structure that holds 16 mini modules. The parts for the floating structure were constructed of basic shapes that looked more or less similar to the floats used in the Clicfloats system. Four small poles with strings attached would serve as anchoring for the floats.

Consideration was also given to the implementation of additional environmental impacts. Two features were considered. First, the effect of wind by adding fans that blow towards the modules and secondly a water heating and cooling system to regulate water temperature. After analysing the cost and complexity of a water chiller and heater, it became clear that this would be an expensive feature to add. The heating or cooling of the water would need to happen fast for the audience to see the effect within a reasonable amount of time. A system that could do this would be large, heavy, and expensive. Furthermore, this would most likely represent a misleading effect. In reality, based on conclusions of literature and this thesis, the cold temperature of the water will only have a direct effect on module temperature if the modules are really close to the water. This is true for this miniature design, so the effect would most likely be visible. However, this is not the case for a real FPV system. Adding fans to the demonstrator could be a nice addition. Although it is unclear how well the effect will be visible given the very small scale of the setup. In this first design, movable fans were added using rails between the four corners of the table frame.

Rendered shots of the Inventor CAD model of this first design can be seen in Figures 59 and 60. The colours for all the parts in this design are chosen to improve visibility but have no further meaning.

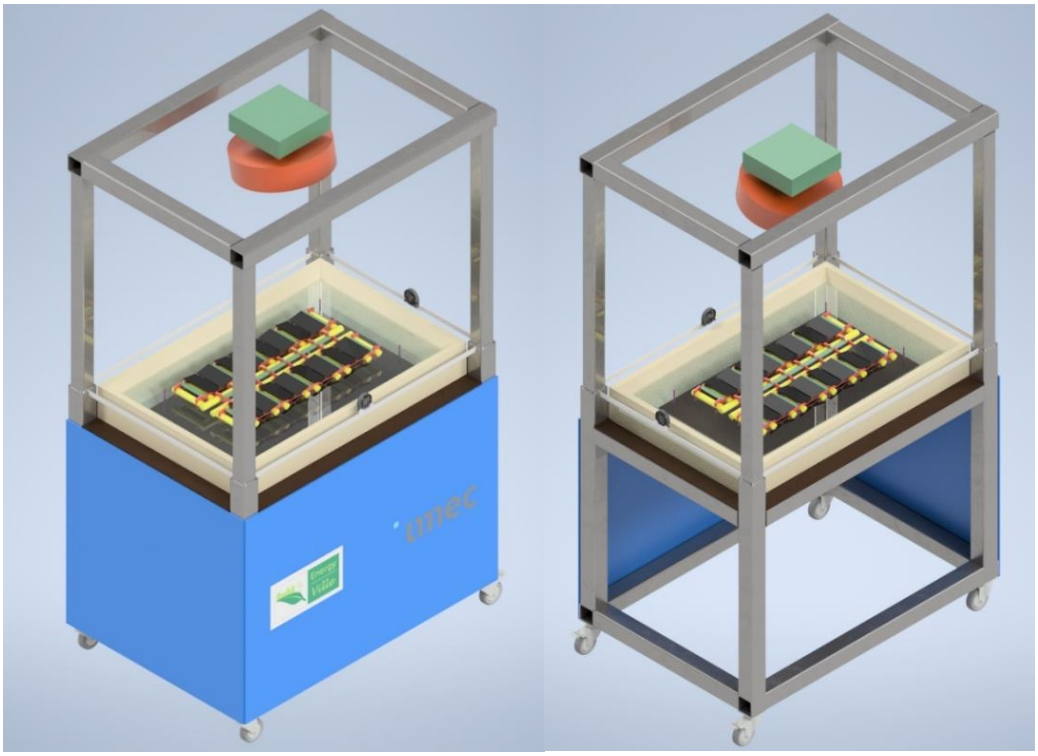

Figure 59: Front and back shot from first design

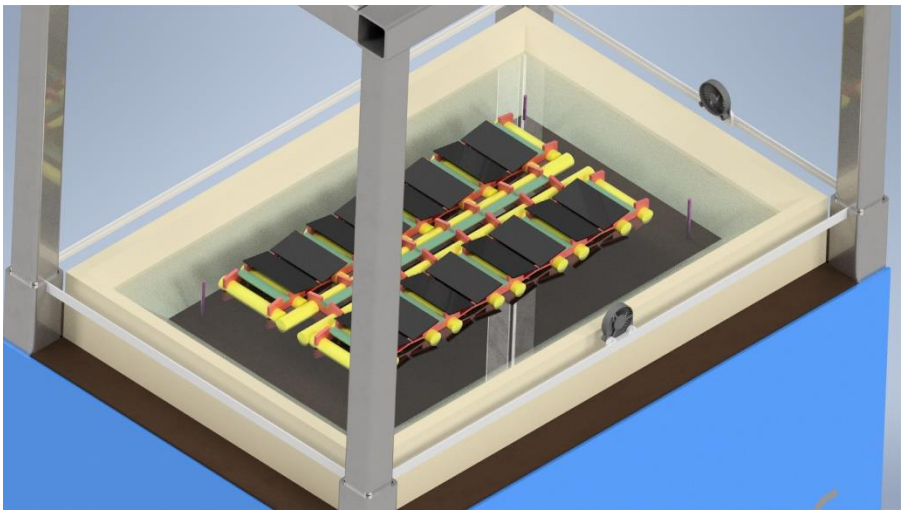

Figure 60: Close-up shot of floating structure from first design

6.1.2. Reworked design

After the first design was presented to the promotors, feedback was received. The first point was about the portal construction to support the lamp. This construction was very heavy and blocked some of the view to the floating structure. The idea that the lamp would be movable in all directions was not really necessary. It was suggested to go with a lighter design that does not block the view as much. A second point of feedback was about the artificial basin. It was suggested to make this see through by having the water in a plexiglass container. This way, the floats can be seen from afar and the demonstrator becomes more visually appealing. A final point of feedback was the recommendation to leave the fans out for now. It was not clear whether the effect of the wind blown by the fans would be visible. Therefore, it was decided to first measure the output of the modules when the demonstrator was being built.
A reworked design was made, taking into account the feedback that was given. The portal construction of the lamp was replaced by just one arm holding the lamp. The artificial basin was replaced with a plexiglass container. Using this container instead of the artificial basin also created more room for the floating structure.

The floating structure was also further developed. The bigger water area that was created by using the plexiglass container allowed for more modules to be used. The parts of the floats were designed with more detail and now looked very similar to the actual Clicfloats. The parts of the floats would be 3D-printed, and buoyancy is provided by PVC tubes. A close-up shot of how the floats are put together is shown in Figure 61.

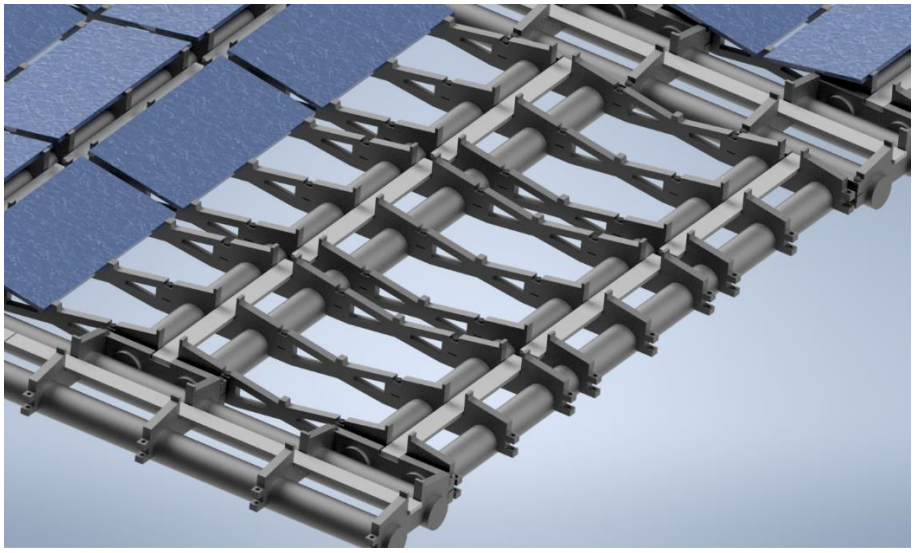

Figure 61: Close-up shot of assembled floats

Finally, the steel framework of the table was replaced with aluminium ITEM profiles. These are light, modular and are easy to assemble.

Rendered shots of the Inventor CAD model of this reworked design can be seen in Figures 62 and 63.

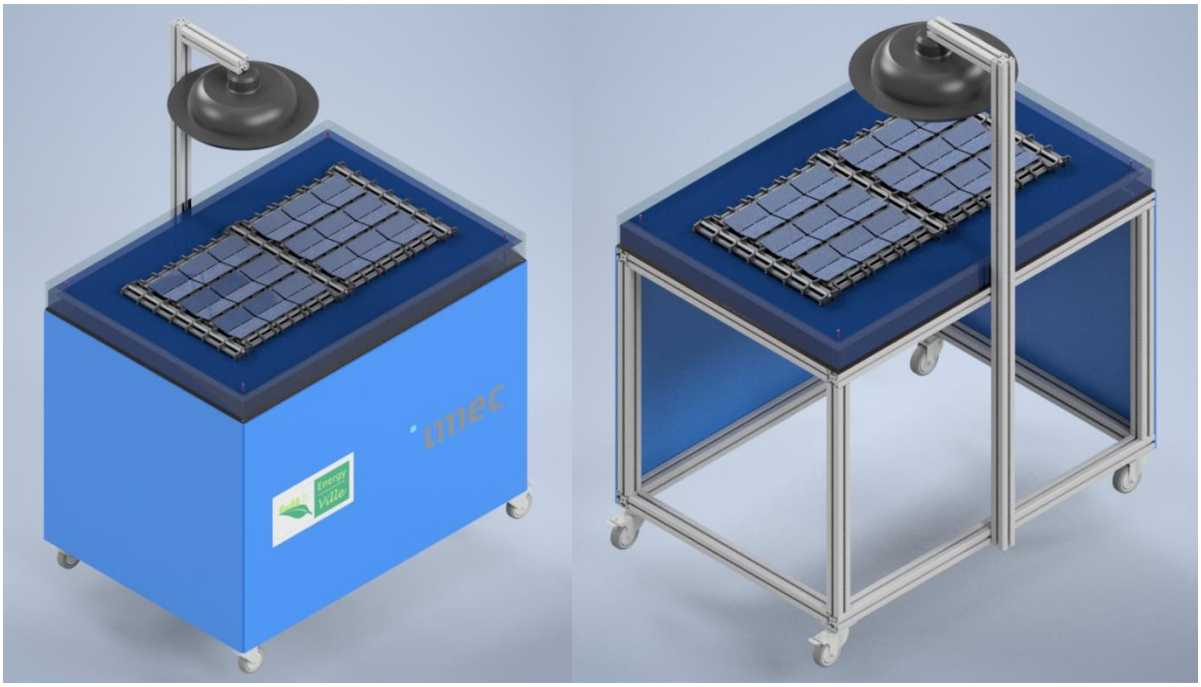

Figure 62: Front and back shot from reworked design

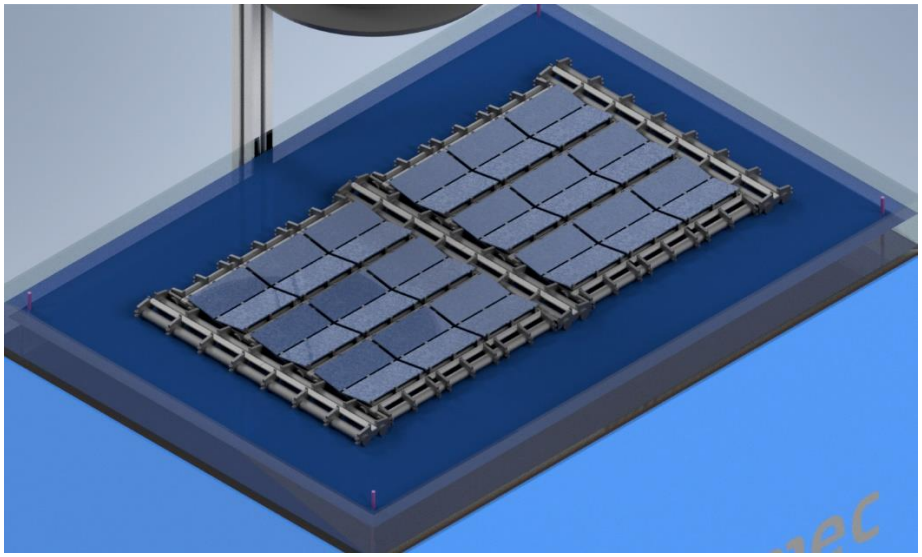

Figure 63: Close-up shot of floating structure from reworked design

6.1.3. Design with parts to order

Around this time in the design process, there were discussions about which PV modules would be used for the demonstrator. The first idea was to make the modules at Energyville, but this would take quite a lot of time and work. It was later decided to simply buy the modules. Bought modules would also look aesthetically better. The modules that were suggested and later ordered provide 6V, 1W and are ideal for DIY purposes [58]. They are 60 by 110 mm² in size and are 2 mm thick.

The next step in the design process was determining the exact components needed and compiling an order list. The technical staff of Energyville suggested ordering most of the parts at Item, since they order there regularly. At Item's website, it is possible to download CAD files of the products. This allowed for a CAD model to be created that had the exact parts that will be ordered.

Before creating the CAD model with Item parts, a few changes were made to the design. First is the size of the table. It was agreed upon that the water container will have a size of 700 by 1000 mm² since this will fit a good number of modules on the water. The height of the container is 100 mm, and the thickness is 8 mm. The container was ordered from Teblick. Until now, the container used the full area of the table. The table size in this design is 850 by 1300 mm², which ensures that there is a perimeter of 15 cm free space around the container. This extra space on the table could be used to place leaflets or other promotional material on. Second, is the number of PV modules. Now that the exact modules that will be used are known, the parts of the floating structure were adjusted to fit with the modules. This made the floating structure bigger than before. Therefore, the decision was made to go from 32 modules to 24 modules. Third, is the addition of a wooden sheet underneath the table. This makes it possible to use the space under the table to store equipment like electronics, etc. A final change is made to the arm holding the lamp. This now uses wider ITEM profiles to grant more support. The mounting pieces on the part that holds the lamp can also be adjusted to change the height of the lamp.

Figures 64 and 65 show an Inventor CAD model constructed of parts from the Item website. A list of the products used is given below.

- ITEM profiles of size 40 x 40 mm² to make the frame of the table
- Wider ITEM profiles of size 80 x 40 mm² to use as an arm for the lamp
- Mounting pieces (corners) to mount the profiles together
- Castor wheels of diameter 125 mm, two with and two without brake
- A plastic-coated chipboard of size 850 x 1300 mm², 25 mm thick as tabletop
- The same sheet is used underneath the table frame. Although, it will need to be sawn to size to fit on the profile frame
- Cold rolled aluminium sheets as cover panels on the front and sides of the table. These have sizes 1300 x 1000 mm² and 850 x 1000 mm². The back of the table frame will be left open
- Screws and nuts for fastening the wheels, profiles, and plates

The demonstrator is about 1200 mm high from the ground to the tabletop and about 2000 mm from the ground to the top of the lamp's arm.

Figure 64: Front and back shot from design with parts to order

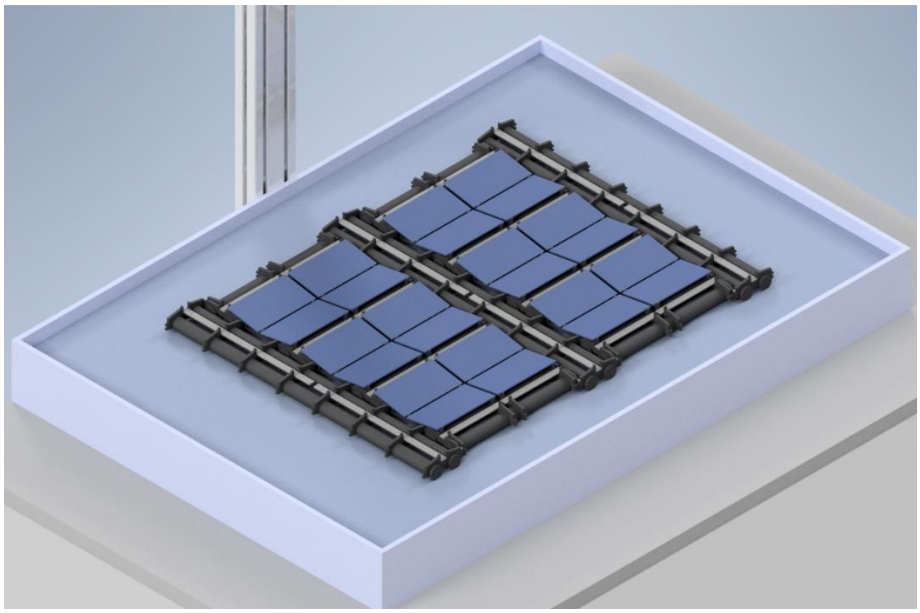

Figure 65: Close-up shot of floating structure from design with parts to order

6.1.4. Final design

During the building process of the demonstrator, it was noticed that the tabletop was a bit higher than expected. This was not a problem for taller people however it could be an issue for smaller people or children since they would not be able to see the floating structure properly from their point of view. To lower the demonstrator, the framing around the wheels was changed. A picture of the reworked bottom side framing is shown in Figure 66. The demonstrator now has a height of about 1050 mm from the ground to the tabletop and about 1940 mm from the ground to the top of the lamp's arm.

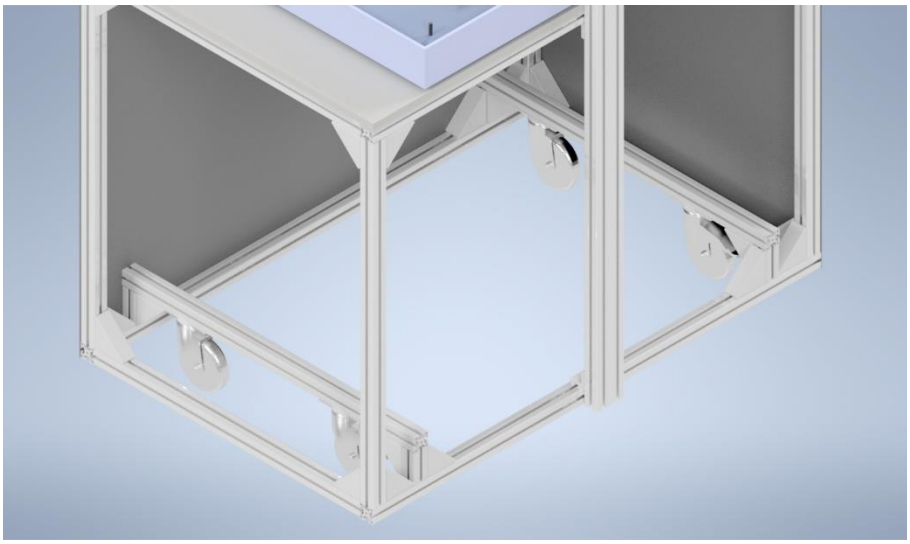

Figure 66: Reworked bottom side framing

Stickers showing the parties involved were designed to place on the aluminium cover sheets. Anchoring poles and artificial walkways for the floats were designed to be 3D printed. The walkways have a U-shape and cut-outs for the cables. Figures 67 and 68 show the Inventor CAD model of the final design. The colours in these figures more or less correspond to reality.

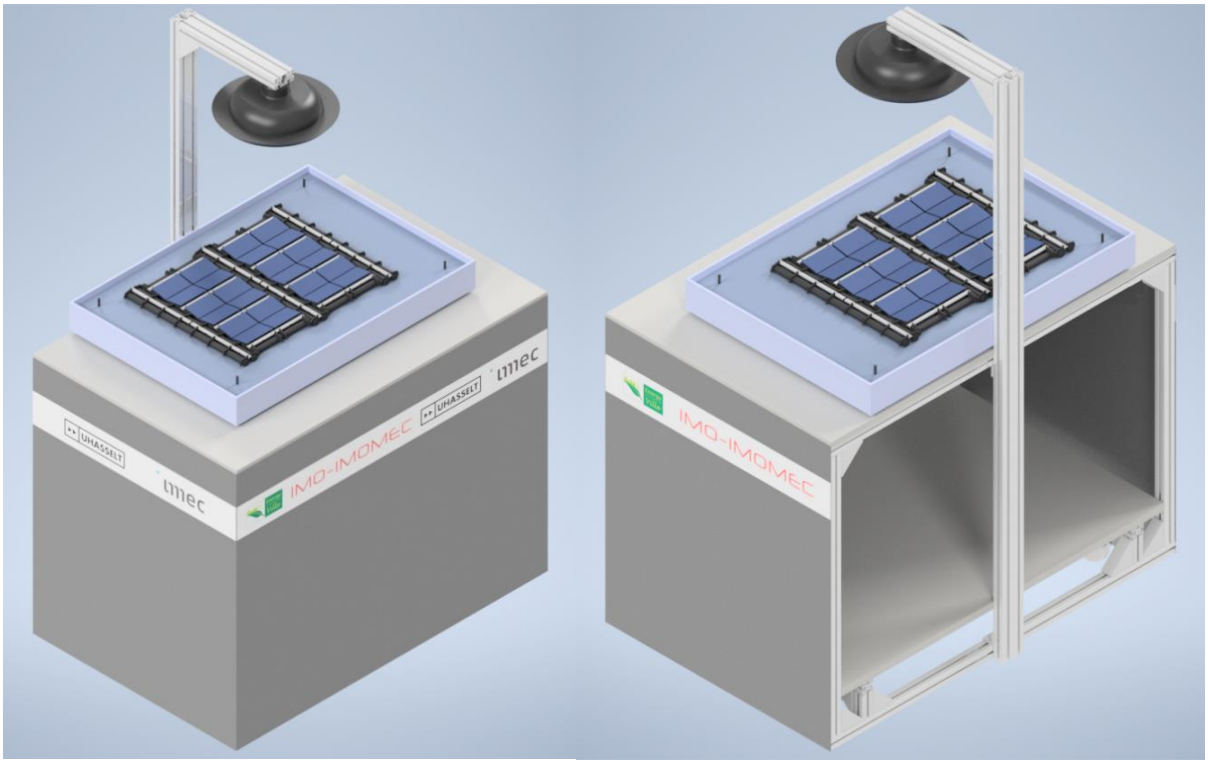

Figure 67: Front and back shot from final design

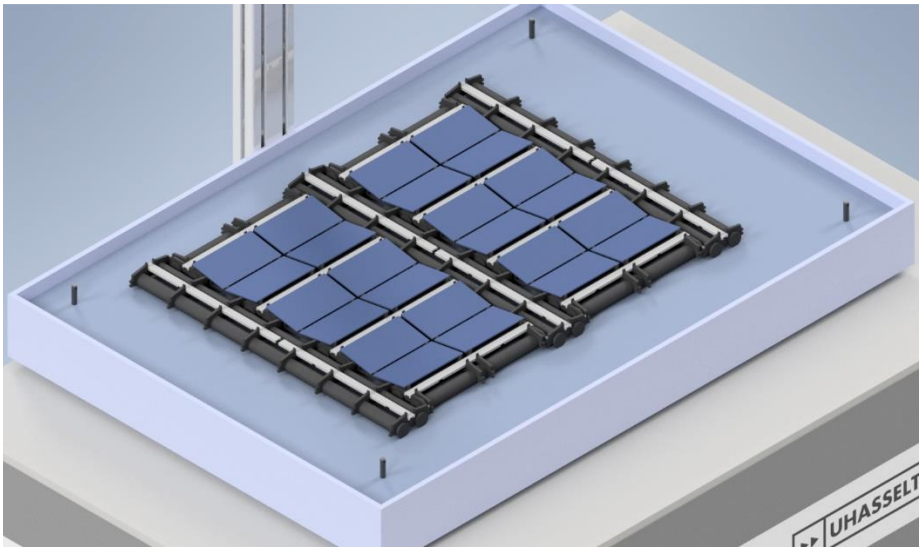

Figure 68: Close-up shot of floating structure from final design

6.2. Building process

The building process started after the order from Item arrived at Energyville. The table frame was assembled first, as designed in the CAD model. But after seeing the height of the table, adjustments were made to the framing around the wheels as mentioned in section 6.1.4. To mount the lamp to the arm, a groove was milled into the profile for a bolt to fit through. Eighty millimetres were then sawn off from the bottom plate to fit underneath the table. The tabletop and bottom plate were screwed to the ITEM profiles with corner pieces that were bought from Brico. Holes were drilled in the cover plates and were then spray painted. Figures 69 and 70 show pictures of the adjustment and the assembled table.

Figure 69: Adjustment to lower table height

Figure 70: Assembled table without container

Simultaneously, the floats, walkways and anchor poles were 3D-printed, cleaned, and assembled. Figure 71 illustrates the assembled floating structure.

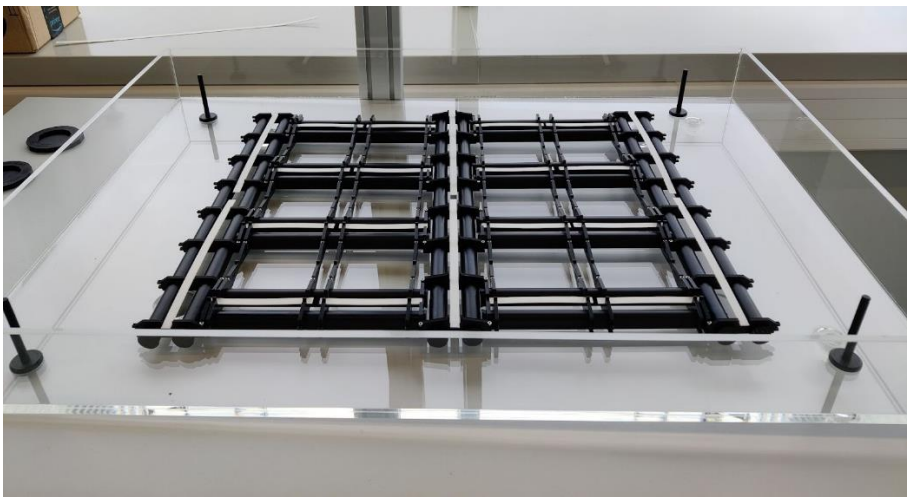

Figure 71: Assembled floating structure

When the floating structure was assembled, a test was done to see if the structure was buoyant enough. The floating structure was placed in the container and water was poured in. Overall, the structure floated, and no modules got wet. But it was noticed that, towards the middle of the structure, the floats sagged a few millimetres. To fix this problem and provide more buoyancy in the middle section, the floats were adjusted to hold four tubes instead of two. After reassembling, there was no more sagging in the middle section. Pictures of this adjustment are shown in Figures 72 to 74.

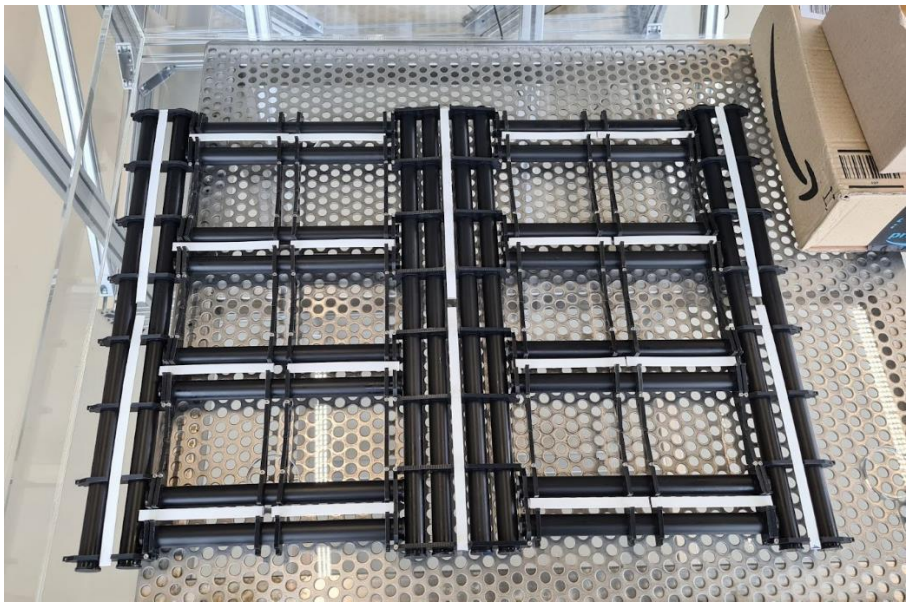

Figure 72: Addition of two tubes in the middle section of the floating structure

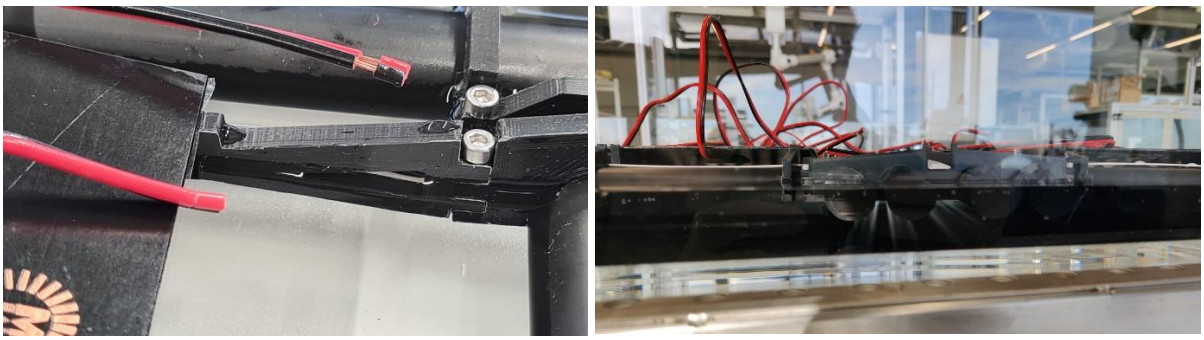

Figure 73 and 74: Sagging of floats (left) and buoyancy after fix (right)

Additionally, two taps were installed under the top sheet of the setup to drain the water. Four circular supports were also 3D printed to keep the container in the correct position using a thin wire. Figure 75 show a picture of the taps.

Figure 75: Taps under top sheet of demonstrator

With the mechanical part of the demonstrator more or less complete, it was time to start the process of electrically connecting the modules and the measuring setup. The 24 PV modules are divided into six strings of four modules in series which are then connected together in parallel. This choice is made because the modules are separated into groups of four by the walkways and thus it would be very hard to manage the cables if another configuration were chosen. Before each connection was properly soldered together, the short-circuit current was measured using the previously mentioned configuration. Figure 76 shows a picture of the measurements being taken.

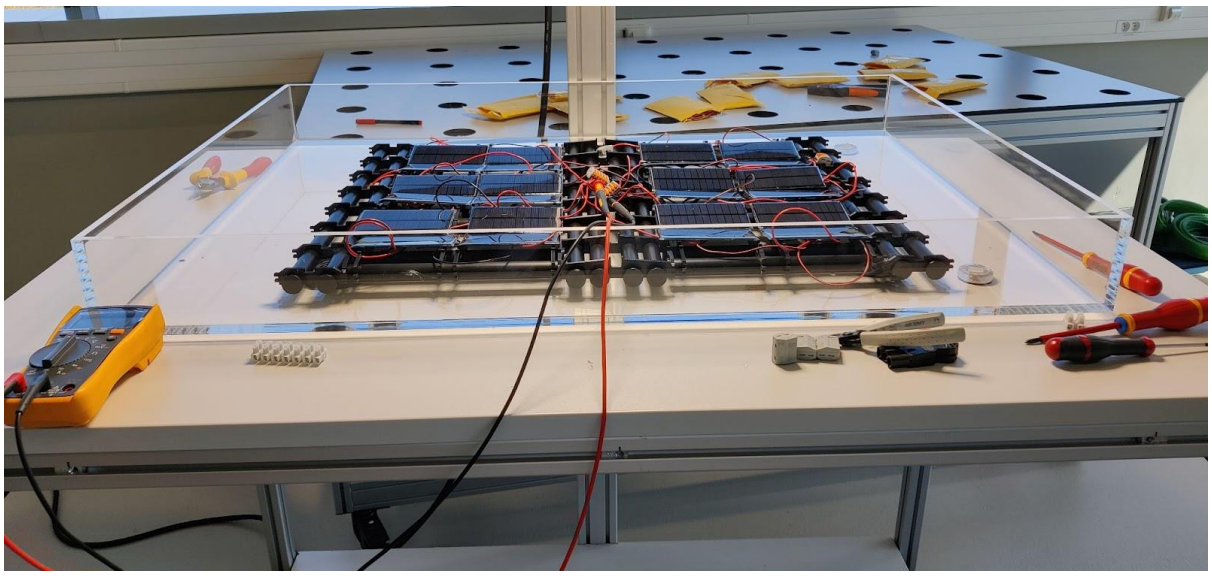

Figure 76: Measuring of PV modules

While the system was placed below the lamp, around 0,080 A was measured. This is much lower than what the array should be able to generate. A single module should produce 1 W of power at 6 V. This means the current should be around 0,166 A. Since six of the system's strings are connected in parallel, the short-circuit current should be around 1 A. For testing purposes, the system was then measured in outside, clear-sky conditions to see if higher currents could be measured. On the roof of the Energyville 2 building, the circuit reached a maximum of 0,7 A which is closer to what the specifications suggest. This means it is likely that the lamp is emitting certain wavelengths that the modules can not properly convert to electricity.

Based on these low current measurements below the lamp, a few important decisions were made. First, it was decided that the final measurement setup would stick with measuring just the short circuit current. The low output of the system would make the benefit of an MPPT negligible and not worth the additional investment. Next to this, the decision was made to no longer include wind simulation using fans. Due to the modules working at a very low-capacity factor, the heat generation will be very low. Therefore, the cooling effect will be negligible. Finally, it was decided that the measured short circuit current would be displayed as a percentage.

Besides all of these decisions based on the measurements, it could also be concluded that all modules were operational. So, with the arrangement of the modules decided, the cables could be properly routed. The cables were connected using tin and a soldering iron after which they were hidden under the 3D-printed walkways. In the middle, all strings come together at two busbars and are routed to the side of the container. Figures 77 and 78 show the routing of the cables.

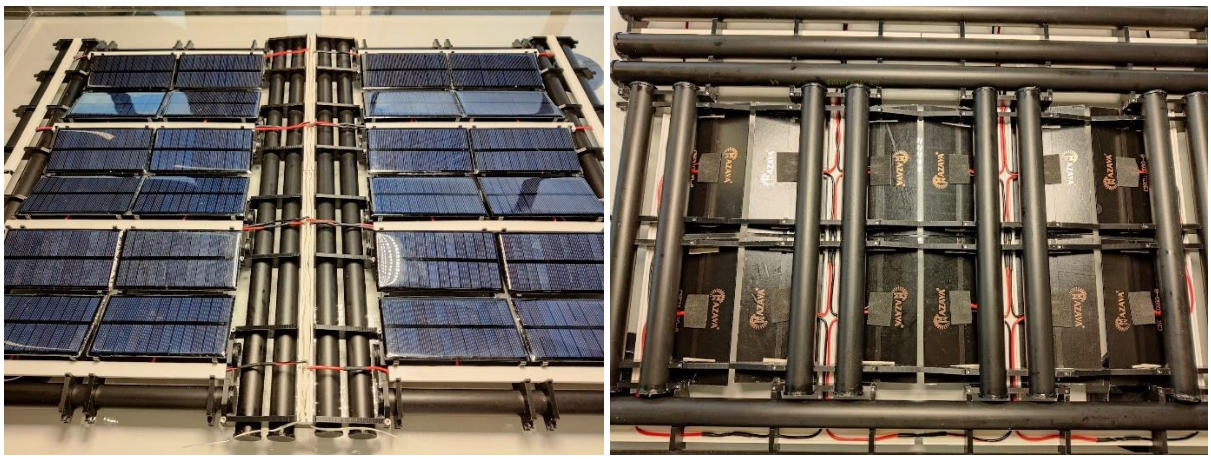

Figure 77 and 78: PV modules cable routing

Finally, to create the proper measuring setup, a Raspberry Pi is used together with a DC current and voltage sensor. The Raspberry Pi is connected to a monitor using a mini-HDMI to HDMI cable. A script on the Pi reads the measurements from the DC current sensor and then displays it on a monitor. The current sensor is a INA219 I2C DC current and voltage sensor that works up to 3,2 A with a resolution of 0.8 mA. The Raspberry Pi is a Raspberry Pi 4 Model B with 4 GB of RAM. A schematic of this is illustrated in Figure 79.

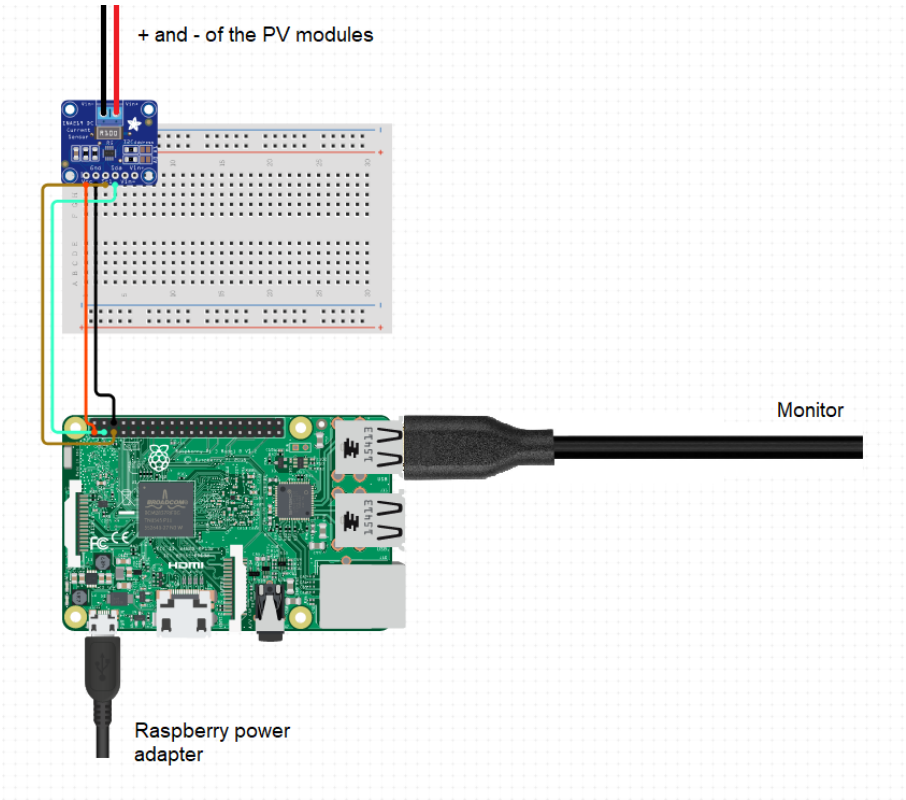

Figure 79: Measuring setup with Raspberry Pi [59]

6.3. Final result

The final demonstrator consists of a setup with a plexiglass container holding a miniature FPV system. The table frame is built using ITEM profiles, has aluminium cover sheets on the front and sides and is mounted on wheels. On top of the table frame the miniature FPV system is placed. This is based on the Clicfloats system and consists of 24 PV modules. The short-circuit voltage of these 24 panels is measured with a Raspberry Pi and shown on a monitor as an indication of the energy yield. The estimated and actual cost of the demonstrator are listed in Attachment 1. Figures 80 to 82 show pictures of the final result.

Figure 80: Front view of final demonstrator

Figure 81: Side view of final demonstrator

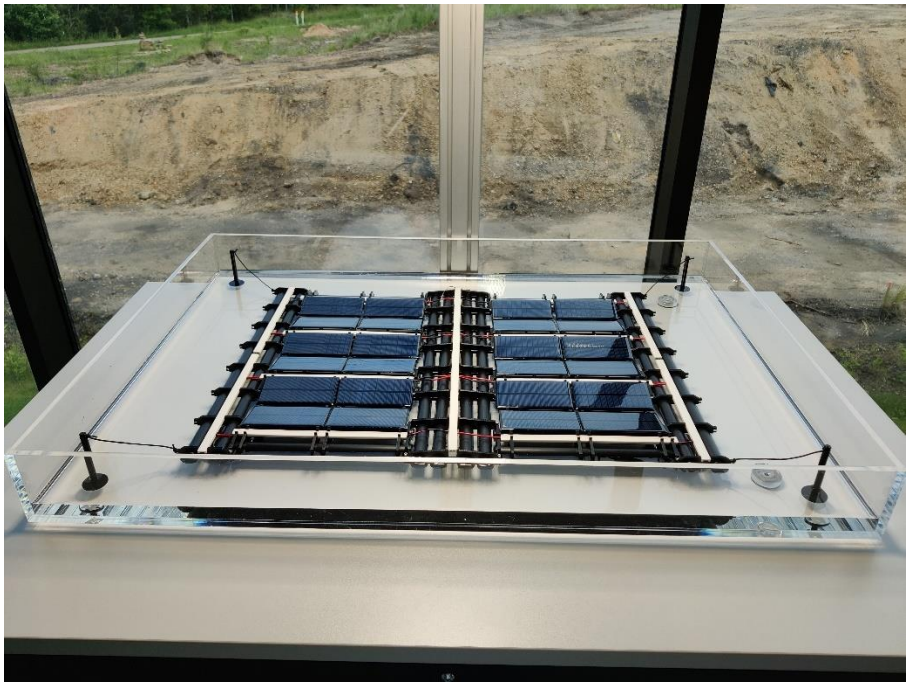

Figure 82: Close-up view of final floating structure

7. Conclusion

This Master's thesis covered three main topics. The first part dealt with simulating an FPV system using commercially available software. The results of this were then compared with measured values and the results of imec's framework. Secondly, a data analysis was performed using the measurements from the Clicfloats FPV plant. This was done to determine the influence of water temperature and wind velocity on module temperature. Finally, the process of designing and building an FPV demonstrator was discussed.

The results of the PVSyst simulation, performed on the Clicfloats FPV system, show that PVSyst underestimates the AC power output with a normalised MBE of 5.93%. This error can likely be attributed to an overestimation in module temperature. When only the predetermined important power range is analysed, the accuracy of the model improves. In a comparison between PVSyst, imec's framework and the measured data, PVSyst shows slightly better results for power output estimation. The causes for PVSyst's better performance are determined to be the poor shunt resistance calculation used in imec's electrical model and the underestimation in module temperature of PVSyst. This in comparison to the very accurate model used by imec. Future research could compare the PVSyst simulation with the newer version of imec's framework.

From the data analysis it can be concluded that module cooling, in the Clicfloats system, is mostly a result of convective cooling done by wind. This is in line with conclusions from literature that claim the module temperature in FPV systems is affected more by the wind velocity than the water temperature. Additionally, wind originating from the north and the south proved to be the most beneficial for module cooling. Next to this, it is found that the water level in the Clicfloats system seems to have no effect on the energy yield. The possible additional shading thus seems to be negligible. A possible combined cooling effect between wind and water was also analysed but no definite conclusion could be drawn. Further research is needed surrounding this topic. A direct comparison between the Clicfloats system and a similar GPV system would also be interesting for future research since it could verify the claimed increased energy yield of FPV.

The constructed FPV demonstrator is comprised of a table frame that supports a plexiglass container. This container is filled with water on which 24 miniature PV modules float. The design of the floating structure is based on the one used in the Clicfloats system. A lamp provides light to the modules so they can operate, and their short circuit current can be measured. This is displayed on a monitor using a Raspberry Pi. In the future, the interactivity of the demonstrator could be improved by adding better modules that would benefit from convective cooling supplied by fans as a means of wind simulation.

Reference list

[1] "Where Sun Meets Water FLOATING SOLAR MARKET REPORT," 2019. [Online]. Available: www.worldbank.org

[2] H. Vella, "Inside the world's largest dam-based floating solar power project," *Power-technology*, Jan. 12, 2021.

[3] "Riding the wave of solar energy: Why floating solar installations are a positive step for energy generation." Accessed: Oct. 02, 2021. [Online]. Available: www.recgroup.com

[4] G. Gijo and P. Pranav, "Floating PV systems – an overview of design considerations," Dec. 2019, doi: 10.1002/pip.3039.

[5] G. M. Tina, F. Bontempo Scavo, L. Merlo, and F. Bizzarri, "Analysis of water environment on the performances of floating photovoltaic plants," *Renewable Energy*, vol. 175, pp. 281–295, Sep. 2021, doi: 10.1016/j.renene.2021.04.082.

[6] Marco. Rosa-Clot and Giuseppe. Marco Tina, *Floating PV Plants*. San Diego : Academic Press, 2020.

[7] M. Haggag, "Exploring the Thermal Dynamics of a Floating Photovoltaic System," 2021.

[8] S. Oliveira-Pinto and J. Stokkermans, "Assessment of the potential of different floating solar technologies – Overview and analysis of different case studies," *Energy Conversion and Management*, vol. 211, May 2020, doi: 10.1016/j.enconman.2020.112747.

[9] D. G. As, "RECOMMENDED PRACTICE Design, development and operation of floating solar photovoltaic systems," 2021.

[10] "Where Sun Meets Water FLOATING SOLAR HANDBOOK FOR PRACTITIONERS," 2019. [Online]. Available: www.worldbank.org

[11] "Solar Integration: Inverters and Grid Services Basics ," *Solar Energy Technologies Office*. https://www.energy.gov/eere/solar/solar-integration-inverters-and-grid-services-basics (accessed Dec. 06, 2021).

[12] J. 'Smalley, "What is a combiner box?," *Solar Power World*, Jun. 30, 2015. https://www.solarpowerworldonline.com/2015/06/what-is-a-combiner-box/ (accessed Dec. 06, 2021).

[13] "Solar Resource Glossary," *National Renewable Energy Laboratory*. https://www.nrel.gov/grid/solar-resource/solar-glossary.html#watervapor (accessed Dec. 10, 2021).

[14] "Glossary of meteorology - Precipitation," *American Meteorological Society*. https://web.archive.org/web/20081009142439/http://amsglossary.allenpress.com/glossary/search?id=precipitation1 (accessed Dec. 04, 2021).

[15] S. S. ' 'Wyer, *A treatise on producer-gas and gas-producers*, 2nd ed. New York: McGraw-Hill, 1906. Accessed: Dec. 04, 2021. [Online]. Available: https://archive.org/details/treatiseonproduc00wyerrich/page/22/mode/2up

[16] W. Porter, "BIFACIAL MODULES: THERE ARE TWO SIDES TO EVERY SOLAR PANEL," 2019.

[17] B. Müller, S. Dittmann, D. Dirnberger, and U. Kräling, “Uncertainties of Laboratory Measurements for Energy Rating,” Sep. 2012, doi: 10.4229/27thEUPVSEC2012-4BV.2.24.
[18] P. Dwivedi, K. Sudhakar, A. Soni, E. Solomin, and I. Kirpichnikova, “Advanced cooling techniques of P.V. modules: A state of art,” *Case Studies in Thermal Engineering*, vol. 21, 2020, doi: 10.1016/j.csite.2020.100674.
[19] “Application Note - How to Simulate a SolarEdge PV System in PVsyst,” *Solar Edge*. Jan. 2021.
[20] G. Barbose and N. Darghouth, “Tracking the Sun: Pricing and Design Trends for Distributed Photovoltaic Systems in the United States - 2019 Edition,” Oct. 2019. [Online]. Available: https://escholarship.org/uc/item/5422n7wm
[21] “Heat Generation in PV Modules,” *pv education*. https://www.pveducation.org/pvcdrom/modules-and-arrays/heat-generation-in-pv-modules (accessed Apr. 10, 2022).
[22] “Heat Loss in PV Modules,” *pv education*. https://www.pveducation.org/pvcdrom/modules-and-arrays/heat-loss-in-pv-modules (accessed Apr. 10, 2022).
[23] S. Z. Golroodbari and W. van Sark, “Simulation of performance differences between offshore and land-based photovoltaic systems,” *Progress in Photovoltaics: Research and Applications*, vol. 28, no. 9, pp. 873–886, Sep. 2020, doi: 10.1002/pip.3276.
[24] H. S. Jeong, J. Choi, H. H. Lee, and H. S. Jo, “A study on the power generation prediction model considering environmental characteristics of floating photovoltaic system,” *Applied Sciences (Switzerland)*, vol. 10, no. 13, Jul. 2020, doi: 10.3390/app10134526.
[25] I. M. Peters and A. M. Nobre, “On Module Temperature in Floating PV Systems,” in *Conference Record of the IEEE Photovoltaic Specialists Conference*, Jun. 2020, vol. 2020-June, pp. 0238–0241. doi: 10.1109/PVSC45281.2020.9300426.
[26] T. Kjeldstad, D. Lindholm, E. Marstein, and J. Selj, “Cooling of floating photovoltaics and the importance of water temperature,” *Solar Energy*, vol. 218, pp. 544–551, Apr. 2021, doi: 10.1016/j.solener.2021.03.022.
[27] “Are wind speeds the same over land as they are over the ocean?,” *National data buoy center*. https://www.ndbc.noaa.gov/educate/windspeed_ans.shtml (accessed Apr. 11, 2022).
[28] W. C. L. Kamuyu, J. R. Lim, C. S. Won, and H. K. Ahn, “Prediction model of photovoltaic module temperature for power performance of floating PVs,” *Energies (Basel)*, vol. 11, no. 2, Feb. 2018, doi: 10.3390/en11020447.
[29] H. Ziar *et al.*, “Innovative floating bifacial photovoltaic solutions for inland water areas,” *Progress in Photovoltaics: Research and Applications*, vol. 29, no. 7, pp. 725–743, Jul. 2021, doi: 10.1002/pip.3367.
[30] E. Skoplaki and J. A. Palyvos, “On the temperature dependence of photovoltaic module electrical performance: A review of efficiency/power correlations,” *Solar Energy*, vol. 83, no. 5, pp. 614–624, May 2009, doi: 10.1016/j.solener.2008.10.008.
[31] H. Goverde *et al.*, “Spatial and temporal analysis of wind effects on PV module temperature and performance,” *Sustainable Energy Technologies and Assessments*, vol. 11, pp. 36–41, Sep. 2015, doi: 10.1016/j.seta.2015.05.003.

[32] Y. Y. Wu, S. Y. Wu, and L. Xiao, “Numerical study on convection heat transfer from inclined PV panel under windy environment,” *Solar Energy*, vol. 149, pp. 1–12, 2017, doi: 10.1016/j.solener.2017.03.084.

[33] O. Turgut and N. Onur, “Three dimensional numerical and experimental study of forced convection heat transfer on solar collector surface,” *International Communications in Heat and Mass Transfer*, vol. 36, no. 3, pp. 274–279, Mar. 2009, doi: 10.1016/j.icheatmasstransfer.2008.10.017.

[34] M. Redón Santafé, J. B. Torregrosa Soler, F. J. Sánchez Romero, P. S. Ferrer Gisbert, J. J. Ferrán Gozálvez, and C. M. Ferrer Gisbert, “Theoretical and experimental analysis of a floating photovoltaic cover for water irrigation reservoirs,” *Energy*, vol. 67, pp. 246–255, Apr. 2014, doi: 10.1016/j.energy.2014.01.083.

[35] A. Glick *et al.*, “Influence of flow direction and turbulence intensity on heat transfer of utility-scale photovoltaic solar farms,” *Solar Energy*, vol. 207, pp. 173–182, Sep. 2020, doi: 10.1016/j.solener.2020.05.061.

[36] M. J. Wilson and M. C. Paul, “Effect of mounting geometry on convection occurring under a photovoltaic panel and the corresponding efficiency using CFD,” *Solar Energy*, vol. 85, no. 10, pp. 2540–2550, Oct. 2011, doi: 10.1016/j.solener.2011.07.013.

[37] G. Gan, “Effect of air gap on the performance of building-integrated photovoltaics,” *Energy*, vol. 34, no. 7, pp. 913–921, 2009, doi: 10.1016/j.energy.2009.04.003.

[38] P. ’Brian, “Kyocera to drop NYSE listing,” *pv magazine*, Feb. 26, 2018. https://www.pv-magazine.com/2018/02/26/kyocera-to-drop-nyse-listing/ (accessed Apr. 15, 2022).

[39] “Floating pv systems,” *solar float*. https://www.solarfloat.com/en-nl/floating-pv-systems (accessed Apr. 15, 2022).

[40] “Clicfloats,” *Connectum*. https://www.connectum.biz/clicfloats?lang=en (accessed Nov. 02, 2021).

[41] L. Rodriguez, “Solar panel orientation: How using East-West structures improves the performance of your project,” *Ratedpower*, 2021. https://ratedpower.com/blog/solar-panel-orientation/ (accessed Apr. 16, 2022).

[42] M. Rosa-Clot and G. M. Tina, “Cooling systems,” in *Floating PV Plants*, Elsevier, 2020, pp. 67–77. doi: 10.1016/B978-0-12-817061-8.00006-3.

[43] M. Rosa-Clot and G. M. Tina, “Submerged PV Systems,” in *Submerged and Floating Photovoltaic Systems*, Elsevier, 2018, pp. 65–87. doi: 10.1016/b978-0-12-812149-8.00004-1.

[44] S. C. Ng, K. S. Low, and N. H. Tioh, “Newspaper sandwiched aerated lightweight concrete wall panels - Thermal inertia, transient thermal behavior and surface temperature prediction,” *Energy and Buildings*, vol. 43, no. 7, pp. 1636–1645, Jul. 2011, doi: 10.1016/j.enbuild.2011.03.007.

[45] M. Piotrowicz and W. Maranda, “The effect of thermal inertia in photovoltaic module simulation; The effect of thermal inertia in photovoltaic module simulation,” 2012.

[46] B. Tuncel, T. Ozden, R. S. Balog, and B. G. Akinoglu, “Dynamic thermal modelling of PV performance and effect of heat capacity on the module temperature,” *Case Studies in Thermal Engineering*, vol. 22, Dec. 2020, doi: 10.1016/j.csite.2020.100754.

[47] G. H. Yordanov and J. D. Moschner, “Meteorological and Metrological Data Acquisition for Connectum / ClicFloats,” 2021.

[48] I. M. Peters and A. M. Nobre, “Deciphering the thermal behavior of floating photovoltaic installations,” *Solar Energy Advances*, vol. 2, p. 100007, 2022, doi: 10.1016/j.seja.2021.100007.
[49] N. Umar, B. Bora, C. Banerjee, and B. S. Panwar, “Comparison of different PV power simulation softwares: case study on performance analysis of 1 MW grid-connected PV solar power plant,” 2018.
[50] “Multi-MPPT inverters,” *PVSyst*. https://www.pvsyst.com/help/multi_mppt_use.htm (accessed Nov. 11, 2021).
[51] “Power sharing,” *PVSyst*. https://www.pvsyst.com/help/powersharing.htm (accessed Nov. 11, 2021).
[52] “Array Thermal losses,” *PVSyst*. https://www.pvsyst.com/help/thermal_loss.htm (accessed Nov. 11, 2021).
[53] O. Dupon, “An overview of the PV-System simulation framework,” *imec*.
[54] J. Suh, Y. Jang, and Y. Choi, “Comparison of electric power output observed and estimated from floating photovoltaic systems: A case study on the hapcheon dam, Korea,” *Sustainability (Switzerland)*, vol. 12, no. 1, Jan. 2020, doi: 10.3390/su12010276.
[55] N. Manoj Kumar, S. Chakraborty, S. Kumar Yadav, J. Singh, and S. S. Chopra, “Advancing simulation tools specific to floating solar photovoltaic systems – Comparative analysis of field-measured and simulated energy performance,” *Sustainable Energy Technologies and Assessments*, vol. 52, p. 102168, Aug. 2022, doi: 10.1016/j.seta.2022.102168.
[56] J. K. Kaldellis, M. Kapsali, and K. A. Kavadias, “Temperature and wind speed impact on the efficiency of PV installations. Experience obtained from outdoor measurements in Greece,” *Renewable Energy*, vol. 66, pp. 612–624, Jun. 2014, doi: 10.1016/j.renene.2013.12.041.
[57] Y. Du *et al.*, “Evaluation of photovoltaic panel temperature in realistic scenarios,” *Energy Conversion and Management*, vol. 108, pp. 60–67, Jan. 2016, doi: 10.1016/j.enconman.2015.10.065.
[58] “3 Pièces Mini Panneau Solaire Dc 6 V Polysilicium Module de Chargeur de Cellule époxy Solaire Kits de Système de Bricolage Solaire Avec Câble de 30 cm,” *Amazon.fr*. https://www.amazon.fr/dp/B08THTGHG6 (accessed Nov. 10, 2021).
[59] “Circuito.io,” *Circuito.io*. https://www.circuito.io/ (accessed May 18, 2022).

Attachments

Attachment 1: Price of the demonstrator

Estimated price of the demonstrator:

Quantity	Item	Assumed price (complete quantity)	Note
1	microcontroller	€ 80,00	Raspberry Pi starter kit
1	powersupply for electronics	€ -	Already have this on Energyville
1	display	€ -	Already have this on Energyville, with table
24	mini solar cells	€ 230,00	2 extra calculated in price:
6 16	walkways floats	€ 88,00	Material: PVC - Price when costum made, propably lower
4	poles for anchoring	€ 20,00	
6 16	tubes for floats	€ -	~7m in total - Already have these on Energyville
104	pins for floats	€ 20,00	2.5M RVS bolts
2 2	wheels (with and without brake)	€ 80,00	
1 2 2	coverpanels	€ 60,00	Material: aluminium
1 1	basepanel + planel under demonstrator for electronics	€ 120,00	Material: HPL - glad wit 8 mm
1 5 9	ISB profiles (different lengths)	€ 230,00	~11m in total - 40x40 aluminium isb profiles
2 2 4 1 6 18	mountingpieces for isb profiles	€ 70,00	
1	plexiglass container	€ 805,00	Requested quotation
16 36 72 44	floating parts (3 different parts) + caps for tubes	€ 40,00	PLA filament
1	lamp	€ -	Reuse of previous demonstrator
		Estimated price for demonstrator:	
		€ 1.843,00	

Actual price of the demonstrator:

Item	Actual price	Note
Measuring unit	€ 123,20	Raspberry Pi + sensor + peripherals
Plexiglass container	€ 805,00	Ordered at Teblick
Materials for table frame	€ 1.485,67	Ordered at ITEM
Mini solar cells	€ 230,00	Ordered at Amazon
3D printer filament	€ -	Was available at Energyville
Tubes for floats	€ -	Was available at Energyville
Bolts for mounting floats	€ -	Was available at Energyville
Lamp	€ -	Reused from older demonstrator setup
Stickers	€ 34,50	Ordered at drukland.be
Mounting brackets	€ 10,00	Bought at Brico
Paint cover panels	€ 50,00	Bought at local store
Taps	€ -	Was available at Energyville
	Actual price for demonstrator:	
	€ 2.738,37	